Zoological Journal of the Linnean Society, 2020, **190**, 654–708. With 29 figures.

Phylogenetic analysis of the subfamily Prodidominae (Arachnida: Araneae: Gnaphosidae)

BRUNO V. B. RODRIGUES[1,2*] and CRISTINA A. RHEIMS[1]

[1]*Laboratório Especial de Coleções Zoológicas, Instituto Butantan. Av. Vital Brasil, 1500, CEP 05503-900, São Paulo, SP, Brazil*
[2]*Departamento de Zoologia, Instituto de Biociências, Universidade de São Paulo, São Paulo, SP, Brazil*

Received 16 August 2019; revised 17 January 2020; accepted for publication 2 February 2020

Prodidominae was recently re-established as a subfamily of Gnaphosidae, comprising 316 species placed in 33 genera. In this study, we conduct a cladistic analysis including 59 species of Prodidominae and 32 outgroup species. The matrix is composed of 291 morphological characters and the data are analysed under the parsimony criterion, using differing weighting regimes. Prodidominae is not recovered as monophyletic, because *Anagrina* did not arise within the subfamily. *Cryptotoerithus*, *Molycria*, *Myandra*, *Nomindra*, *Wesmaldra* and *Wydundra* arise to form a clade. Thus, we re-establish Molycriinae as a distinct subfamily in Gnaphosidae, sister to Prodidominae. We redefine the limits of Prodidominae to include the genera *Austrodomus*, *Brasilomma*, *Caudalia*, *Chileomma*, *Chileuma*, *Chilongius*, *Eleleis*, *Indiani*, *Katumbea*, *Lygromma*, *Lygrommatoides*, *Moreno*, *Namundra*, *Neozimiris*, *Nopyllus*, *Paracymbiomma*, *Plutonodomus*, *Prodidomus*, *Purcelliana*, *Theuma*, *Theumella*, *Tivodrassus*, *Tricongius*, *Zimirina* and *Zimiris*. Species of these genera share the presence of anterior lateral spinnerets with pyriform gland spigots associated with patches of long setae and the presence of a large protrusion between coxae IV with erect setae and unsclerotized margins. In addition, we propose three new synonymies: *Oltacloea* as a junior synonym of *Tricongius*, and *Prodida* as junior synonym of *Prodidomus*. *Lygromma ybyguara* is transferred to *Tricongius*.

ADDITIONAL KEYWORDS: Araneae – Taxa, morphology – Anatomy, phylogenetic systematics – Phylogenetics.

INTRODUCTION

Gnaphosids are predominantly nocturnal, free-living spiders that are widely distributed around the world (Ubick *et al.*, 2005; World Spider Catalog, 2020). They are originally ground-dwellers and can be found in leaf litter, beneath rocks and within and under decomposing wood. Few species are found in arboreal habitats (Ubick *et al.*, 2005). Some species are also capable of occupying synanthropic habitats, such as *Urozelotes rusticus* (L. Koch, 1872), *Scotophaeus blackwalli* (Thorell, 1871) and *Zimiris doriai* Simon, 1882 (Dippenaar-Schoeman & Jocqué, 1997; Platnick & Penney, 2004). Gnaphosids do not spin webs but use silk for draglines, retreats and egg sacs. They are mostly generalized predators that capture a wide variety of prey (including other spiders) using speed, force and agility (Dippenaar-Schoeman & Jocqué, 1997; Ubick *et al.*, 2005; Dippenaar Schoeman, 2014). Recently, Wolff *et al.* (2017) observed that morphological modifications of the pyriform gland spigots allow functional modifications in some Gnaphosidae, and the silk of these spigots became mainly used for prey capture. Gnaphosidae is the fourth most diverse spider family with 2539 known species distributed across 159 genera (World Spider Catalog, 2020). The family includes nine subfamilies, including Prodidominae, although several genera are not allocated to any subfamily (Azevedo *et al.*, 2018).

The taxonomic status of prodidomine spiders has always been controversial, because the group has historically alternated between family and subfamily status (Simon, 1884; Platnick & Shadab, 1976; Platnick, 1990; Azevedo *et al.*, 2018). Simon (1884) originally described Prodidomidae to include *Prodidomus* Hentz, 1847, *Trocantheria* Karsch, 1878 and *Zimiris* Simon, 1882. It retained family status for almost a

*Corresponding author. E-mail: bruno.vbrodrigues@gmail.com
[Version of record, published online 27 March 2020; http://zoobank.org/urn:lsid:zoobank.org:pub:B45352ED-D736-49E7-B387-F4374406A129]

© 2020 The Linnean Society of London,

century, until Platnick & Shadab (1976) reclassified it as a subfamily of Gnaphosidae. At the time, the authors suggested that Prodidominae Simon, along with Molycriinae Simon and Anagraphidinae Simon, form a monophyletic group within Gnaphosidae. This group is supported by the presence of a distinct lobe of the sternum, projecting between the coxae IV. Platnick (1990) again raised Prodidomidae to family rank based on spinneret morphology and transferred Molycriinae and Anagraphidinae from Gnaphosidae to Prodidomidae. Platnick & Baehr (2006) later transferred *Anagraphis* Simon, 1893 back to Gnaphosidae and proposed Theuminae Platnick & Baehr for the remaining genera of the former Anagraphidinae. Prodidomidae remained a well-established family, comprising the subfamilies Prodidominae Simon, Theuminae Platnick & Baehr and Molycriinae Simon, although, with the exception of Molycriinae (Platnick & Bird 2007), their monophyly was never tested.

Prodidominae comprises 88 species in 11 genera, grouped together by the presence of peculiar minor ampullate gland spigots, in which the shaft is reduced to a needle-like extension of the base (Platnick 1990). *Prodidomus* is the largest genus with 53 species occurring worldwide. *Austrodomus*, *Eleleis* and *Purcelliana* are endemic to South Africa, and *Katumbea* and *Plutonodomus* are restricted to Tanzania. *Zimirina* is mostly Palaearctic, with one species described from South Africa, while *Prodida* occurs in the Phillipines and the Seychelles Islands. *Neozimiris* occurs from Mexico to Ecuador. *Caudalia* is endemic to Cuba. *Zimiris* includes one species from Yemen and another, *Z. doriae* Simon, 1882 with a circumtropical distribution, having been introduced to several countries throughout the world (World Spider Catalog, 2020).

Theuminae includes 88 species in 14 genera characterized by the sternum with a large protrusion between the coxae IV lacking a sclerotized margin (Platnick *et al.*, 2005; Platnick & Baehr, 2006). The group is mostly Neotropical, with the exception of *Anagrina* from eastern Africa and Niger, *Lygrommatoides* from Japan, *Theuma* from South Africa and Namibia, and *Theumella* from Ethiopia. *Paracymbiomma* and *Brasilomma* are endemic to Brazil and *Tivodrassus* is endemic to Mexico. *Lygromma* occurs from Mexico to Brazil. *Tricongius* occurs in Colombia, Venezuela and Brazil. *Chileomma*, *Chileuma* and *Chilongius* are endemic to Chile. *Moreno* is recorded from Chile and Argentina and *Otalcloea* from Argentina and Brazil.

Molycriinae is by far the largest and best-known prodidomid subfamily, with 139 species in seven genera (*Cryptoerithus* Rainbow, 1915, *Molycria* Simon, 1887, *Myandra* Simon, 1887, *Namundra* Platnick & Bird, 2007, *Nomindra* Platnick & Baehr, 2006, *Wesmaldra* Platnick & Baehr, 2006 and *Wydundra* Platnick & Baehr, 2006). Their members are recognized by the extraordinarily elongated anterior lateral spinnerets, which originate far in advance from the other spinneret pairs, near the middle of the ventral abdominal surface (Platnick & Baehr, 2006). It is predominantly Australian, with the exception of the African genus *Namundra*.

Studies on the phylogenetic relationships between Prodidomidae genera are scarce. Platnick & Baehr (2006) studied intensively the Australian genera and carried out a phylogenetic analysis including *Prodidomus* and Molycriinae. Although the analysis included only 11 taxa and 11 characters, the study helped elucidate the relationships between these genera, confirming the monophyly of the group. However, the analysis did not include the African genus *Namundra*, the single non-Australian genus that also has such characteristics. Thus, even though the relationships between the Australian genera were studied, the relationships between this group and other Prodidomidae are still uncertain.

Recently, several studies including morphological and molecular data were carried out to elucidate the relationships between spider families (Ramírez, 2014; Garrinson *et al.*, 2016; Wheeler *et al.*, 2017; Fernández *et al.*, 2018). Traditionally, Prodidomidae was associated with other families (Ammoxenidae Simon, Cithaeronidae Simon, Gallienellidae Millot, Gnaphosidae Pocock, Lamponidae Simon and Trochantheriidae Karsch) that comprised Gnaphosoidea, by sharing irregular and flattened posterior median eyes and obliquely depressed endites (Platnick, 1990). Nevertheless, Ramírez (2014) did not recover Gnaphosoidea and its representatives were distributed in several other groupings. Prodidomidae was included in the CTC clade (Claw Tuft Clasper), characterized by the development of a new mechanism for moving the claw tuft setae of the legs.

In a study involving only molecular data, Wheeler *et al.* (2017) also did not recover Gnaphosoidea as monophyletic and the relations of Prodidomidae and Gnaphosidae became more distant. The authors obtained the Australian genera separated from other Prodidomidae and grouped with other subfamilies of Gnaphosidae. Despite suggesting that Prodidomidae is not monophyletic, taxonomic changes were not carried out and the authors recommended that more studies be performed to better understand the phylogenetic position of their genera.

The most recent analysis including Prodidomidae was carried out by Azevedo *et al.* (2018), in which ten Prodidomidae genera were included. In this study, the authors treated Prodidomidae as a subfamily and placed it in Gnaphosidae, suggesting that Prodidominae, as currently delimited, could be a

group derived from Gnaphosidae, as per Platnick & Shadab (1976). Thus, Prodidominae is characterized by an incomplete distal article of the anterior lateral spinnerets composed of patches of setae closely associated with the pyriform gland spigots, with their base longer than the shaft (Platnick, 1990; Azevedo *et al.*, 2018). Although important taxonomic decisions were made about this group of spiders in this study, nothing was discussed about the relationships within the group.

A phylogenetic analysis of Prodidominae, including most of its accepted genera, will contribute towards the elucidation of the internal relationships, especially considering the position of the less studied genera, such as the African ones. In addition, this analysis could also contribute to a better understanding of the evolution of some characters within this poorly explored group. To continue and expand the recent morphological studies involving Prodidominae, this study aims to carry out a phylogenetic analysis, based on morphological characters, test the monophyly of the subfamily and propose a relationship hypothesis for their genera.

MATERIAL AND METHODS

Material examined

The examined material belongs to the following institutions (abbreviations and curators in parentheses): Agricultural Research Council, National Collection of Arachnida, Petroria, South Africa (ARC.LNR, R. Lyle); American Museum of Natural History, New York, USA (AMNH, L. Prendini); Australian Museum, Sydney, Australia (AM, G. A. Milledge); Instituto Butantan, São Paulo, Brazil (IBSP, A. D. Brescovit); Instituto de Ciencias Naturales, Universidad Nacional, Bogotá, Colombia (ICN, E. Florez); Instituto de Ecología y Sistemática, La Havana, Cuba (IES, L. F. Armas); Instituto Nacional de Pesquisas da Amazônia, Manaus, Brazil (INPA, A. L. Henriques); Iziko South African Museum, Cape Town, South Africa [SAMC (SAM), D. Larson]; Museo Argentino de Ciencias Naturales 'Bernardino Rivadavia', Buenos Aires, Argentina (MACN, M. Ramírez); Museu de Ciências e Tecnologia da Pontifícia Universidade Católica do Rio Grande do Sul, Porto Alegre, Brazil (PUCRS, R. Teixeira); Museu de Ciências Naturais da Fundação Zoobotânica do Rio Grande do Sul, Porto Alegre, Brazil (MCN, R. Ott); Museu Paraense Emílio Goeldi, Belém, Brazil (MPEG, A. B. Bonaldo); Museum National d'Histoire Naturelle, Paris, France (MNHN, C. Rollard); Museum of Comparative Zoology, Harvard University, Cambridge, Massachusetts, USA (MCZ, G. Giribet); National Museum Bloemfontein, Bloemfontein, South Africa (NMBA, L. Lotz); National Museum of Namibia, Windhoek, Namibia [NMNW (SMN), B. Muramba]; Oxford University Museum of Natural History, Oxford, England (OUMNH, Z. M. Simmons); Queensland Museum, Brisbane, Australia (QMB, R. Raven); Royal Museum of Central Africa, Tervuren, Belgium (RMCA, R. Jocque); Senckenberg Research Institute and Museum, Frankfurt am Main, Germany (SMF, P. Jäger); Universidade de Brasília, Distrito Federal, Brazil (UNB, P. C. Motta); Western Australian Museum, Welshpool, Australia (WAM, M. Harvey).

Specimen preparation

The material was examined immersed in 70–80% ethanol under a Leica MZ125 stereomicroscope. For visualization of internal structures of the female genitalia, the epigyne was detached from the body and digested with contact lens cleaner enzyme Ultrazime. Compound digital photographs were taken using a DFC295 camera mounted on a Leica M205A stereomicroscope. Extended focal range images were composed with the program Leica Application Suite v.3.3.0. Scanning electron micrograph (SEM) images were taken using a FEI Quanta 250 Scanning Electron Microscope at Instituto Butantan and a FEI XL 30 TMP Scanning Electron Microscope at Museo Argentino de Ciencias Naturales 'Bernardino Rivadavia'. For SEM preparations, specimens were cleaned with brushes or with ultrasonic cleaner. The material was dissected and dehydrated through a series of graded ethanol (80 to 100%), critical point dried, fixed on metal stubs with adhesive copper tape and sputter coated with gold.

Data matrix

The data matrix is composed of 91 terminal taxa, 32 comprising the outgroup and 59 the ingroup (Supporting Information, Data S1). Whenever possible, the type species of the genus was used to preserve nomenclatural stability. The outgroup composition was chosen based on recent studies (Murphy, 2007; Ramírez, 2014; Wheeler *et al.*, 2017; Azevedo *et al.*, 2018) and includes representatives of Anyphaenidae Bertkau, Cithaeronidae Simon, Corinnidae Karsch, Gallieniellidae Millot, Lamponidae Simon, Miturgidae Simon, Phrurolithidae Banks,Trochanteriidae Karsch and different genera of Gnaphosidae. The latter were selected based on groups and subfamilies proposed by Murphy (2007) and Azevedo *et al.* (2018), respectively. Genera from all biogeographic regions were selected. The Gnaphosidae genera *Hypodrassodes* Dalmas, 1919 and *Zelanda* Özdikmen, 2009, were scored based on matrix data from Azevedo *et al.* (2018), since they showed an important relationship with Prodidominae. *Xiruana gracilipes* (Keyserling, 1891), Anyphaenidae,

was used to root the tree based on recent phylogenetic analyses (Ramírez, 2014; Wheeler *et al.*, 2017; Azevedo *et al.*, 2018). Of the 32 outgroup species, 24 are type species of genera.

The ingroup is composed of representatives of 32 of the 33 valid genera of Prodidominae and four possibly new genera. In total, 59 species of Prodidominae were included, of which 26 are type species of genera. The monotypic genus *Lygrommatoides* was not included in the analysis, because the type specimen was not located and is probably lost. In addition, the original description is imprecise and without illustrations, which makes it difficult to identify additional material. In the few cases when females and males from different species of the same genus were studied, we treated them as a single chimera taxon, such as *Namundra griffinae* Platnick & Bird, 2007 and *Namundra* sp. Whenever possible, the genera were represented by more than one species to better represent the intergeneric relationship.

Several characters were scored based on SEM images and this procedure cannot be done for some of our terminal taxa, because only the holotype was analysed. This resulted in a dataset with several missing entries. However, when possible, complementary observations were taken from literature and reported in the voucher list (Supporting Information, Data S2).

The data matrix is composed of 291 morphological characters (Appendix), of which 66 are herein proposed and 225 are characters previously used in cladistic analyses that included Prodidominae species (Platnick, 1990, 2000, 2002; Platnick & Baehr, 2006; Ramírez, 2014; Azevedo *et al.*, 2018). Some of these characters were slightly altered and these modifications are indicated in the character list. For characters used by more than one author, only the first is cited. The description of characters follows Sereno (2007). All characters are treated as unordered and the autapomorphies were kept in the analysis, since they can be useful in future analyses.

Cladistic analysis

The phylogenetic analysis was performed under the parsimony criterion, using TNT 1.5 (Goloboff *et al.*, 2008; Goloboff & Catalano, 2016). The dataset was analysed with New Technology Search under equal weights and weighting regimes against homoplasy with the implied weighting option (Goloboff, 1993), using different values of concavity constant (k = 3–10, 15, 20, 25). The analysis was carried out using the following parameters: *Sectorial Search* (default mode), *Ratchet* (default mode), *Drift* (default mode) and *Tree Fusing* (five rounds) (Goloboff, 1999) until the most parsimonious trees (MPTs) was reached 50 times independently. The strict consensus of the different weighting regimes (EW and IW) were compared to evaluate the frequency and stability of clades (Goloboff *et al.*, 2008; Magalhaes & Santos, 2012; Azevedo *et al.*, 2018). Navajo-rugs were used to indicate the frequency of a clade in the preferred tree. Bremer relative support was used to evaluate clade support (Bremer, 1994; Goloboff & Farris, 2001), searching for suboptimal trees with one to ten steps more than the MPTs and retaining 2000–20 000 trees, respectively (*sub 1 hold 2000; bb=tbr fillonly; unique**). A comparative analysis, using SPR-distances for the strict consensus of different MTPs under weighting regimes, was used to determine topology stability (Robinson & Foulds, 1981; Goloboff *et al.*, 2008). The tree with the highest mean was chosen for the discussion and optimization of characters. WinClada v.1.00.08 (Nixon, 2002) was used for character state optimizations (Supporting Information, Fig. S1). Some topology tests were conducted to evaluate the stability of taxonomic groups established within Prodidominae, as well as groups established in recent analyses (Ramírez, 2014; Wheeler *et al.*, 2017; Azevedo *et al.*, 2018), but not supported by our results. Topologies with constrained searches were analysed through relative FIT difference (RFD), in which RFD is the measure of the difference of evidences contradicting the constrained tree in relation to the evidence favouring that tree (Goloboff & Farris, 2001). This measurement is calculated by the formula 1 – (C/F), where C is the sum of character FITs that had their values increased (favourable evidence) and F represents the character FITs that had their values decreased (contradictory evidence). Both values were calculated using TNT. Thus, the highest value of RFD in constrained trees indicates a low support for these clades and, therefore, favours the relationship hypotheses of the most parsimonious unconstrained trees.

Terminology

The terminology and abbreviations follow Ramírez (2014) and Azevedo *et al.* (2018): A, atrium; Ac, aciniform gland spigot; AF, anterior fold; AFH, anterior fold hood; ALS, anterior lateral spinnerets; C, conductor; CbRmP, cymbial retromedian process; CbTS, cymbial thick setae; CbVG, cymbial ventral groove; CD, copulatory duct; CO, copulatory opening; CSS, claw slit suture; Cy, cylindrical gland spigot; dRTA, dorsal retrolateral tibial apophysis; DTA, dorsal tibial apophysis; E, embolus; FD, fertilization duct; HCD, hyaline copulatory duct; IM, inflatable membrane; LETe, laminar extension of tegulum; LFF, lateral fold furrow; LFS, lateral fold suture; MA, median apophysis; MaAm, major ampullate gland spigot; MiAm, minor ampullate gland spigot;

Pa, patella; Pcb, paracymbium; PEs, promarginal escort seta; PH, posterior hood; Pi, pyriform gland spigots; PiB, pyriform spigot base; PIn, postepigastric invaginations; PiS, pyriform spigot shaft; PLS, posterior lateral spinnerets; PMS, posterior median spinnerets; PN, posterior notch; PRk, promarginal rake seta; PS, primary spermathecae; PWh, promarginal whisker seta; REs, retromarginal escort seta; ReT, reduced tooth; RRk, retromarginal rake seta; RTA, retrolateral tibial apophysis; RWh, retromarginal whisker seta; S, septum; SBP, setae bearing projection; Sc, scape; Sk, serrated keel; T, tegulum; TA, terminal apophysis; TEx, tegular excavation; Ti, tibia; Tr, trochanter; TSP, tegular spine-like process; vRTA, ventral retrolateral tibial apophysis; VTA, ventral tibial apophysis; **S**, septum; **SS**, secondary spermathecae.

RESULTS

The cladistic analysis under equal weights results in 314 most parsimonious trees (MPTs) with 1407 steps (CI = 22; RI = 65). The strict consensus shows that relationships between the Prodidominae genera are generally well resolved with two well-defined clades (Fig. 1). The topologies obtained under implied weighting with different concavity values (*K*) show few changes regarding the number of MPTs and steps. The analysis with k = 3–10 results in five MPTs, while the analyses with the other k values results in one most parsimonious tree. Thus, considering the tree with the highest mean similarity and stability of the results of strict consensus (Table 1), we decided to choose the trees obtained with k = 9 to discuss the relationships of Prodidominae (Fig. 2; Supporting Information, Fig. S1). The analysis with k = 9 resulted in five MPTs with total fit of 206.55708 (CI = 22; RI = 65).

Gnaphosidae is not recovered as monophyletic in our analysis, because *Micaria* Westring, 1851 arose as sister to Cithaeronidae (Fig. 2). Trochanteriidae, represented by the genera *Platyoides* O. Pickard-Cambridge, 1891, *Hemicloea* Thorell, 1870 and *Vectius* Simon, 1897, is recovered as monophyletic in all analyses.

Azevedo *et al.* (2018) defined the group Gnaphosidae *s.s.*, to include all taxa with pyriform gland spigots longer and wider than major ampullate gland spigots, therefore excluding all problematic taxa. In our analysis, this group recovers as monophyletic, with *Lampona* (Lamponidae) as sister-group (Fig. 2; Supporting Information, Fig. S1). Some relationships found by Azevedo *et al.* (2018) within this clade are also recovered in our analysis, such as the subfamilies Leptodrassinae Azevedo *et al.*, Zelotinae Platnick and Gnaphosinae Pocock (Suppoting Information, Fig. S1).

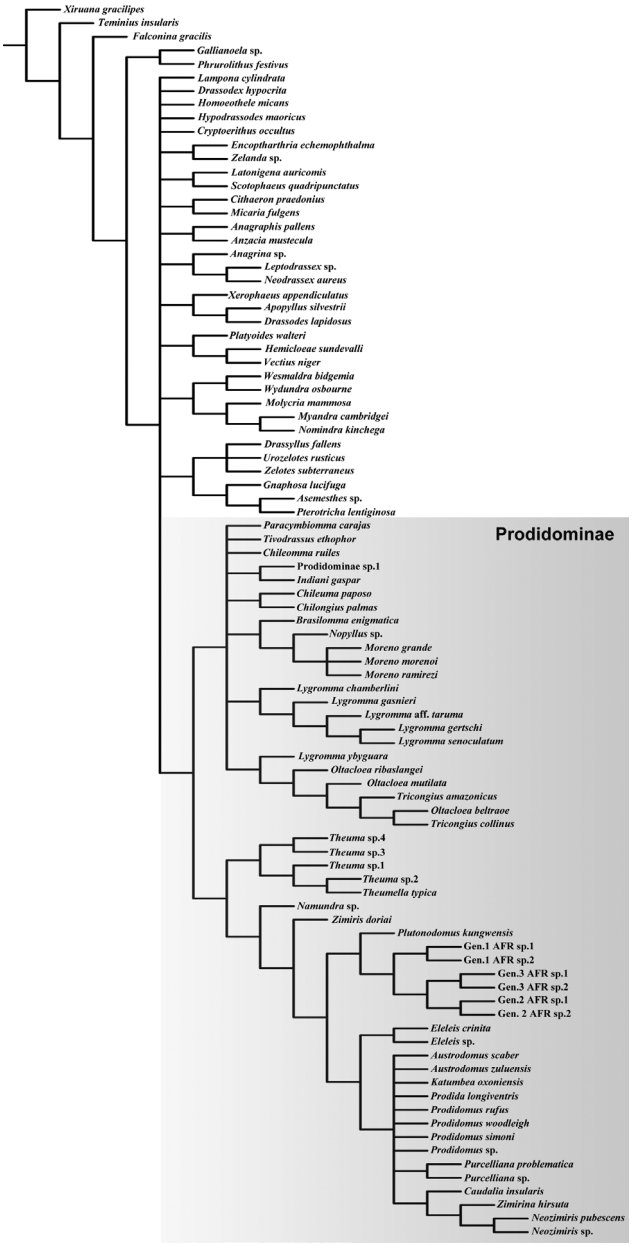

Figure 1. Strict consensus of the 314 most parsimonious trees obtained under equal weights analyses.

Prodidominae, as defined by Azevedo *et al.* (2018), is not recovered as monophyletic in our analysis (Fig. 2), because *Anagrina* arose as sister to Leptodrassinae (*Leptodrassex* Murphy, 2007 + *Neodrassex aureus* Ott, 2012). The genera *Cryptotoerithus*, *Molycria*, *Myandra*, *Nomindra*, *Wesmaldra* and *Wydundra* do not show the main synapomorphy of Prodidominae, the ALS with pyriform gland spigots with long base and associated with plumose setae (Fig. 23; char. 190). They arise as a monophyletic group supported by ALS extremely elongate and situated far in advance of the posterior

Table 1. Mean similarity calculated through SPR distances (150 replications) to strict consensus of trees under different weighting regimes. Value highlighted indicates the highest mean between the topologies. EW= equal weighting

Analysis	SPR Mean
EW	0.84966
$k = 3$	0.76799
$k = 4$	0.81818
$k = 5$	0.83333
$k = 6$	0.84576
$k = 7$	0.84576
$k = 8$	0.83902
$\boldsymbol{k = 9}$	**0.85038**
$k = 10$	0.84376
$k = 15$	0.82861
$k = 20$	0.82861
$k = 25$	0.82861

spinnerets (Fig. 21C, D; char. 165, 166) and distal article of ALS with retractile area (Fig. 22J, K, char. 190). Thus, we re-establish the subfamily Molycriinae as a distinct subfamily in Gnaphosidae (Fig. 2).

Prodidominae, as redefined in our study, is supported by ALS with pyriform gland spigots with long base and associated with plumose setae (char. 190). *Nopyllus* Ott, 2014, a genus that was not assigned to any subfamily in Azevedo *et al.* (2018), arose within Prodidominae (Fig. 2; Supporting Information, Fig. S1).

The subfamily Prodidominae is divided into two large clades (Fig. 2, clades 38 and 59). Clade 38 is composed of exclusively Neotropical genera, supported by the presence of a classic claw tuft clasper (Fig. 18A–D, char. 134) and postepigastric invaginations on the abdomen (Fig. 13K, char. 146). In this group, *Lygromma*, *Oltacloea* and *Tricongius* were not recovered as monophyletic. *Lygromma ybyguara* Rheims & Brescovit, 2004, a troglobitic species, is more closely related to *Oltacloea* and *Tricongius*, by the presence of a ventral bunch of thick setae on the cymbium (Fig. 27E, J, char. 245). *Oltacloea* and *Tricongius* are also not recovered as monophyletic, since *O. beltraoe* Brescovit & Ramos, 2003 arises as sister to *T. collinus* Simon, 1893 by characteristics of female genitalia (Supporting Information, Fig. S1, char. 269, 275, 285).

Clade 59 is composed of genera with predominantly African distribution, with the exception of the Neotropical *Neozimiris* and *Caudalia*. It is supported, among other characters, by the absence of leg claw teeth (Fig. 18E–I, char. 128), ALS with sclerotizaton close to base (Fig. 21H, char. 168) and insertion of pyriform gland spigots on well-defined base (Figs 23F, S1, char. 187). The genera *Austrodomus* and *Prodidomus* are not recovered as monophyletic (clades 82, 84). *Prodida* is found along with *Prodidomus* supported by the massive PLS (Fig. 21L, char. 224). *Austrodomus* and *Katumbea* are recovered as closely related by sharing the longer patella (similar to tibia) and copulatory ducts wider and closer to the copulatory openings (Figs 13A, 29I, char. 70, 288). *Theuma* and *Theumella* arise as a monophyletic group, supported mainly by the thin and conical protrusion between coxae IV (Fig. 11L, char. 40) and metatarsus III with scopula continuous (clade 60, char. 102). *Namundra*, a genus previously assigned to Molycriinae, arises as sister to other African genera of Prodidominae (clade 64). We recovered a well-supported clade, formed by six new species (clade 66). This group is supported mainly by having pyriform gland spigots with cracked texture (Fig. 23I; Supporting Information, Fig. S1, char. 185). Three well-supported groups arise within this clade.

Topology tests were performed to evaluate the robustness of previously defined groups that were not recovered in our analysis, such as the former subfamiliy Theuminae (Neotropical Prodidominae, *Anagrina*, *Theuma* and *Theumella*). However, the high RFD values indicate that all alternative hypotheses that considered such groups monophyletic, are poorly supported, favouring our unconstrained hypothesis (Table 2).

The genus *Nopyllus* is forced outside of Prodidominae. The value of RFD favoured the unconstrained hypothesis, since the constrained topology results in a polytomy between *Nopyllus*, Molycriinae and several other genera of Gnaphosidae and Trochanteriidae (Fig. 3A).

The topology obtained from forcing the monophyly of the former subfamily Theuminae shows that this clade would be supported only by the homoplastic synapomorphy of AME smaller ALE (Figs 3B, 9H, char. 24). The high value of RFD obtained in this analysis indicates that the genera included in the former Theuminae do not constitute a monophyletic group.

The monophyly of *Lygromma* was forced and the strict consensus resulted in a polytomy together with other Neotropical Prodidominae (Fig. 3C). The topology obtained indicates the lack of character to support the monophyly of genus and, therefore, favours our hypothesis that *Lygromma* is not monophyletic.

Forcing the monophyly of *Tricongius* resulted in the maximum value of RFD, because no character favoured the monophyly of *Tricongius*, indicating that this hypothesis is not supported, favouring our unconstrained hypothesis. The strict consensus of this analysis resulted in a polytomy with *Tricongius* and *Oltacloea* (Fig. 3D), reinforcing our hypothesis that both genera are synonymous.

The topology obtained from forcing the monophyly of the subfamily Molycriinae, including *Namundra*

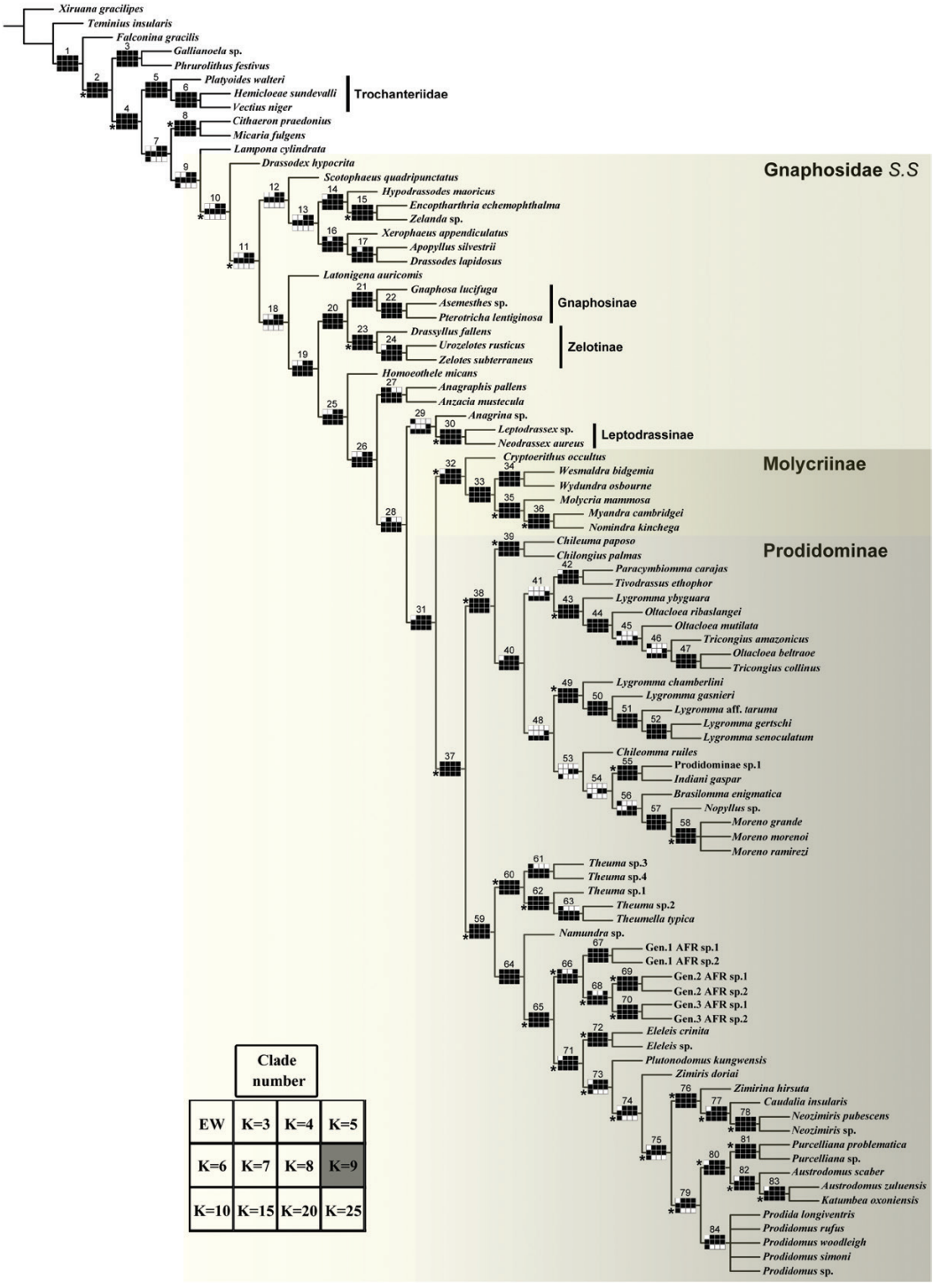

Figure 2. Strict consensus of phylogenetic hypothesis of Prodidominae, found under implied weighting (k=9). Clades with the sensitivity to different weighting regimes; white squares represent absence of clade in corresponding analyses and black squares represent its presence. Relative Bremer supports higher 70% are indicates with asterisk.

(according to Platnick & Baehr, 2006), recovered the group within Prodidominae and was supported mainly by the large size and advanced positions of ALS (Fig. 21C, D, J, char. 165, 166). The strict consensus showed that Molycriinae would be more related to the African genera (Fig. 3E).

Table 2. Alternative hypothesis using constrained searches with their respective steps number, total fit, RFD value and fit difference of those characters more favoured to constrained tree

Constraint	Steps (MPTs)	Total Fit (MPTs)	RFD	Fit difference of characters more favoured
Nopyllus outside Prodidominae	1450	204.54259	0.537210	0.100 (char. 116), 0.081 (char. 114), 0.080 (char. 126)
Former subfamily Theuminae monophyletic	1438	205.34486	0.594489	0.129 (char. 287), 0.068 (char. 135)
***Lygromma* monophyletic**	1424	206.42755	0.505981	0.033 (char. 277)
***Tricongius* monophyletic**	1422	206.49017	1.000000	-
Molycriinae + *Namundra* monophyletic	1431	206.31163	0.121970	0.081 (char. 37), 0.081 (char. 39), 0.081 (char. 165)
Single origin of hood	1434	205.22094	0.328888	0.181 (char. 209), 0.080 (char. 126)
Unconstrained	1420	206.55708	-	-

We also tested a constrained hypothesis of a single origin of hood in ALS. In this case, Prodidominae remains monophyletic and sister to the genera that have hoods (Molycriinae + *Hypodrassodes* Dalmas, 1919 + *Asemesthes* Simon, 1887 + *Encoptarthria* Main, 1954 + *Zelanda* Özdikmen, 2009) (Fig. 3F). The analysis suggests weak evidence to constrained hypothesis, indicating that the hood arose independently in these taxa.

DISCUSSION

OUTGROUP

Azevedo *et al.* (2018) recently redefined the taxonomic limits of Gnaphosidae by means of a phylogenetic analysis based on morphological characters. They did not recover the family as monophyletic, since the genera *Micaria* Westring, 1851, *Nauhea* Forster, 1979 and *Verita* Ramirez & Grismado, 2016 arose more closely related to other families. Nevertheless, considering that the limits of these genera are still unclear, the authors preferred to keep them in Gnaphosidae, rather than place them in other well-established families. They proposed Gnaphosidae *s.s.* to include all genera that have pyriform gland spigots longer and wider than the major ampullate gland spigots (Figs 22C, J, 23B), excluding the above-mentioned genera, considering them problematic taxa. *Homoeothele* Simon, 1908 and *Matua* Forster, 1979, were not included in their analysis, but were also deemed problematic taxa and excluded from Gnaphosidae *s.s*. The authors suggested further studies to confirm the placement of these genera.

In our study, we tested the placement of two of these problematic taxa, *Micaria* and *Homoeothele*. *Micaria* was included in several of the latest phylogenetic analyses (Ramírez, 2014; Wheeler *et al.*, 2017; Azevedo *et al.*, 2018), but there has been no consensus on its position. Ramírez (2014) recovered *Micaria* as sister to Gnaphosidae + Prodidomidae. In Wheeler *et al.* (2017), *Micaria* arose within Gnaphosidae, but sister to Molycrinnae. Azevedo *et al.* (2018) recovered a well-supported clade in which *Micaria* is sister to Cithaeronidae + Ammoxenidae. Our analysis corroborates the relationship between *Micaria* and *Cithaeronidae*, which arose as sister to each other (Fig. 2).

Homoeothele was included in the *Anzacia* group (*Anzacia* Dalmas, 1919, *Hypodrassodes*, *Matua*, *Nauhea*) by Murphy (2007), but Azevedo *et al.* (2018) found this group polyphyletic. Our analysis includes representatives of *Homoeothele*, *Anzacia* and *Hypodrassodes* and does not recover the *Anzacia* group as proposed by Murphy (2007). However, *Homoeothele* arises with good support within Gnaphosidae *s.s.*, by sharing the same spinneret characteristics of other Gnaphosidae, contradicting Azevedo *et al.* (2018).

Azevedo *et al.* (2018) rearranged the internal structure of Gnaphosidae. The authors placed the former Prodidomidae as a subfamily of Gnaphosidae (Prodidominae), redefined the limits of Gnaphosinae, Zelotinae, Herpyllinae Platnick and Drassodinae Simon, and proposed the new Leptodrassinae. In contrast, several genera were considered unplaced and could not be assigned to any subfamily due to the low support and unstable relationships. Among these unplaced genera, our analysis includes representatives of *Anzacia*, *Apopyllus* Platnick & Shadab, 1984, *Drassodex* Murphy, 2007, *Hypodrassodes*, *Nopyllus*, *Scotophaeus* Simon, 1893, *Xerophaeus* Purcell, 1907 and *Zelanda*. We also include *Anagraphis*, which was maintained in the monogeneric subfamily Anagraphidinae by Azevedo *et al.* (2018).

Our results show a poorly supported clade including *Apopyllus*, *Drassodes*, *Encoptarthria*, *Hypodrassodes,*

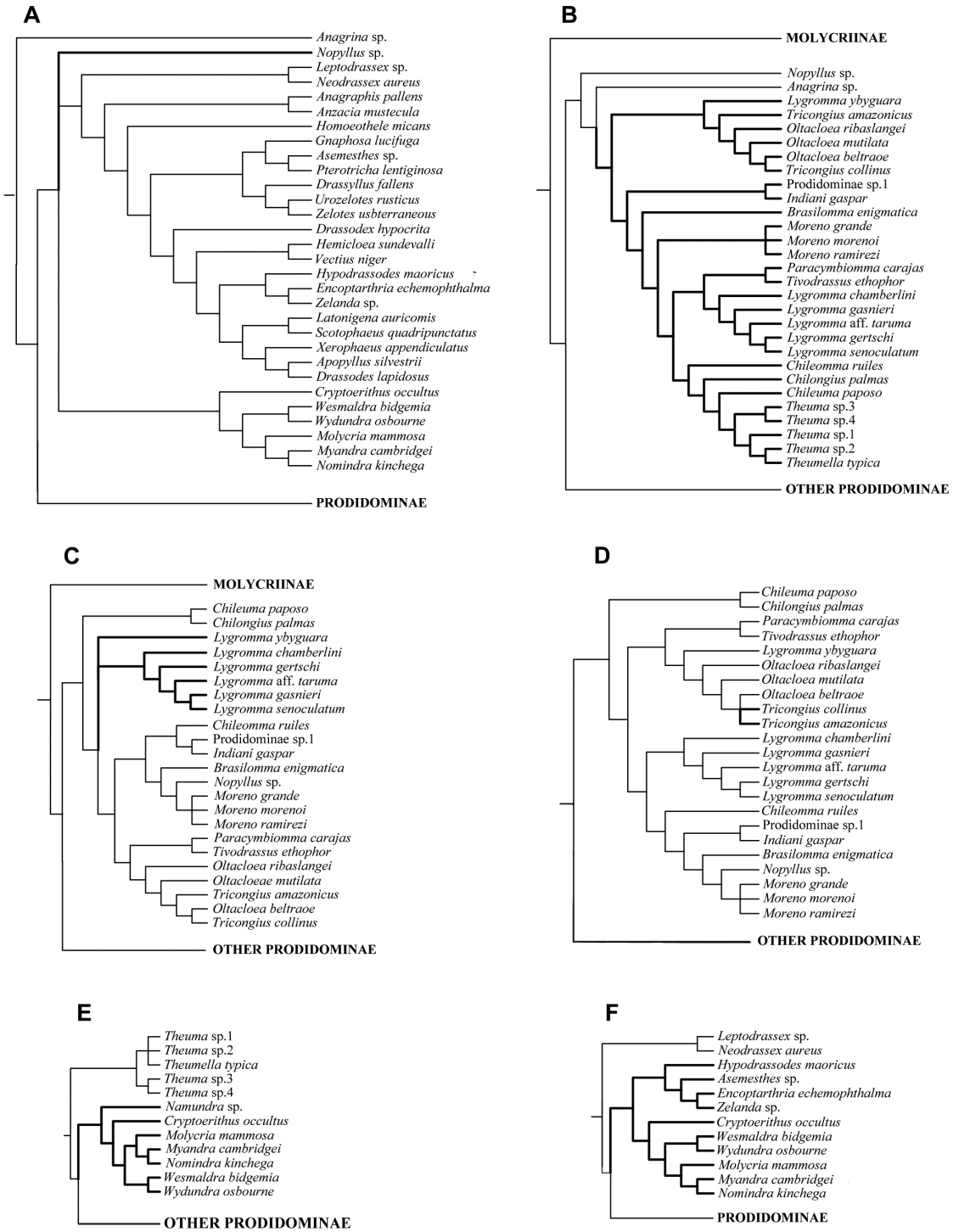

Figure 3. Strict consensus of constrained trees. A, *Nopyllus* outside Prodidominae; B, former subfamily Theuminae monophyletic; C, *Lygromma* monophyletic; D, *Tricongius* monophyletic; E, Molycriinae + *Namundra* monophyletic; F, hood monophyletic. Taxa submitted to constrain are with thickened branch.

Scotophaeus, *Xerophaeus* and *Zelanda* (clade 12). Of these, only *Drassodes* had been assigned to a subfamily (Drassodinae Platnick) by Azevedo *et al.* (2018). In addition to the above-mentioned genera, our analysis also includes a representative of the genera *Encoptarthria*, not included in the study of Azevedo

et al. (2018). Our results show a relationship between the latter, *Hypodrassodes* and *Zelanda*, another Australian genus (clade 14) (Fig. 2; Supporting Information, Fig. S1). The group is supported by spinneret characters, such as pyriform gland spigots with the base longer and wider than the shaft.

The position of *Anagraphis* is still controversial within Gnaphosidae. Platnick & Baehr (2006) redefined Anagraphidinae to include *Anagraphis* and *Talanites* Simon, 1893. Azevedo *et al.* (2018) did not recover this relationship in analyses performed under implied weighting, in which *Anagraphis* emerged as sister to *Anzacia*. Nevertheless, despite having found a supported relationship between these taxa, they suggested not using the name Anagraphidinae for the group until more studies are carried out. Their results show this group as sister to a clade including *Hypodrassodes*, *Notiodrassus* Bryant, 1935 and *Echemus* Simon, 1878, sister to Prodidominae. Our results corroborate the relationship between *Anagraphis* and *Anzacia* found by Azevedo *et al.* (2018).

Leptodrassinae was recovered as monophyletic and sister to *Anagrina* (formerly allocated in Prodidominae) (Fig. 2). Thus, we removed *Anagrina* from Prodidominae but refrain from allocating it in any other already established group, because the relationships involving these taxa are apparently unstable.

Nopyllus was considered unplaced within Gnaphosidae by Azevedo *et al.* (2018). Originally described by Ott (2014), the genus was considered closely related to *Apodrassodes* Vellard, 1924 and *Apopyllus* by the presence of a long filiform embolus. Our results show that this character arises independently in these genera and *Nopyllus* appears nestled within a well-established clade of Neotropical Prodidominae (clade 38).

Molycriinae

Platnick & Baehr (2006) performed a cladistic analysis to test the monophyly of Molycriinae and to understand the relationships between their genera. The authors characterized the subfamily by the position of the anterior lateral spinnerets, which are located far in advance of the posterior spinnerets. Wheeler *et al.*'s (2017) molecular analysis recovered Molycriinae as monophyletic and sister to *Micaria*, nestled within Gnaphosidae and not related to the other prodidomids. However, the authors refrained from making any taxonomic decisions until both groups were more adequately studied. Azevedo *et al.* (2018), using only morphology, recovered Prodidominae, including *Cryptoerithus* (Molycriinae), as monophyletic within Gnaphosidae, based on the presence of extremely elongated pyriform gland spigots that are associated with patches of plumose setae. These patches of setae are interpreted as being an incomplete ring of the distal article of ALS (Ramírez, 2014; Azevedo *et al.*, 2018). According to Ramírez (2014), this ring is sclerotized and barely visible, but can be inferred by the presence of setae or their insertions.

In our study, we reinterpret the morphology of the distal article in Molycriinae. In SEM images, we noted that Molycriinae genera have extremely elongated pyriform gland spigots that are not associated with plumose setae. The ALS of Molycriinae are distinct from those of other Gnaphosidae. They have a structure that is able to retract the pyriform gland spigots, leaving only the shaft tip exposed (Fig. 22K, L, char. 190). The latter is protected by a hood, projected from the basal article of the ALS (Fig. 22H, L, char. 209). This structure clearly has setae and apparently are present only in the anterior part. Thus, we coded this structure of the ALS of Molycriinae as a distal article with incomplete distal ring without patches of setae at the base of the pyriform gland spigots. In some specimens, when the spigots are partially retracted, it is possible to observe the setae close to the spigots, giving the impression that both are closely related (Fig. 22F, H). Perhaps this situation has induced previous authors to determine this condition as similar to that observed in Prodidominae.

The morphology of the setae are also different in both subfamilies: in Molycriinae they are completely covered by barbs (Fig. 22H), while in Prodidominae the surface in close contact with the spigots is completely smooth (Fig. 23D, H). Therefore, although additional morphological studies are needed to elucidate the structures of the spinnerets of Molycriinae, the absence of associated patches of setae at the base of the pyriform gland spigots is evident. Thus, Molycriinae is here re-established as a subfamily to include the genera *Cryptoerithus*, *Molycria*, *Nomindra*, *Wesmaldra* and *Wydundra*, supported by the presence of ALS extremely elongated and situated far in advance of the posterior spinnerets (Fig. 21C, D, char. 165, 166), pyriform gland spigots elongated with retractile area (Fig. 22I–K, char. 190) and presence of an apical hood in the basal article (Fig. 22H, L, char. 209).

Molycriinae and Prodidominae share the sternum with a large posterior protrusion between the coxae IV (Fig. 11G–P, char. 37), although less pronounced in some Molycriinae. This characteristic was considered a synapomorphy of the former subfamily Theuminae (Platnick *et al.*, 2005), but we observe that all Prodidominae and Molycriinae have this protrusion, as already suggested by Wunderlich (2011). In Molycriinae, this structure has sclerotized margins (Fig. 11G, H, char. 39), different from Prodidominae (Fig. 11I–N), except for *Namundra* and *Zimiris* where it is weakly sclerotized (Fig. 11O, P).

The relationships between Molycriinae genera obtained in this study corroborate those obtained by Platnick & Baehr (2006), with *Cryptoerithus* sister to the remaining genera (Fig. 2, clade 32). *Wesmaldra* is sister to *Wydundra*, supported by the presence of a lateroventral row of long and strong spines on female palpal femur (Fig. 26A, char. 229). Both genera are sister to *Molycria*, *Nomindra* and *Myandra*, which share the chelicerae fang with wide venom gland opening (Fig. 12C, char. 47).

Namundra was originally proposed by Platnick & Bird (2007) as the only African Molycriinae. The authors considered it more related to *Wesmaldra* and *Wydundra* by the presence of a tarsal onychium, tarsal cracks and female palpal spine row, although all were considered less pronounced in *Namundra*. In addition, the authors also suggested that the wide separation between ALS shared only with *Wyndundra* could indicate a closer relationship between the two genera. In SEMs, we observe that *Namundra* does not have a tarsal onychium or tarsal cracks (Fig. 18I, char. 110–113, 132), and although the female palpal femur apparently has differentiated setae, they are not the same as in *Wesmaldra* and *Wydundra* (Fig. 26B). In our analysis, the separation between ALS, shared with *Wydundra*, appears independently in both genera, but this condition is even more pronounced in *Namundra* (Fig. 21J, char. 167). Therefore, despite *Namundra* having been originally assigned to Molycriinae by sharing mainly the ALS position and size, the genus is herein removed from the subfamily and transferred to Prodidominae, since the genus clearly has patches of long setae around the pyriform gland spigots in ALS (Fig. 23G, char.190). In addition, *Namundra* appears nestled within a group of predominantly African genera (Fig. 2, clade 64). We tested an alternative hypothesis forcing the monophyly of Molycriinae plus *Namundra*, but this hypothesis has low support (Table 2).

Molycriinae and Prodidominae share the elongated pyriform gland spigots (Fig. 4, char. 193). However, Azevedo *et al.* (2018) suggest that this elongation might have evolved before the patches of long setae in Prodidominae, and that these could serve to protect the long spigots. Our observations corroborate this suggestion. The elongation of spigots appeared in both subfamilies and, apparently, each subfamily developed an independent protection mechanism for their spigots (Fig. 4). Prodidominae developed patches of setae, in which the internal surface of the setae is smooth, enabling a close contact association with the spigot and protecting the part that would be exposed to the external environment. In contrast, Molycriinae developed a structure connected to the pyriform gland spigots that is able to retract these spigots inside the basal article, leaving only the shaft exposed, which is protected by an apical hood of the basal article. Nevertheless, behavioural studies are important to clarify the real function of these structures in these spiders.

The advanced position of the ALS in Molyriinae is the most notable characteristic of the group, although (in different degrees of advance) it can also be found in other genera (i.e. *Namundra*, *Theuma*, *Theumella* and *Zimiris*). This advance is probably related to the expansion and/or reduction of opisthosomal segments. It is known that the spinnerets are located on abdominal segments 4 (anterior spinnerets) and 5 (posterior spinnerets) (see: Pechmann *et al.*, 2010). The current posterior positioning of spinnerets on most spiders is due to the expansion of opisthosomal segment 3 and the reduction of the body segments posterior to opisthosomal segment 5 (Pechmann *et al.*, 2010). Therefore, it is probable that the condition observed in Molycriinae and other genera is the result of the expansion of segment 4 and reduction of segment 3. In addition, all genera that have this advance of the spinnerets also show elongate ALS, but this elongation is also observed in spiders with ALS not advanced. Hilbrant (2008) observed that the elongation of spinnerets can be associated with the expression of gene AP-2, because this gene can be expressed in different ways in opisthosomal segments 4 and 5. The author observed that in *Cupiennius salei* (Keyserling, 1877) the gene is strongly expressed in segment 5 and temporarily expressed in segment 4, and consequently the posterior spinnerets are longer than the anterior. Thus, it is possible to suggest that the more prevalent expression of gene AP-2 in segment 4 could be related to the longer anterior spinnerets. Nevertheless, ontogenetics and genic expression studies are needed to elucidate the development of spinnerets.

Prodidominae

Much has been speculated about Prodidominae relantionships but only recently, representatives of this subfamily were included in phylogenetic analyses (Ramírez, 2014; Wheeler *et al.*, 2017; Azevedo *et al.*, 2018; Fernández *et al.*, 2018). Azevedo *et al.* (2018) performed the most recent analysis, including ten genera. The authors used mainly Neotropical species, and suggested that the inclusion of *Zimiris* and other Australian genera would not challenge the monophyly of the group. In addition, the authors also suggested that a careful examination of African Prodidomidae fauna could be of interest.

In this study, we provide the most complete phylogenetic analysis for Prodidominae spiders with representatives of 33 genera. The subfamily is not recovered as monophyletic, and thus it is here redefined to include genera that share an incomplete distal article of the ALS with patches of long setae

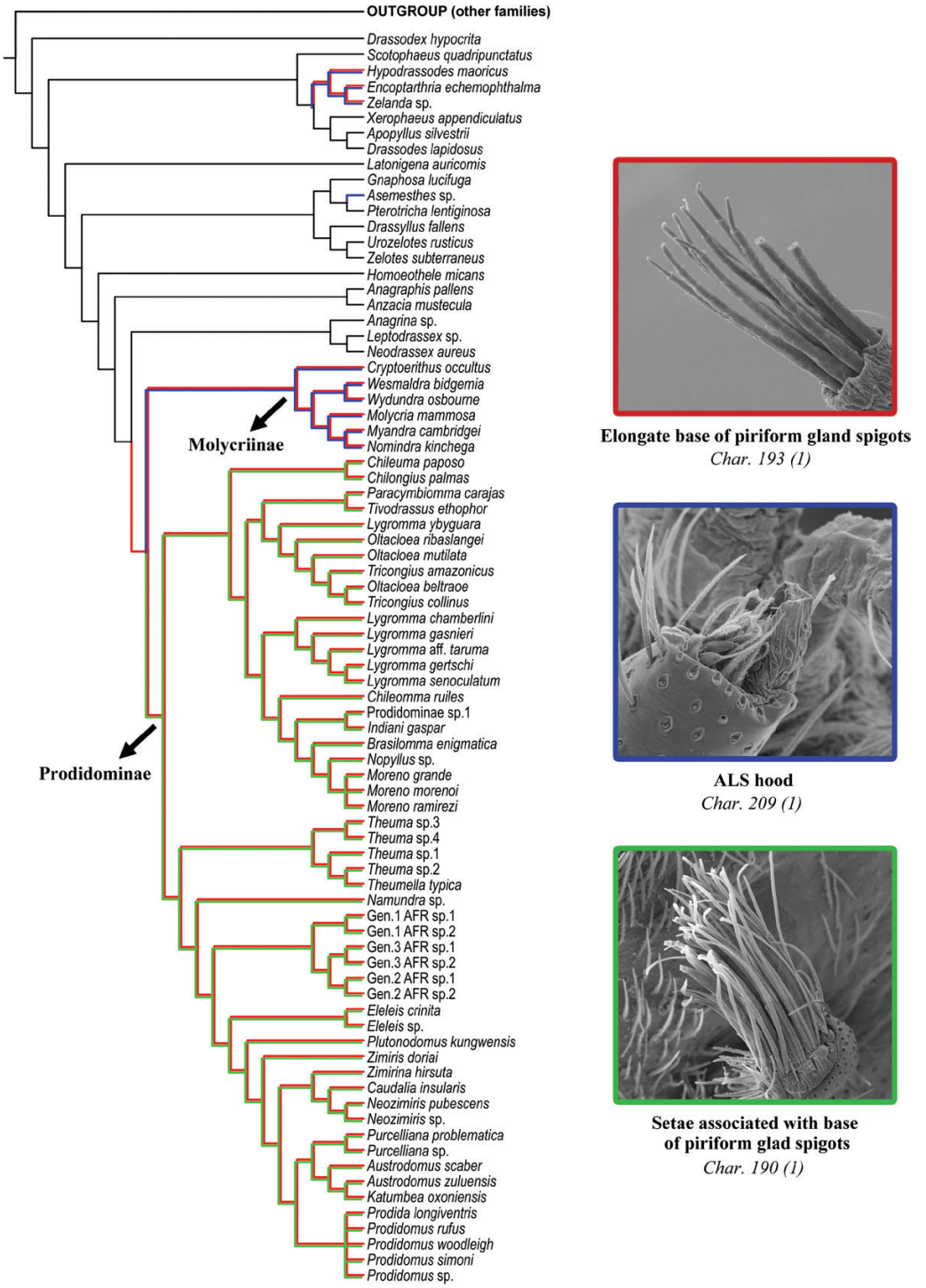

Figure 4. Evolution of elongation of piriform spigots base, the presence of setae associated with these spigots and presence of ALS hood on the Gnaphosidae. Mapping on the working phylogenetic hypothesis according to delayed transformation series (DELTRAN) criteria.

around the pyriform gland spigots (Fig. 23, char. 190). In addition to these patches of setae, the subfamily also shares the presence of a large protrusion between the coxae IV with erect setae and unsclerotized margin (Fig. 11I–N, char. 37–39). Other characteristics related to the spinnerets include the major ampullate gland

spigots located in a well-defined conical article with setae (a characteristic also observed in *Angraphis*, *Encoptarthria*, *Hypodrassodes* and *Zelanda*) and PMS with cylindrical gland spigots mixed with aciniforms and minor ampullates (Figs 23H, I, 24E, F, L, char. 197, 217). *Anagrina* arose sister to Leptodrassinae and was, therefore, removed from Prodidominae and considered an unplaced genus in Gnaphosidae. As suggested by Azevedo *et al.* (2018), the inclusion of *Zimiris* did not influence the monophyly of Prodidominae and it arises nestled within the subfamily.

Platnick *et al.* (2005) observed in some Prodidominae genera a peculiar mechanism formed by several claw teeth appressed together and used to move the tenant setae, the claw tuft clasper (CTC). Ramírez (2014) observed this structure in representatives of several other families and in other genera of Gnaphosidae. The author identified a monophyletic group based on the presence of this structure, which he named the CTC clade. However, Azevedo *et al.* (2018) did not recover the CTC clade as monophyletic, and justified this result with differences in the interpretation of homology of the claw tuft clasper. They divided the clasper into three independent structures located at the base of the tarsal claw, a classic clasper, a folded clasper and a solid clasper, taking into consideration the structural composition. The presence of both the solid clasper and the classic clasper in *Chilongius* (char. 134, 137), observed by the authors and confirmed in our study, strengthen the hypothesis of them being independent structures, although no other species in our dataset shows this condition. In our study, we propose a fourth type of clasper, comprising a thin, flexible, single clasper present in the genus *Zimiris* and in the African genera *Namundra*, *Theuma* and possibly *Theumella* (Fig. 5, char. 138).

According to Ramírez (2014), the claw tuft clasper appeared only once, while Azevedo *et al.* (2018) suggested that this mechanism evolved several times independently. Our results corroborate those of Azevedo *et al.* (2018) and the solid clasper and the flexible single clasper appeared more than once in Prodidominae (Fig. 5, char. 137, 138). Our analysis indicates that the classic clasper evolved once, as suggested by Platnick *et al.* (2005) and corroborated by Azevedo *et al.* (2018). In addition, we observed that the number of teeth in the classic clasper of legs I–II varies among genera (char. 135). The Chilean genera, *Chileumma* and *Chilongiusi*, have four teeth forming the clasper, while the other genera can have two or three teeth.

Ramírez (2014) also suggested that the emergence of the claw tuft clasper was associated with the emergence of the basal ribs on the tenent setae. This correlation was not confirmed by Azevedo *et al.* (2018). Nevertheless, the authors suggested that the evolution of the ribs on the basal section of the tenent setae could be a pre-adaptation to the evolution of a clasper. We do not observe a direct correlation between these two structures, but observe a correlation between the claw tuft clasper and the insertion of the tenent setae, at least in Prodidominae (Fig. 5). Clade 38 has the classic clasper associated with the claw tuft bases packed together, with the bases of the tenent setae (in this case with ribs) close to one another (Fig. 18C, D, char. 134, 144). This condition enables classic clasper to fit in the bases of all tenent setae, since this type of clasper has the tip slightly curved, allowing better movement of the claw tuft. Our results indicate that the claw tuft bases packed together appeared before the classic clasper. Molycriinae also has the claw tuft bases packed together but has a solid clasper instead of a classic clasper. The remaining Prodidominae (clade 59) have the solid clasper and the flexible single clasper, and both are associated because of the presence of a claw tuft plate, in which the tenent setae are inserted in individual sockets (Figs 5, 18E–I). This plate apparently is not articulated as in other groups and the clasper would be the only mechanism involved in tuft movement. The flexible single clasper apparently has a fit mechanism different from those of the species with a classic clasper. Possibly, when the claw moves forward and then returns to its initial position, the space between the flexible single clasper and the claw base work as a notch to move the tenent setae. Perhaps something similar occurs in those species that have a folded clasper. The solid clasper is homoplastic and shows few morphological variations in our dataset. Perhaps a more detailed examination of claws in these genera can indicate other homologies within the morphological condition of the solid clasper.

Neotropical Prodidominae

Clade 38 is composed exclusively of Neotropical genera and is supported by the presence of a claw tuft classic clasper (Fig. 18A–D, char. 134). In addition, the clade also shares the presence of post-epigastric invaginations (Figs 13K, 19E, char. 146) and highly convoluted copulatory ducts (Fig. 29F, char. 286). Platnick & Baehr (2006) included these genera in the former subfamily Theuminae, but this group was not recovered in our analysis, because *Theuma* and *Theumella* are more closely related to other Prodidominae genera. We tested forcing the monophyly of Theuminae, but results indicate that this hypothesis has low support.

Within clade 38, the Chilean *Chileumma* and *Chilongius* arise sister to each other under all tested parameters, corroborating the results obtained by Azevedo *et al.* (2018). In our study, this relantioship was supported by several homoplastic synapomorphies,

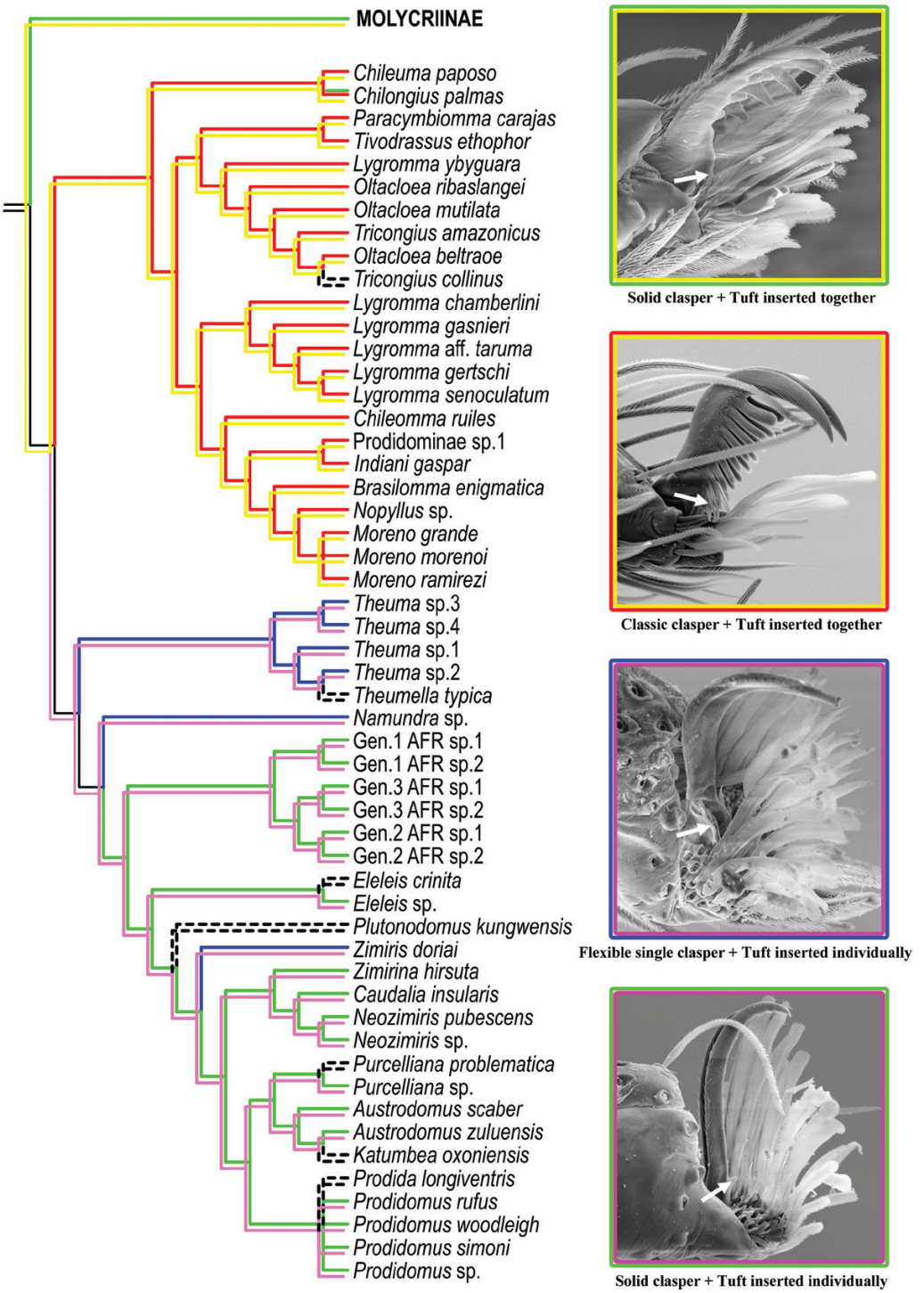

Figure 5. Morphology different of claw tuft clasper and insertion of claw tuft bases found in Prodidominae. Mapping on the working phylogenetic hypothesis according to delayed transformation series (DELTRAN) criteria. Dashed lines indicates missing data. Arrow to claw tuft clasper.

such as the presence of an epigynal atrium (Fig. 28J, char. 276) and fertilization ducts well advanced from the epigastric furrow (Fig. 29K, char. 289). The Chilean *Chileomma*, which was not included in Azevedo *et al.* (2018), arises as sister to a clade including *Brasilomma*, *Indiani*, *Moreno*, *Nopyllus* and one new

genus of Prodidominae (clade 53). This relationship was recovered under fewer parameters and with low support. Our results contradict Platnick *et al.* (2005), who suggested that the Chilean fauna (*Chilongius*, *Chileumma* and *Chileomma*), as typically happens for spider groups that have speciated in Chile, would be entirely distinct from that found in tropical South America.

Lygromma was not recovered as monophyletic, because *L. ybyguara* arose more closely related to *Tricongius* and *Oltacloea*. Thus, *Lygromma* is here redefined to include species that have a ventral tibial apophysis (Fig. 26K, char. 238) and eyes (when present) with PME–PLE and PLE–ALE close, almost touching (Figs 9G, 10D, char. 21, 23). We tested the constrained monophyly of *Lygromma* + *L. ybyguara*, but the results were weakly supported. *Lygromma ybyguara* is considered a troglobitic species and was assigned to *Lygromma* based solely on the absence of eyes (Rheims & Brescovit, 2004), a trait shared by two other cavernicolous species, *L. anops* Peck & Shear, 1987 and *L. gertschi* Platnick & Shadab, 1976. As pointed out by Rodrigues *et al.* (2018), the reduction or absence of eyes is a character, usually related to subterraneous environments, that can vary within the same genus, especially those that include subterranean and epigean representatives. In our analysis, we included five eyeless cavernicolous species (*Brasilomma enigmatica*, *Plutonodomus kungwensis* Cooke, 1964, *L. gertschi*, *L. ybyguara* and *Indiani gaspar*, Rodrigues *et al.*, 2020) and no relationship was recovered between them.

Oltacloea and *Tricongius* are also not recovered as monophyletic in this study (clade 44). *Oltacloea beltraoe* arises as sister to *T. collinus*, both sister to *T. amazonicus* Platnick & Hofer, 1990 with *O. mutilata* Mello-Leitão, 1940 and *O. ribaslangei* Bonaldo & Brescovit, 1997 sister to the remaining species (Fig. 2). Both genera arise close to *L. ybyguara* and the relationship between these six species is recovered and well supported in all analyses. The group (clade 43) shares the carapace with posterior margin truncated (char. 2), anterior margin of sternum less than half of maximum width (Fig. 11K, char. 35) and a bunch of thick setae in the cymbium (Fig. 27E, J, char. 245). Based on this result, we here transfer *L. ybyguara* to *Tricongius* and consider this genus a senior synonym of *Oltacloea*. Thus, the genus is characterized by eyes (when present) widely separated with AME–AME distance shorter than AME–ALE (char. 17), sternum with anterior margin short (less than half of maximum width of sternum) (char. 35) and cymbium with a bunch of thick setae on the ventral-terminal part (char. 245).

Tivodrassus and *Paracymbiomma* arise as sister to each other, supported by the presence of a paracymbium (Fig. 26G, char. 244). These results corroborate the suggestion of Rodrigues *et al.* (2018), who first pointed out the presence and similarity of this structure in both genera. Although both share this important characteristic, they are considered distinct genera based on several characteristics of genital morphology of males and females.

Other Prodidominae

Clade 59 arises as sister to the Neotropical Prodidominae (clade 38) and is composed predominantly of African genera, with the exception of the Neotropical *Neozimiris* and *Caudalia*. *Prodidomus*, *Zimirina* and *Zimiris* are present in Africa, but occur also in other biogeographic regions. In our analysis, we used *Zimirina hirsuta* Cooke, 1964 from the Canary Islands, *Zimiris doriai* (a synanthropic species introduced in several countries around the world) and four species of *Prodidomus*, two African, one Australian and one synanthropic species. All other genera are exclusively Afrotropical. This clade is supported by several homoplastic synapomorphies, such as the presence of dense claw tufts on a well-delimited plate with the tenent setae inserted in individual sockets (Fig. 18E–I, char. 129, 144), pyriform gland spigots with well-defined bases (Fig. 23F, char. 187) and absence of claw teeth (Fig. 18E–I, char. 139), except in *Neozimiris* in which they are reduced.

Some genera in this clade show losses or reduction of several structures that are observed in other Prodidominae, such as the thoracic fovea (char. 0), scales (char. 156–162), serrula (char. 33), cheliceral boss (char. 44), teeth of chelicerae (char. 56, 59), shaft serrula of cheliceral fang (char. 46) and female palpal claw (char. 227). Some of these losses are probably associated with a change in feeding habits and prey capture. Spiders with cheliceral teeth mash up and macerate their prey, while the serrula is used to cut it. In contrast, the absence of these structures indicates that these spiders inflict only a small wound into prey, while the digestive fluid is pumped and the dissolving tissue is gradually sucked out (Foelix, 2011). Perhaps the elongation of the cheliceral fang observed in some of these genera could be associated with the loss of the serrula and reduction or loss of cheliceral teeth (Figs 6, 7). Our results indicate that the loss of these structures may have required different mechanisms to subdue prey more efficiently. The elongation of the cheliceral fang, for example, allows the spider a longer range to insert the fang into the prey, maintaining a safe distance from it. In addition, the absence of fovea in some genera indicates lack of an attachment site for the dorsal muscles of the stomach (Pollard, 1990; Foelix, 2011). The presence of modified ventro-apical setae in tarsi I–II and the reduction or absence of female palpal claw observed in some genera of this group may also

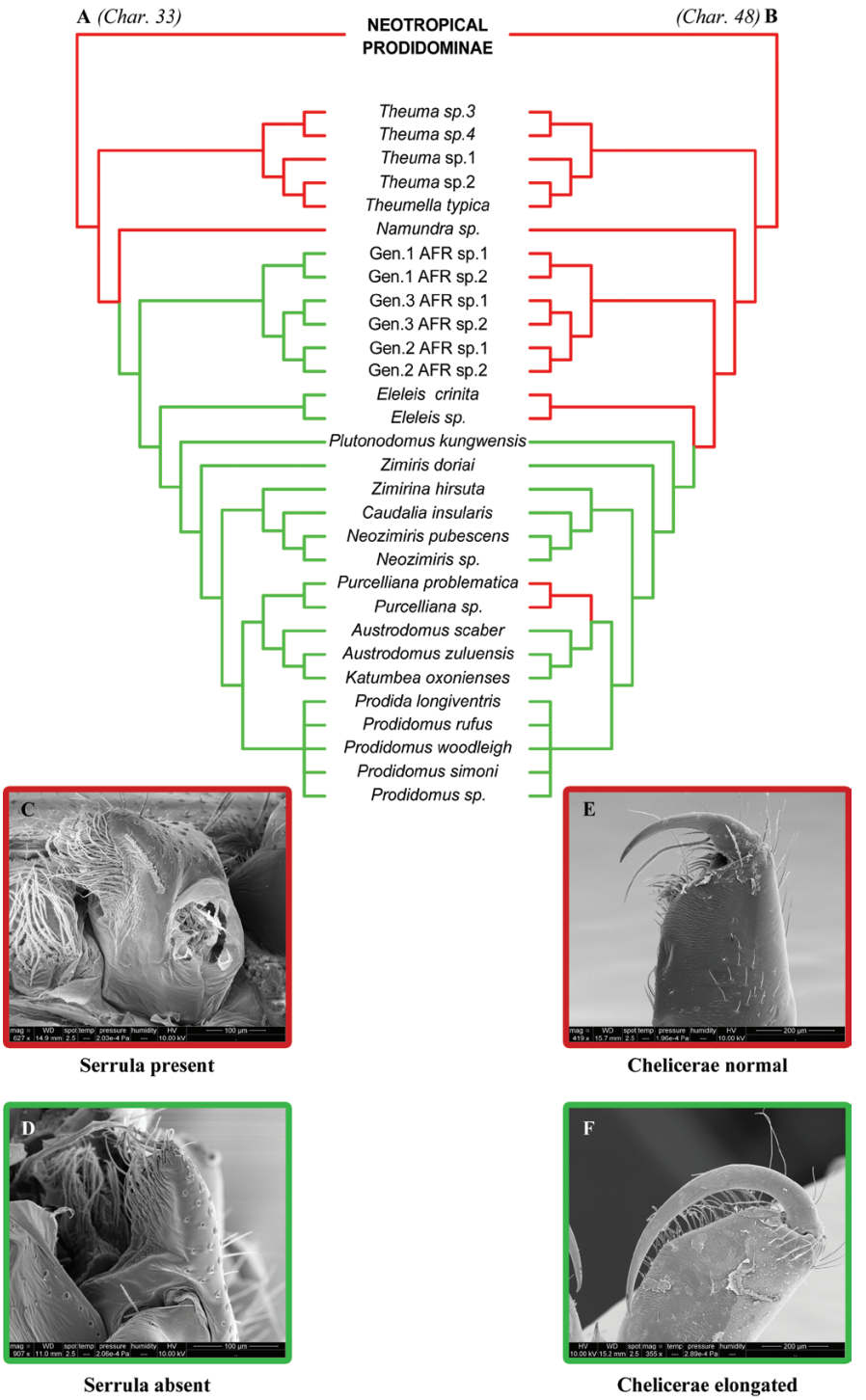

Figure 6. Evolution of characters of occurrence of serrula and cheliceral fang size in Prodidominae. A, mapping of presence and absence of serrula; B, mapping of size of cheliceral fang; C, *Theuma* sp.; D, *Prodidomus woodleigh*; E, *Namundra* sp.; F, *Zimiris doriai*. Mapping on the working phylogenetic hypothesis according unambiguous optimization.

be related to a possible change in feeding habits, since they often play a role during prey capture. However, behavioural studies will be necessary to better explain the absence and morphological modifications of structures in some Prodidominae.

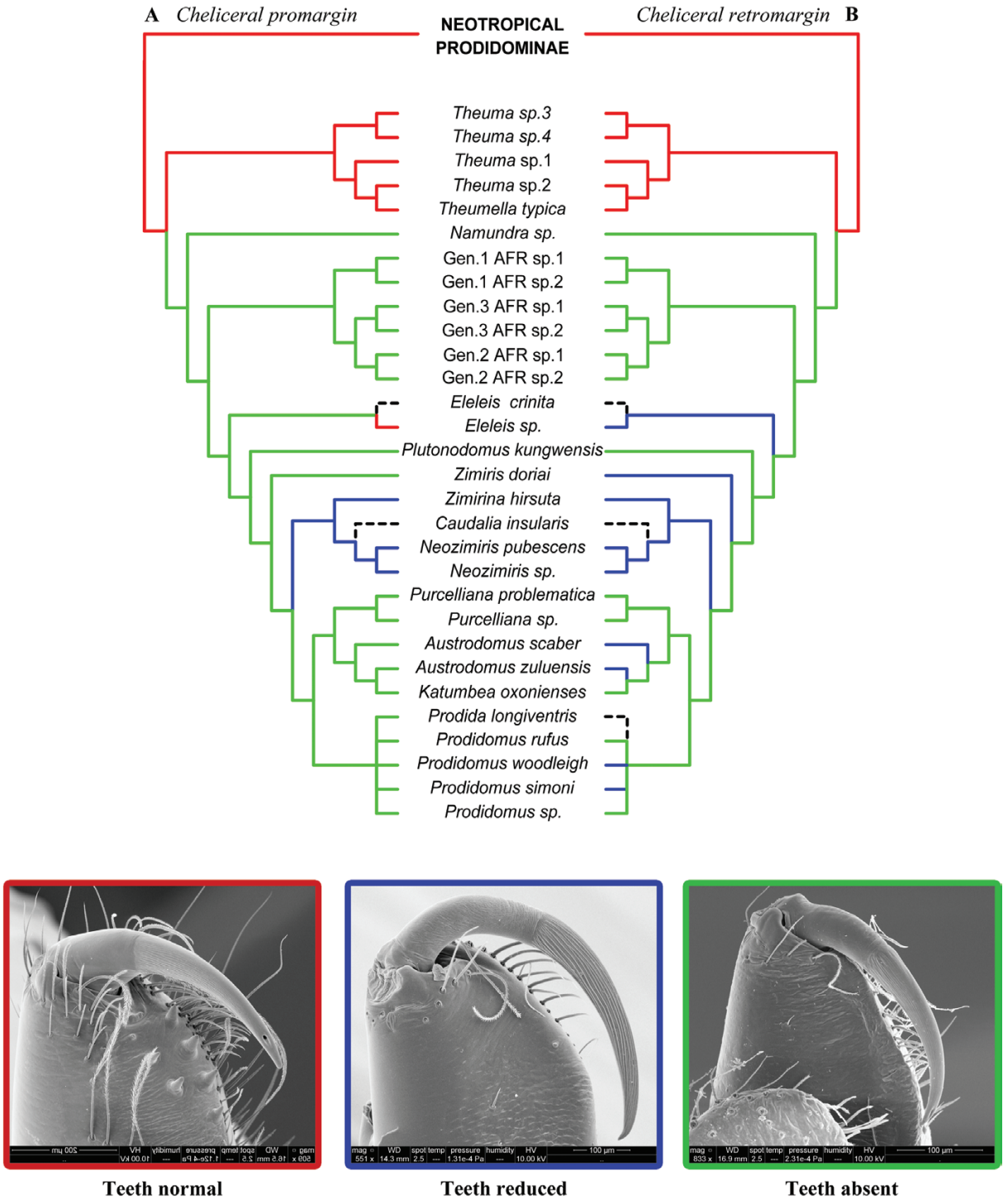

Figure 7. Evolution of characters of teeth in Prodidominae. A, mapping of teeth of cheliceral promargin; B, mapping of teeth of cheliceral retromargin; C, *Theuma* sp.; D, *Prodidomus woodleigh*; E, *Purcelliana*.

Theuma was not recovered as monophyletic. It arises within a well-supported clade including *Theumella,* supported mainly by a thin and conical protrusion of the sternum between the coxae IV (Fig. 11L, char. 40). Although both genera seem to be closely related, we refrain from making any taxonomic changes to their status until further studies are carried out and more species are examined. *Theuma* is a large and abundant

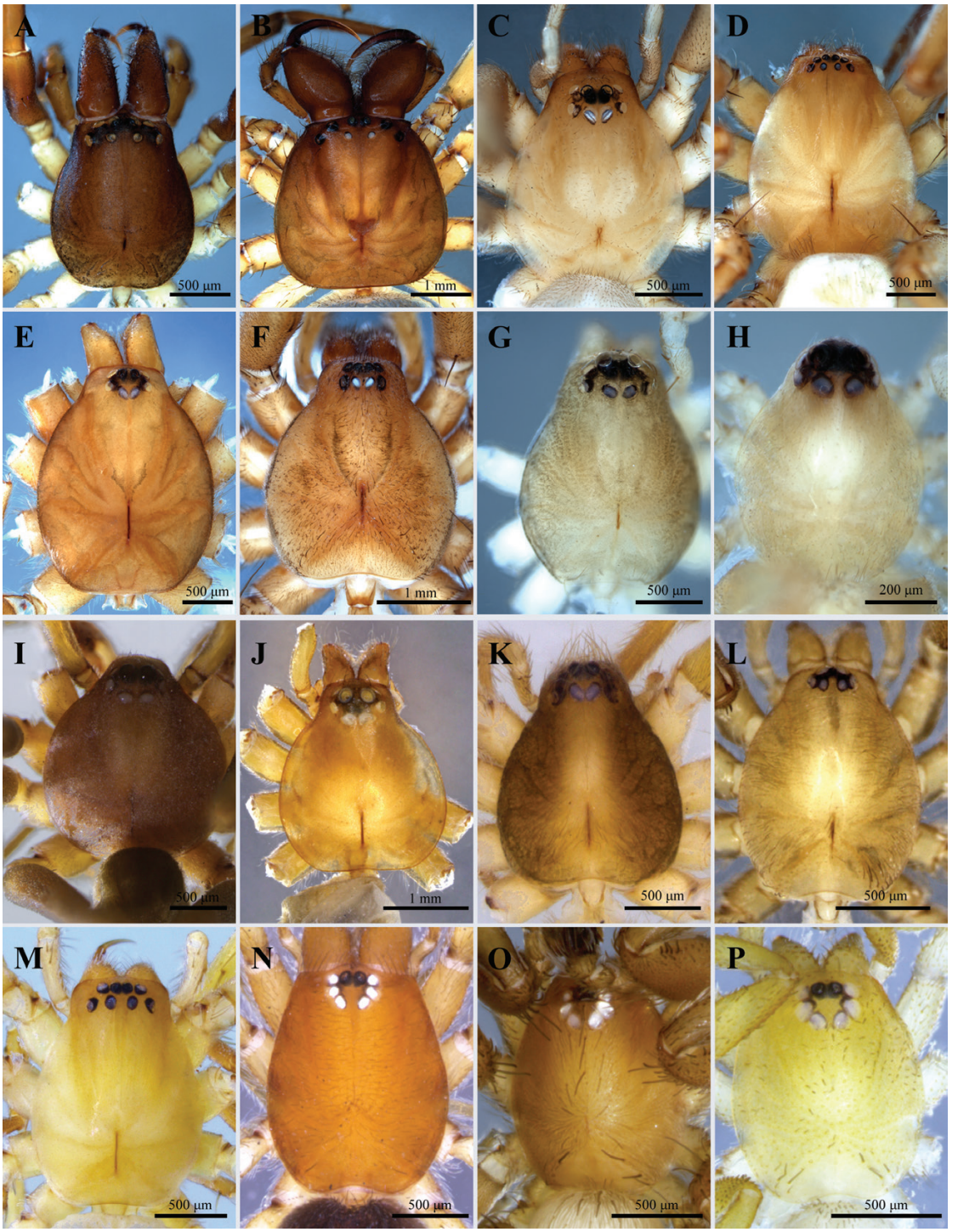

Figure 8. Carapace, dorsal view. A, *Gallianoela* sp., male; B, *Platyoides walteri*, female; C, *Cithaeron praedonius*, female; D, *Anagraphis pallens*, female; E, *Encoptharthria echemophthalma*, female; F, *Pterotricha lentiginosa*, female; G, *Homoeothele micans*, male; H, *Leptodrassex* sp., female; I, *Molycria mammosa*, male; J, *Wydundra osbourne*, female; K, *Namundra* sp., female; L, *Lygromma gasnieri,* male; M, *Theuma* sp.3, female; N, *Prodidomus* sp., male; O, *Eleleis* sp., female; P, *Purcelliana problematica*, male.

Figure 9. Carapace, lateral view. A, *Encoptharthria echemophthalma*, female, arrow to cheliceral boss; B, *Vectius niger*, female. Eyes. C, *Cithaeron praedonius*, female, detail of PME tapetum; D, *Vectius niger*, female, frontal; E, *Urozelotes rusticus*, male, frontal; F, *Neodrassex aureus*, female, frontal; G, *Lygromma gasnieri*, male, frontal; H, *Theuma* sp.3, male, frontal; I, *Molycria mammosa*, female, frontal.

genus in southern Africa. Much of the diversity is still unknown and of the 26 known species, only five are known from both males and females (World Spider Catalog, 2020). *Theumella* is here represented solely by the male holotype of *T. typica* Strand, 1906, and we were not able to examine the specimen with SEM.

Zimiris is a genus considered of interest within Prodidominae, because the morphology of the

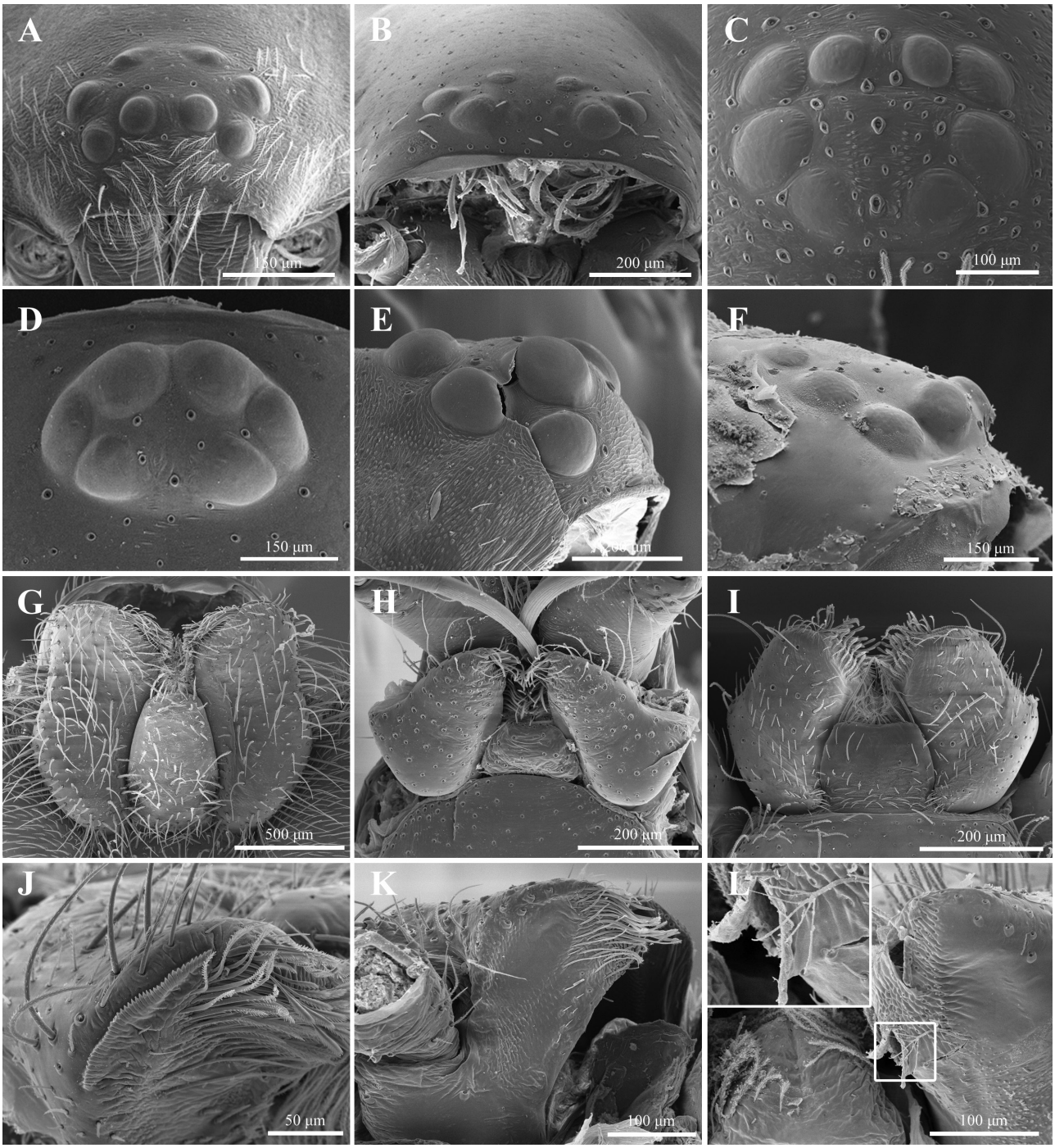

Figure 10. Eyes. A, *Myandra cambridgei*, male, frontal; B, *Paracymbiomma carajas*, male, frontal; C, *Eleleis* sp., male, dorsal; D, *Lygromma gasnieri*, male, dorsal; E, *Wesmaldra bidgemia*, female, lateral; F, *Zimiris doriai*, female, lateral. Endites: G, *Latonigena auricomis*, female, ventral; H, *Austrodomus scaber*, female, ventral; I, *Lygromma gasnieri*, female, ventral; J, same, dorsal, detail serrula; K, *Purcelliana* sp., female, dorsal; L, *Zimiris doriai*, female, dorsal, detail of branched setae.

spinnerets is similar to that of Molycriinae (Deeleman-Reinhold, 2001; Platnick & Penney, 2004; Wheeler *et al.*, 2017; Azevedo *et al.*, 2018). Nevertheless, it was never included in a phylogenetic analysis. Deeleman-Reinhold (2001) suggested a close relationship between *Zimiris* and Molycriinae, based on the anterior position

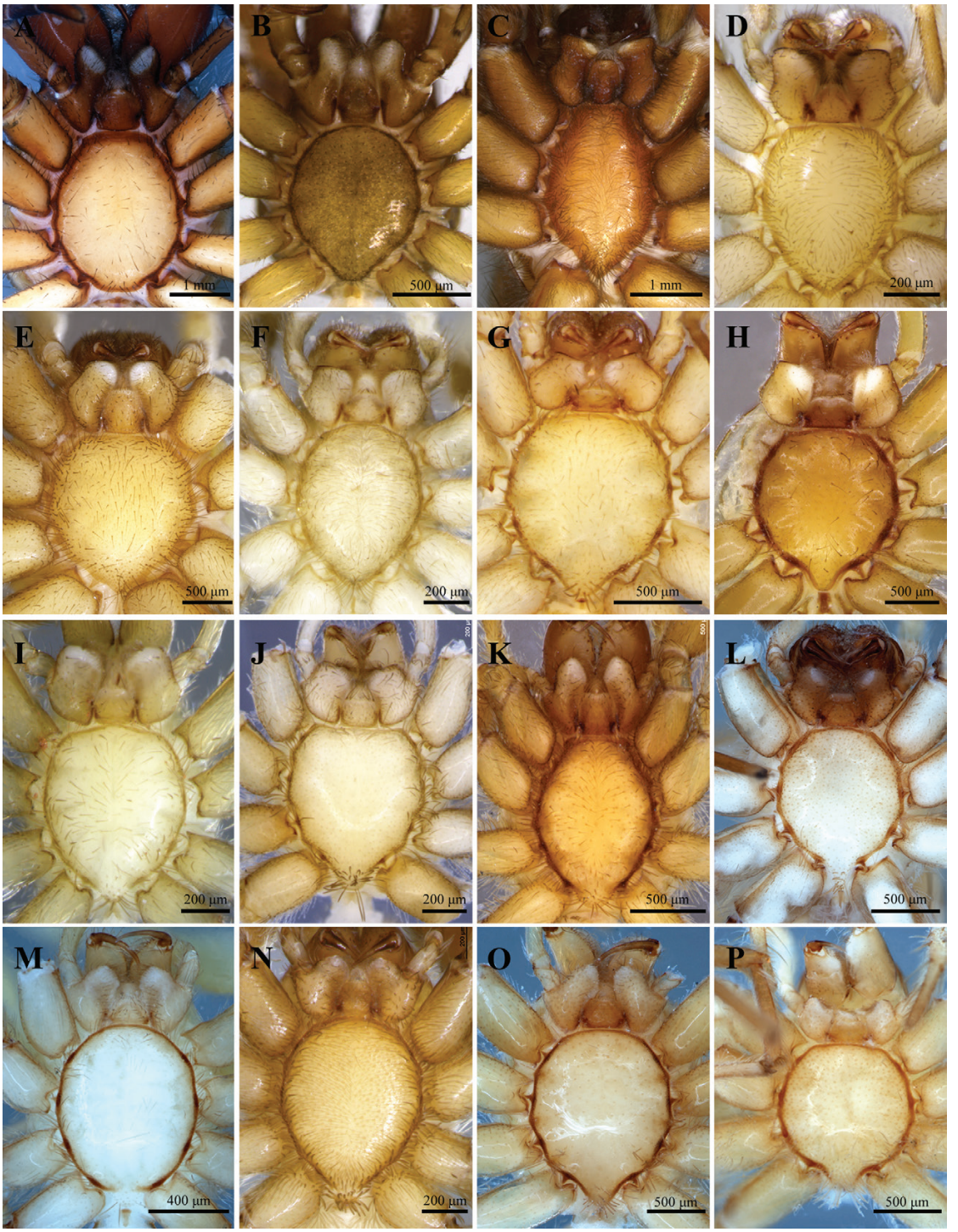

Figure 11. Sternum. A, *Platyoides walteri*, female; B, *Gallianoela* sp., male; C, *Scotophaeus quadripunctatus*, male; D, *Anzacia mustecula*, female; E, *Pterotricha lentiginosa*, female; F, *Homoeothele micans*, male; G, *Wesmaldra bidgemia*, female; H, *Wydundra osbourne*, female; I, *Nopyllus* sp., male; J, *Lygromma gasnieri*, female; K, *Oltacloea beltraoe*, male; L, *Theuma* sp.1, male; M, *Austrodomus zuluensis*, female; N, *Eleleis* sp., female; O, *Zimiris doriai*, female; P, *Namundra* sp., female.

of the ALS (Fig. 21D, K), but Platnick & Penney (2004) observed several characters shared with Prodidominae, such as procurved posterior eye row, enlarged chelicerae with elongated fangs and pyriform gland spigot surrounded by a cluster of sockets (which the authors presumed were insertions of setae).

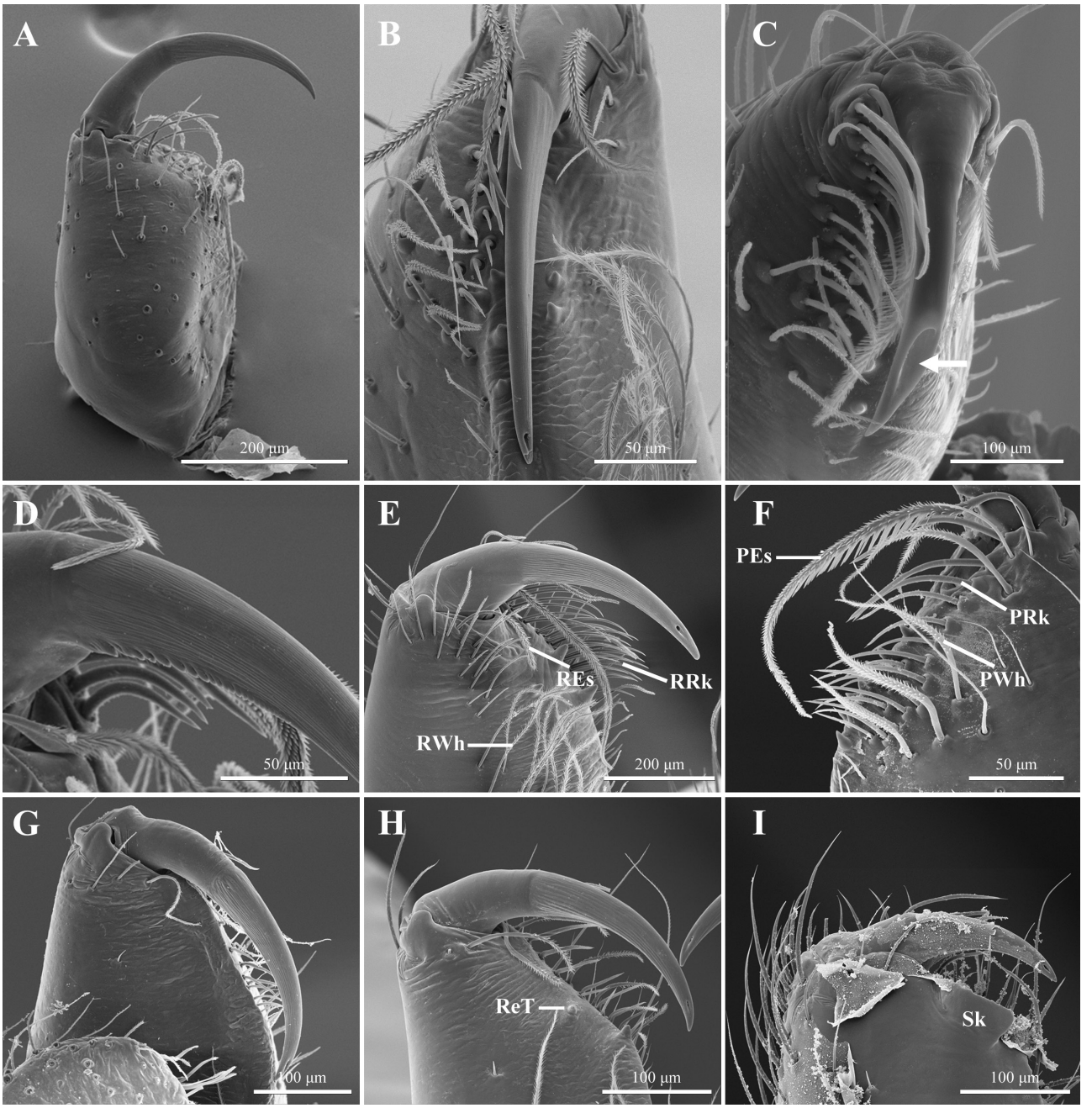

Figure 12. Chelicerae. A, *Neozimiris* sp, male, promargin; B, *Nopyllus* sp., male, frontal; C, *Myandra cambridgei*, male, frontal, arrow to venom gland opening: D, *Lygromma gasnieri*, male, fang shaft serrula; E, *Theuma* sp.3, male, retromargin; F, *Paracymbiomma carajas*, male, promargin; G, *Purcelliana* sp., female, retromargin; H, *Eleleis* sp., male, retromargin; I, *Asemesthes* sp., male, retromargin. PEs, promarginal escort seta; PRk, promarginal rake seta; PWh, promarginal whisker seta; REs, retromarginal escort seta; RRk, retromarginal rake seta; RWh, retromarginal whisker seta; ReT, reduced tooth; Sk, serrated keel.

Thus, the authors concluded that *Zimiris* belonged in Prodidominae and that the advanced ALS was acquired independently. In our analysis, we recovered *Zimiris* within Prodidominae by the presence of patches of long setae around the pyriform gland spigots in ALS (Fig. 23L, char. 190) and confirmed that the ALS position was acquired independently in Molycriinae, as suggested by Platnick & Penney (2004). In addition, the authors suggested that the presence of enlarged and darkened setae, found at the base of the claw tufts,

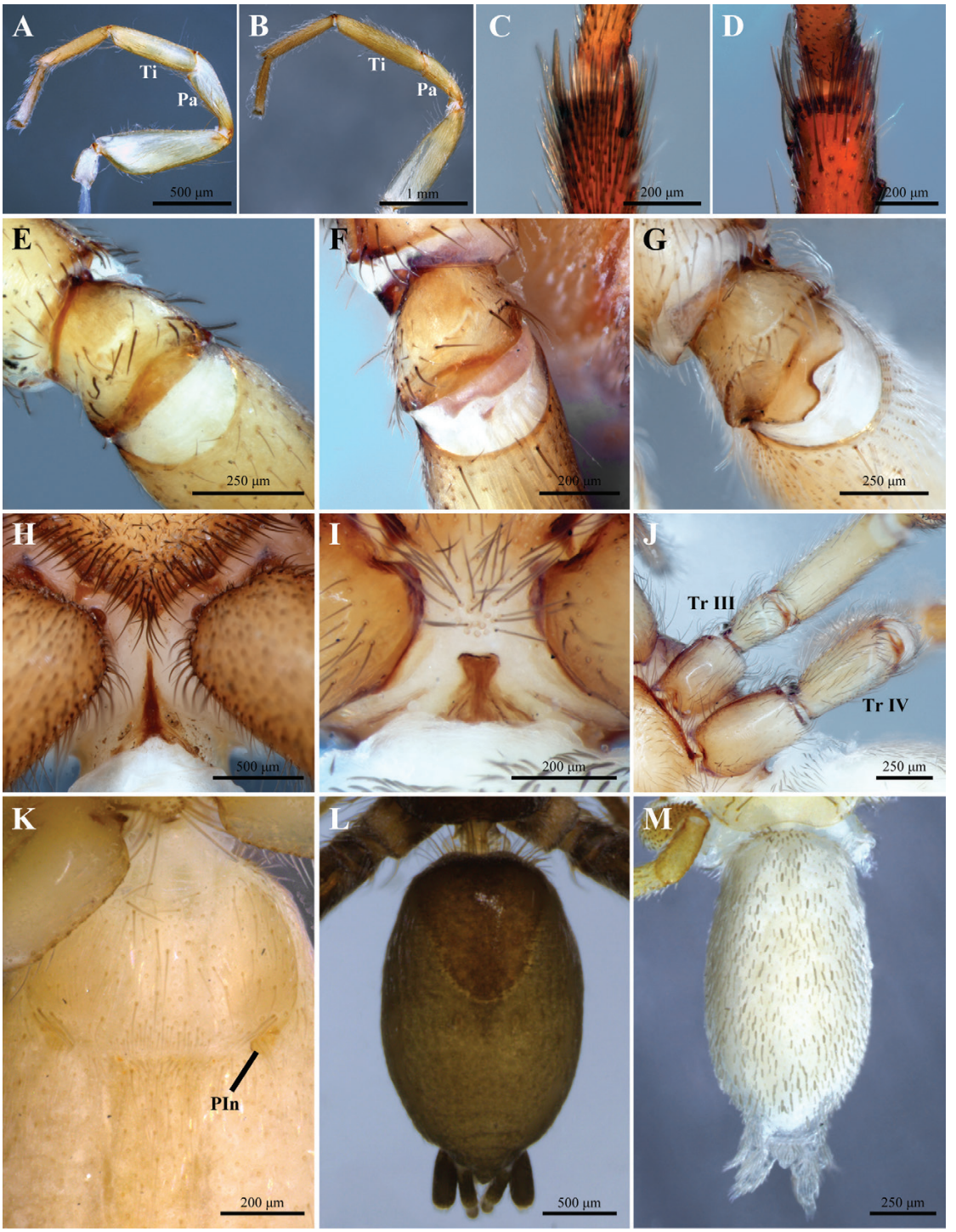

Figure 13. A, *Austrodomus scaber*, female, leg I, prolateral; B, *Namundra* sp., female, leg I, retrolateral; C, *Falconina gracilis*, male, metatarsus I, ventral; D, *Urozelotes rusticus*, male, metatarsus I, ventral; E, *Gallionela* sp., male, trochanter I, ventral; F, *Falconina gracilis*, male, trochanter I, ventral; G, *Xiruana gracilipes*, female, trochanter I, ventral; H, *Pterotricha lentiginosa*, female, pedicel, ventral; I, *Prodidomus simoni*, female, pedicel, ventral; J, same, trochanter III–IV, ventral; K, *Paracymbiomma carajas*, male, abdomen, ventral, detail postepigastric invaginations; L, *Apopyllus silvestrii*, male, abdomen, dorsal; M, *Purcelliana problematica*, male, abdomen, dorsal. Pa, patella; Pin, postepigastric invaginations; Ti, tibia; Tr, trochanter.

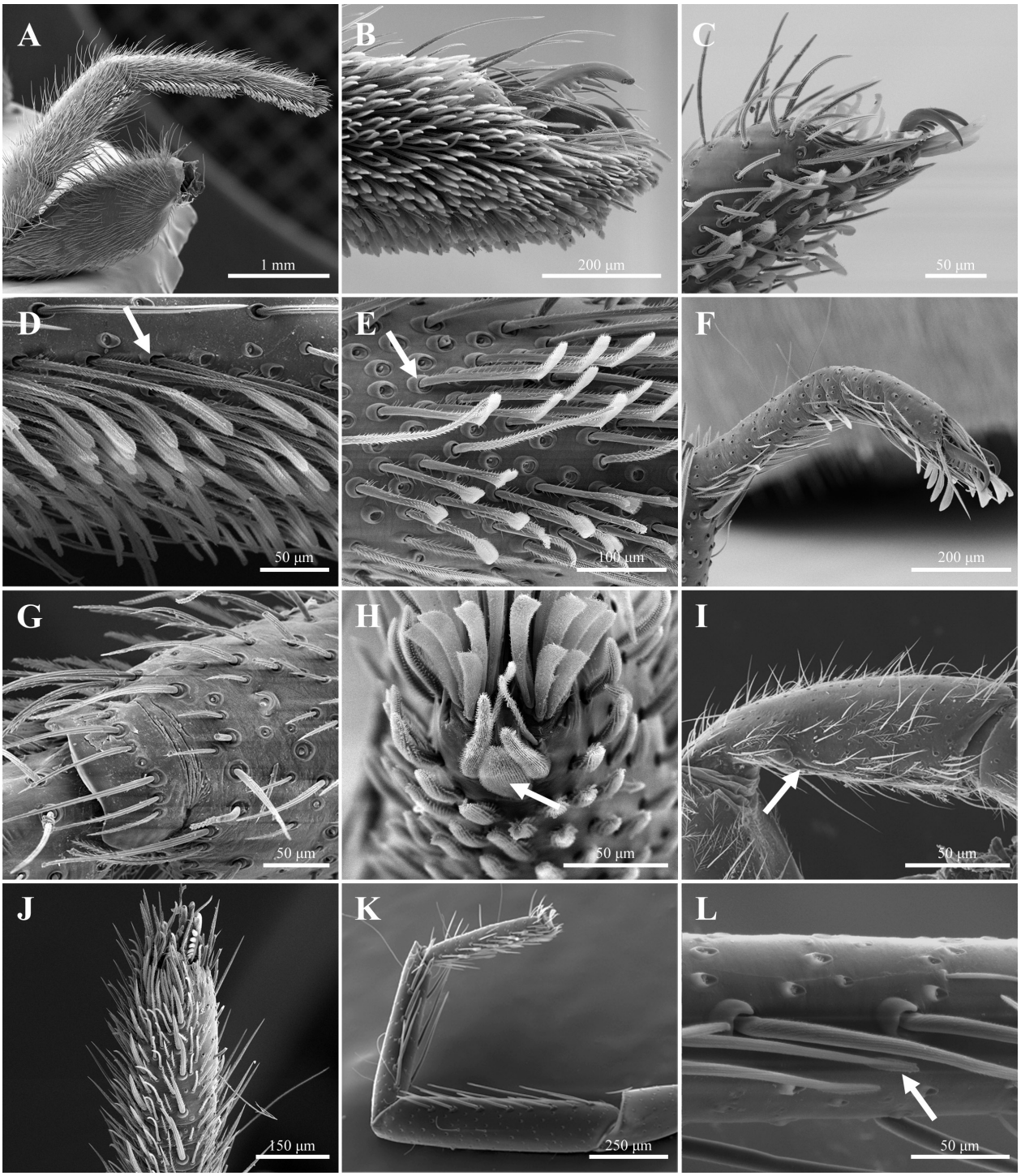

Figure 14. A, *Latonigena auricomis*, female, leg I, prolateral; B, *Scotophaeus quadripunctatus* sp., female, tarsus I; C, *Tricongius beltraoe*, male, tarsus I; D, *Theuma* sp.1, male, tarsus I, scopulae, arrow to socket of tenent setae; E, *Theuma* sp.3, male, tarsus I, scopulae, arrow to socket of tenent setae; F, *Apopyllus silvestrii*, male, tarsus II; G, *Zelotes subterraneus*, male, stopper metatarsus I; H, *Eleleis* sp., male, tarsus I, arrow to modified ventral setae; I, *Anagrina* sp., male, patella I, arrow to indentation; J, *Pterotricha lentiginosa*, male, tarsus I; K, *Chileomma ruiles*, female, leg II; L, same, metatarsus II, arrow to macrosetae with apical tenent surface.

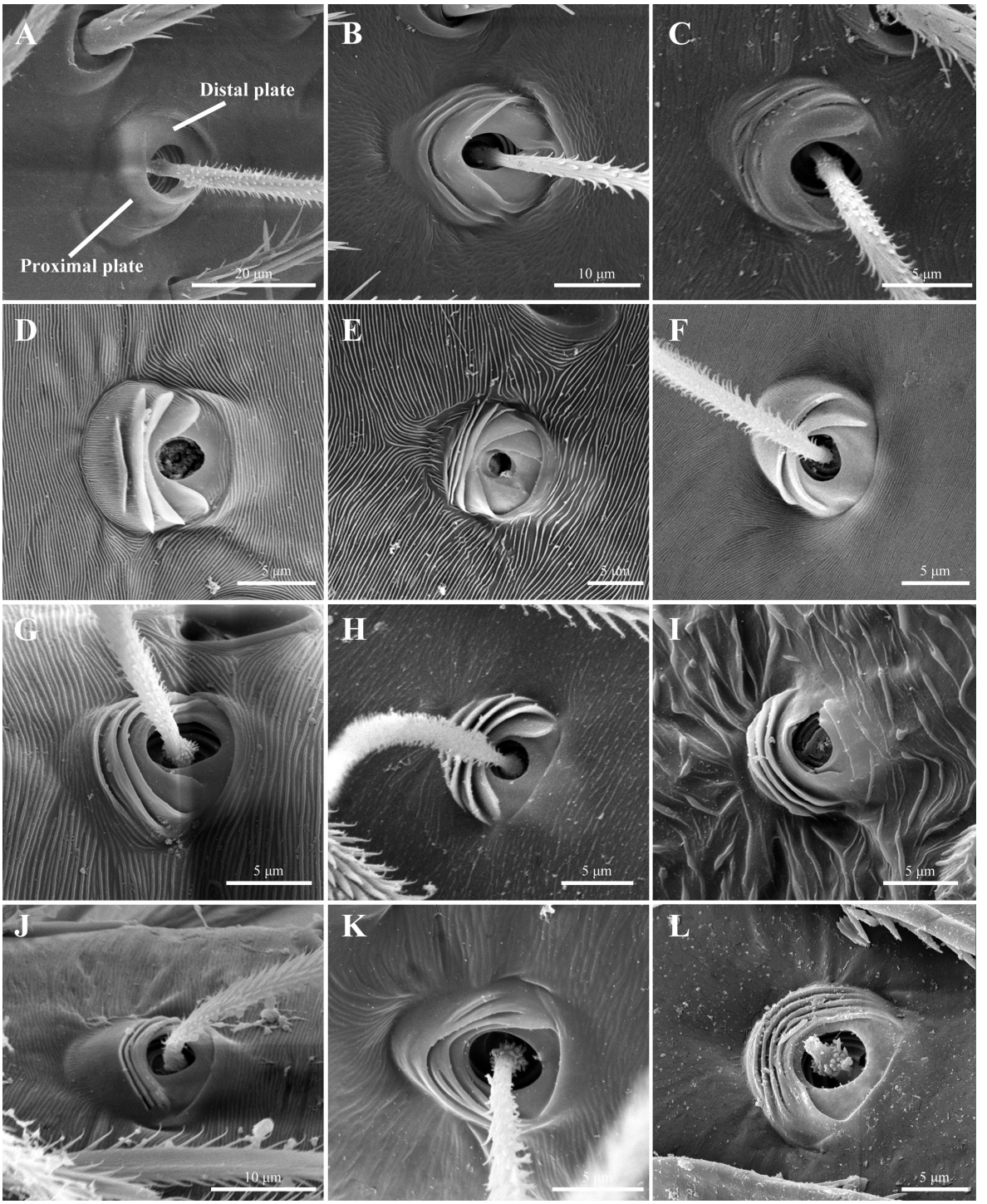

Figure 15. Trichobotria. A, *Pterotricha lentiginosa*, male; B, *Latonigena auricomis*, female; C, *Asemesthes* sp., male; D, *Nopyllus* sp., male; E, *Lygromma gasnieri*, male; F, *Theuma* sp.3, male; G, *Austrodomus scaber*, male; H, *Eleleis* sp., male; I, *Purcelliana* sp., male; J, *Namundra* sp., female; K, *Myandra cambridgei*, female; L, *Wydundra osbourne*, female.

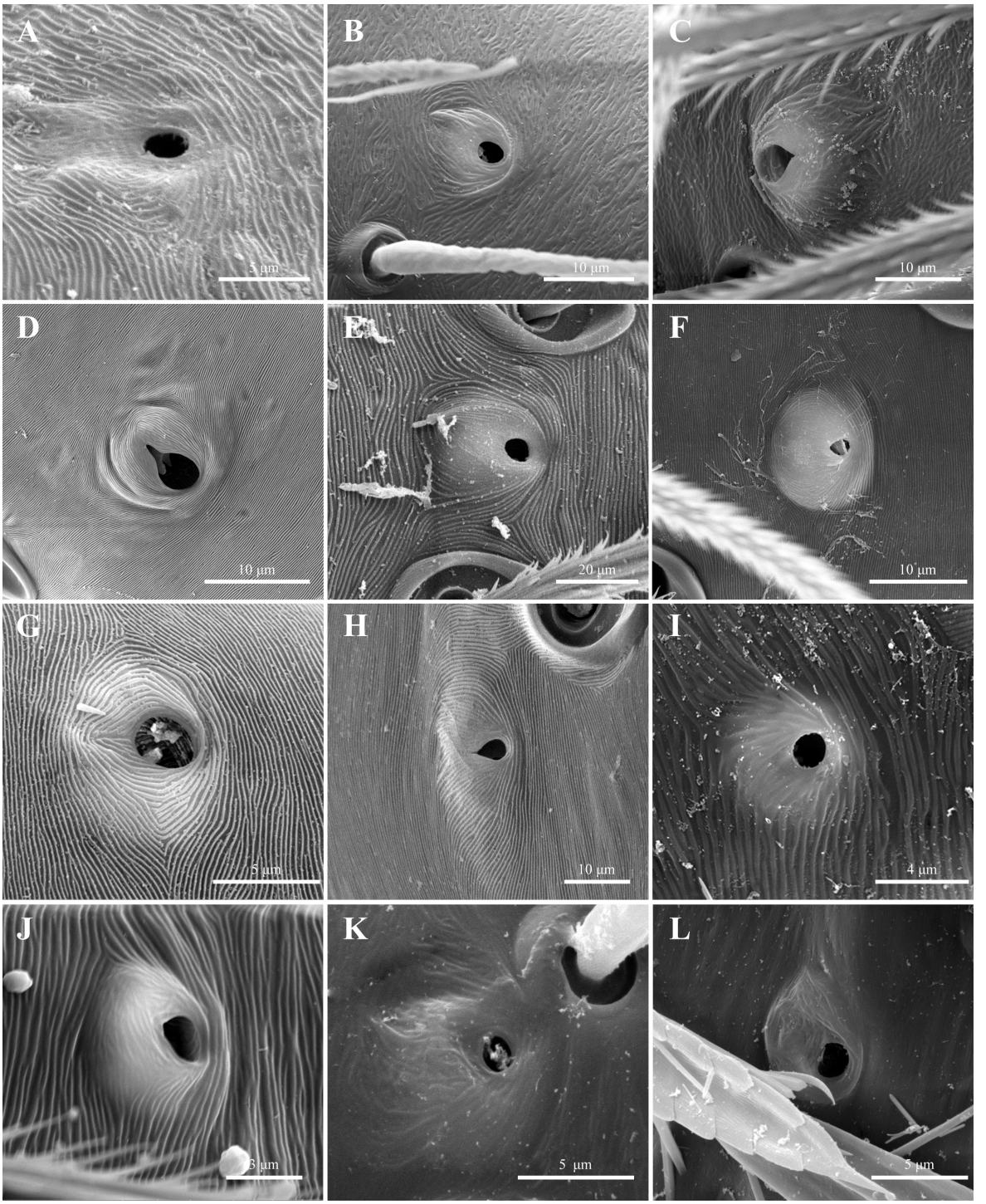

Figure 16. Tarsal organ. A, *Hemicloea sundevalli*, female; B, *Asemesthes* sp., male; C, *Latonigena auricomis*, female; D, *Nopyllus* sp., male; E, *Tricongius amazonicus*, female; F, *Theuma* sp.3, male; G, Gen.1 AFR. sp.1, male; H, *Neozimiris* sp., female; I, *Zimirina hirsuta*, female; J, *Namundra* sp., female; K, *Myandra cambridgei*, female; L, *Wesmaldra bidgemia*, male.

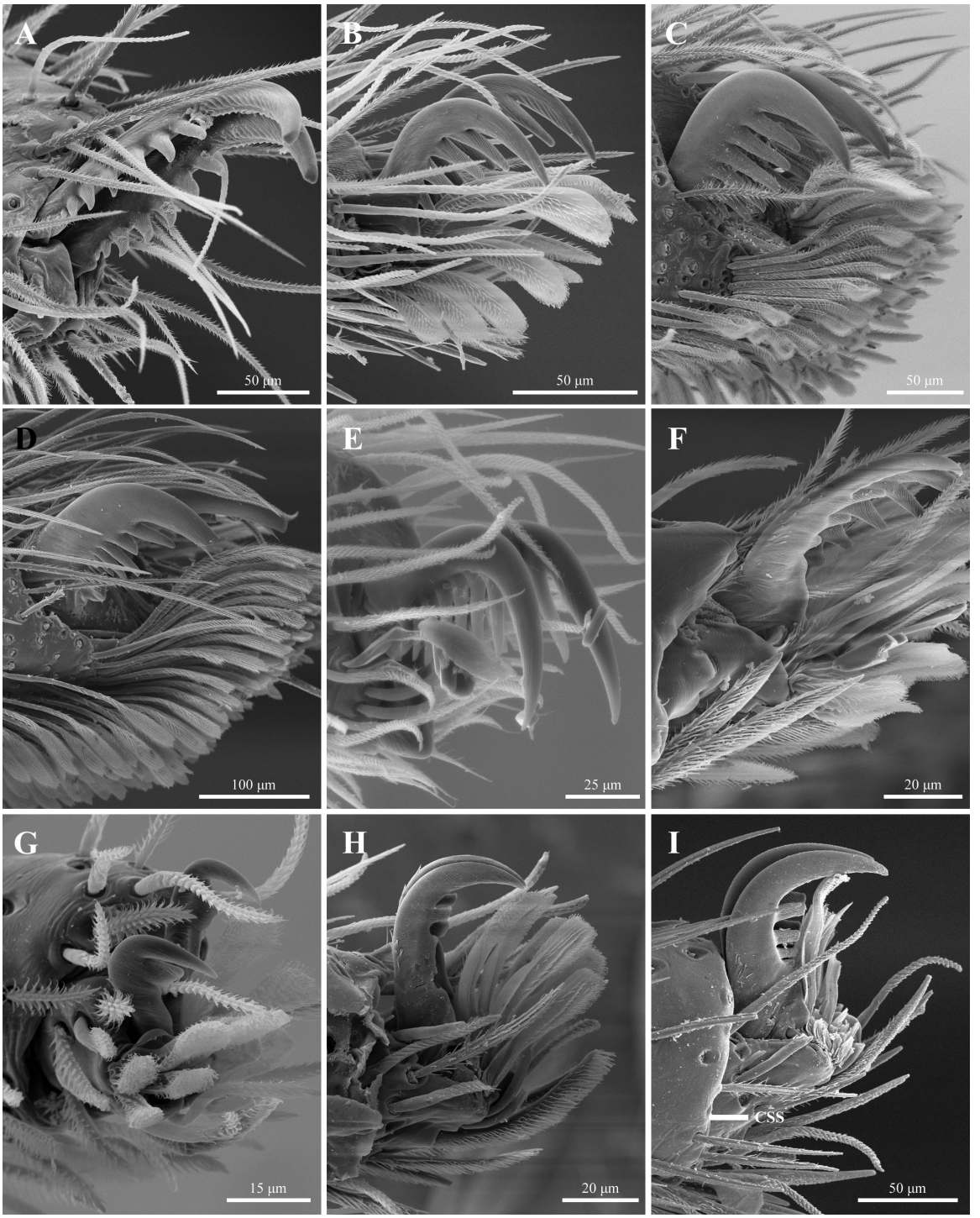

Figure 17. Claws, leg I. A, *Urozelotes rusticus*, male; B, *Asemesthes* sp., male; C, *Xerophaeus appendiculatus*, male; D, *Scotophaeus quadripunctatus*, female; E, *Anagrina* sp., female; F, *Cryptoerithus occultus*, female; G, *Myandra cambridgei*, female; H, *Wesmaldra bidgemia*, male; I, *Wydundra osbourne*, female. CSS, claw slit suture.

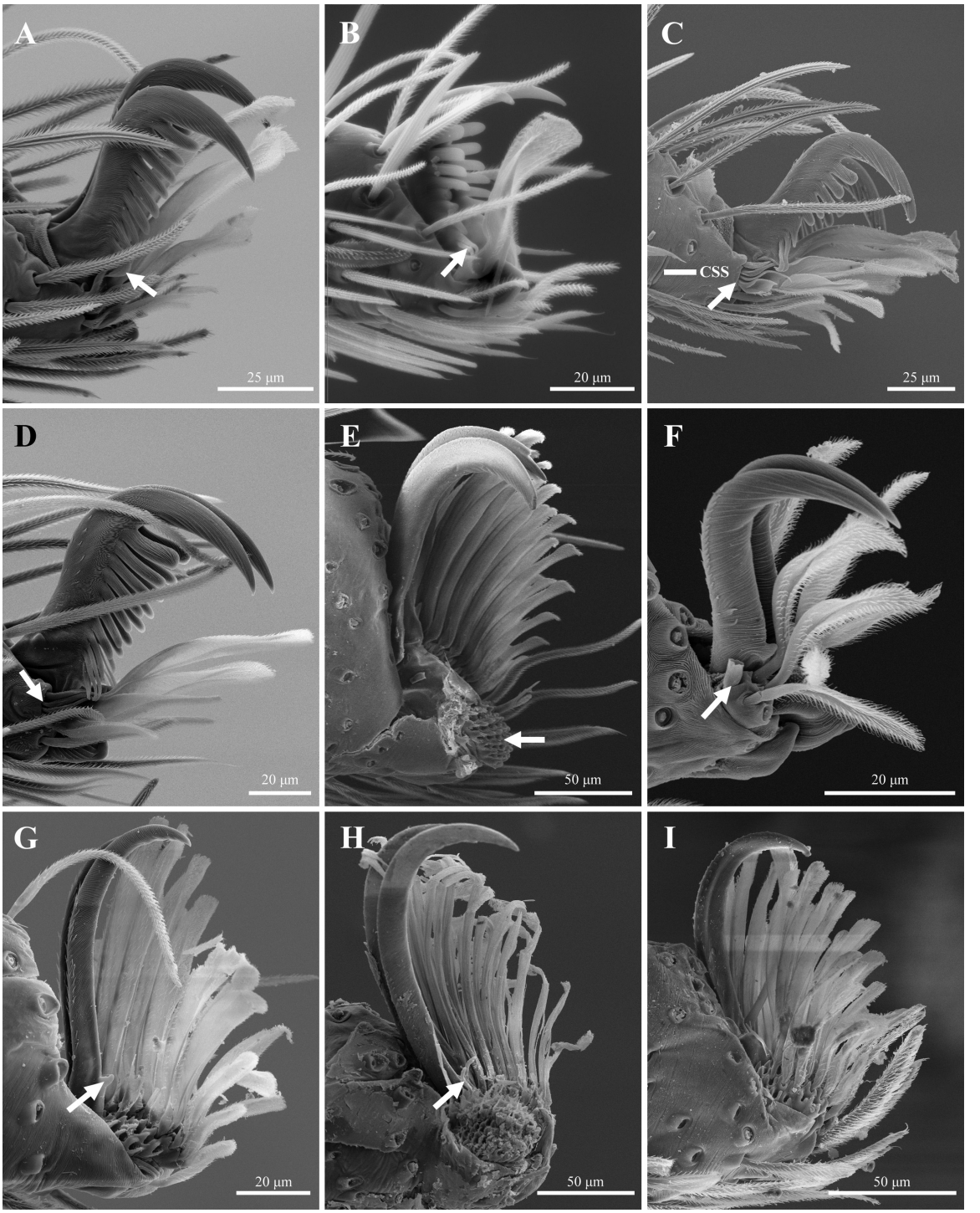

Figure 18. Claws, leg I. A, *Nopyllus* sp., male, leg I, arrow to classic clasper; B, *Chileomma ruiles*, male, leg II, arrow to classic clasper; C, *Tricongius amazonicus*, female, leg I, arrow to claw tuft bases packed together; D, *Paracymbiomma carajas*, male, leg II, arrow to claw tuft bases packed together; E, *Theuma* sp.1, male, leg I, arrow to well delimited plate with the tenent setae inserted in individual sockets; F, Gen.1 AFR. sp.1, male, leg I, arrow to well-delimited plate with the tenent setae inserted in individual sockets; G, *Zimirina hirsuta*, male, leg I, arrow to solid clasper; H, *Zimiris doriai*, female, leg I, arrow to flexible single clasper; I, *Namundra* sp., female, leg I. CSS, claw slit suture.

would be diagnostic for the genus (Fig. 14H, char. 145). However, we observed that all genera within clade 71 of Prodidominae share this characteristic with *Zimiris* (Fig. 14H).

Caudalia and *Neozimiris* are the only exclusively Neotropical genera in clade 59. We recovered both genera as closely related in all analysis under implied weighting and with high support values (clade 77). However, because we examined only the female holotype of *Caudalia insularis*, we prefer not to make any taxonomic decisions until more material is examined. Alayón (1980) has already noted the close relationship between these genera and has suggested that both showed structural similarities with *Austrodomus*. However, our results indicate that *Austrodomus* is more closely related to other African genera. Cooke (1977) suggested that *Zimirina* could be a junior synonym of *Neozimiris*. In our study, *Zimirina* arises sister to *Caudalia* + *Neozimiris* in all analyses and with high support (Fig. 2, clade 76), contradicting the observations of Cooke that *Zimirina* and *Neozimiris* could be synonyms.

Prodidomus and *Prodida* were recovered in several analyses as a polytomy (Fig. 2, clade 84). *Prodida* is a genus comprised of only two species and is restricted to the Philippines and the Seychelles Islands, while *Prodidomus* is a widely distributed genus with 53 species characterized by the presence of massive PLS, much thicker than the anterior spinnerets (Figs 21L, 25J, char. 224). Deeleman-Reinhold (2001) observed that *Prodida* shares with *Prodidomus* characters such as the diverging chelicerae and endites with a pointed, distal margin. She also described the spinnerets of *Prodida* as having ALS anterior-posteriorly compressed, PMS small and laterally compressed, PLS with basal segment more massive than in ALS and with atypical spigots. We observed that all these characters are also present in *Prodidomus*, including the atypical spigots (spigots with shafts widened at the tip). Thus, although only the female holotype of *Prodida longiventris* (from which the epigyne is missing) was scored in this study, the presence of a massive PLS allows us to propose *Prodida* as a junior synonym of *Prodidomus*.

Austrodomus, *Katumbea* and *Purcelliana* arose as a monophyletic group, supported by the presence of simple vRTA (clade 82, char. 234). The male of *Purcelliana problematica* and the female of *Austrodomus scaber* were originally described as *Prodidomus scaber* by Purcell, 1904. Although the specimens were collected together, Cooke (1964) observed that both show characters that separate them from *Prodidomus*. Thus, the author described a new genus to allocate the male specimen and placed the female in *Austrodomus*. Nevertheless, he stated that the examination of additional material was needed to elucidate the limits of these genera. Our results corroborate Cooke's (1964) hypothesis that both genera arose as distinct but closely related (Fig. 2, clade 80). *Purcelliana* was recovered as monophyletic (clade 81) supported by several homoplastic synapomorphies, such as the presence of clavate setae over the entire body (Figs 8P, 13M, char. 7, 154). *Austrodomus* was not recovered as monophyletic, because *Katumbea* arose more closely to *A. zuluensis* Lawrence, 1947 by the presence of conspicuous primary spermathecae (char. 277) and copulatory ducts wider and closer to the copulatory opening (clade 83, char. 288).

Although our results have elucidated several issues involving Prodidominae spiders, some genera remain unresolved and need further studies. *Theuma* and *Prodidomus*, for example, are diverse genera that deserve a taxonomic revision to better define their taxonomic limits. The monotypic genera *Caudalia*, *Plutonodomus* and *Theumella* are known only from one sex and only their holotypes were examined. Perhaps, the study of additional material will help to provide a better taxonomic and phylogentic definition of these groups.

TAXONOMY

GNAPHOSIDAE POCOCK, 1898

MOLYCRIINAE SIMON, 1908 SUBFAMILY REVALIDATED

Molycriinae: Platnick, 1990: 36.
Prodidominae: Azevedo *et al.*, 2018: 35, **syn**.

Type genus: Molycria Simon, 1887.

Genera included: Cryptoerithus Rainbow, 1915; *Molycria*; *Myandra* Simon 1887; *Nomindra* Platnick & Shadab, 2006; *Wesmaldra* Platnick & Shadab, 2006; *Wydundra* Platnick & Shadab, 2006.

Diagnosis: ALS extremely elongated, situated far in advance of the posterior spinnerets (Figs 19D, 21C, D), distal article modified in a retractile area (Fig. 22I–K) and presence of an apical hood in the basal article (Fig. 22H, L); pyriform gland spigots elongated with base longer than shaft (Fig. 22G–I).

Shared characters: ***char. 16—Eyes***, posterior eye row, shape: straight to recurved ➔ procurved; ***char. 39—Sternum***, posterior margin, protrusion, sclerotization marginal: unsclerotized ➔ sclerotized; ***char. 71—Legs*** I–II, trochanters, distal rim: straight ➔ shallow indentation; ***char. 72—Legs*** III–IV, trochanters, distal rim: straight ➔ shallow indentation; ***char. 131—Legs***, tarsus, distal, ventral, claw slit suture (CSS): absent ➔ present; ***char. 132—Legs***, tarsus, distal,

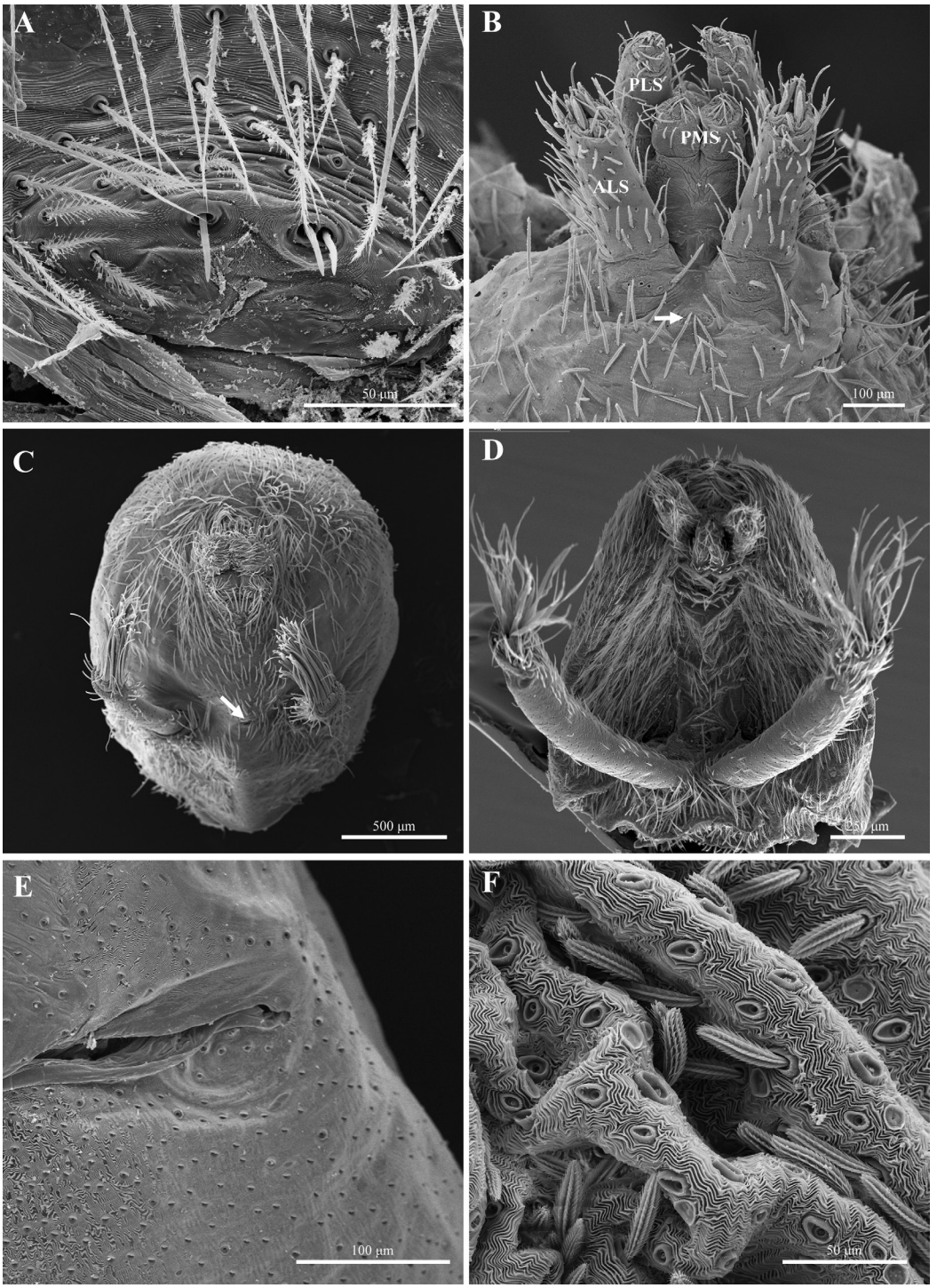

Figure 19. A, *Leptodrassex* sp., male, abdomen, epiandrous spigots; B, *Tricongius amazonicus*, female, spinnerets, arrow to tracheal spiracle; C, *Namundra* sp., female, abdomen, arrow to tracheal spiracle; D, *Molycria mammosa*, female, abdomen; E, *Lygromma gasnieri*, female, abdomen, postepigastric invagination; F, *Purcelliana* sp., male, abdomen, clavate setae. ALS, anterior lateral spinnerets; PLS, posterior lateral spinnerets; PMS, posterior median spinnerets.

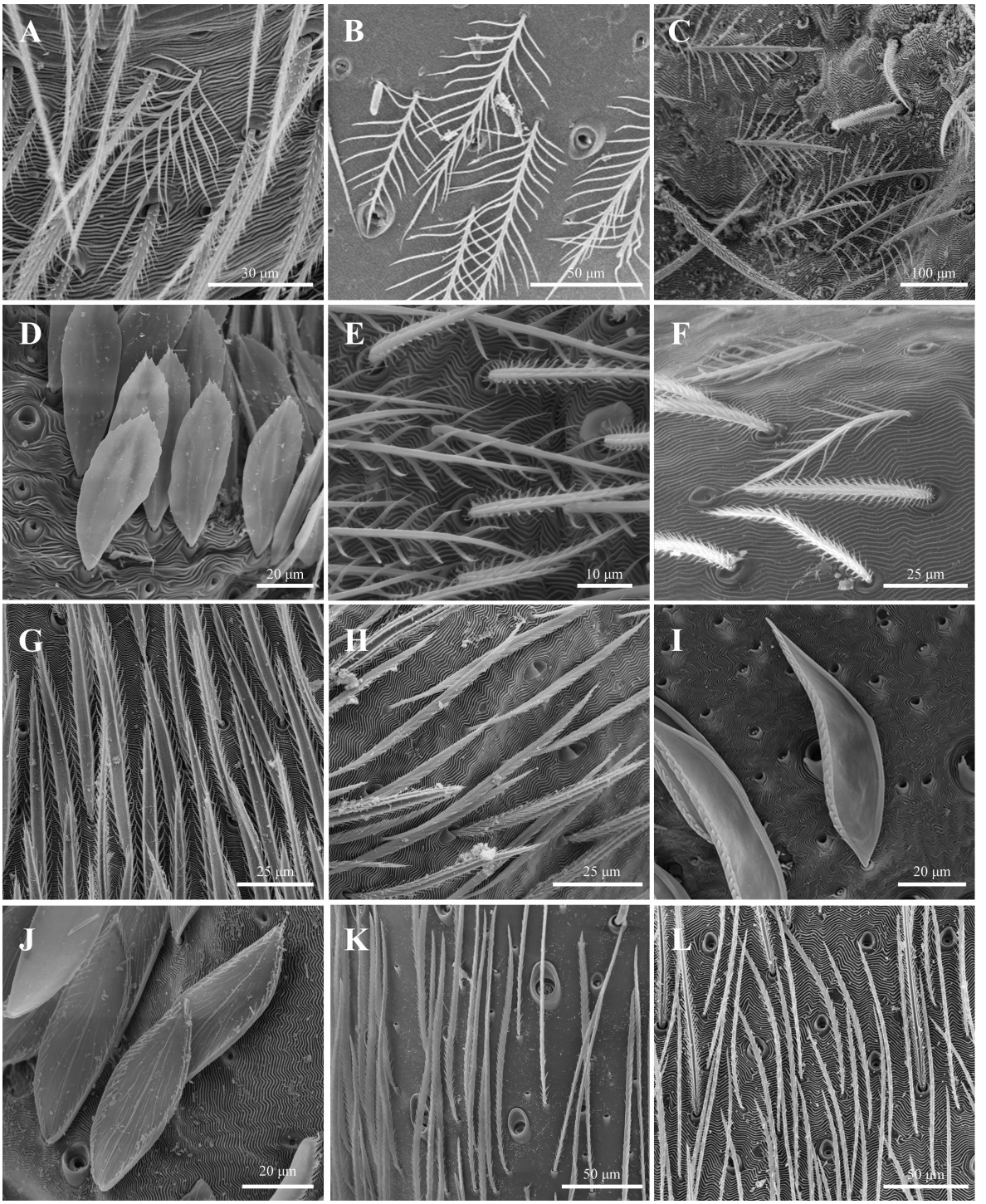

Figure 20. Plumose and squamose setae, abdomen. A, *Apopyllus silvestrii*, female; B, *Asemesthes* sp., male; C, *Cryptoerithus occultus*, female; D, *Wesmaldra bidgemia*, male; E, *Myandra cambridgei*, female; F, *Nomindra kinchega*, female; G, *Tricongius beltraoe*, male; H, *Moreno ramirezi*, male; I, *Paracymbiomma carajas*, male; J, *Lygromma gasnieri*, male; K, *Theuma* sp.1, male; L, *Namundra* sp., female.

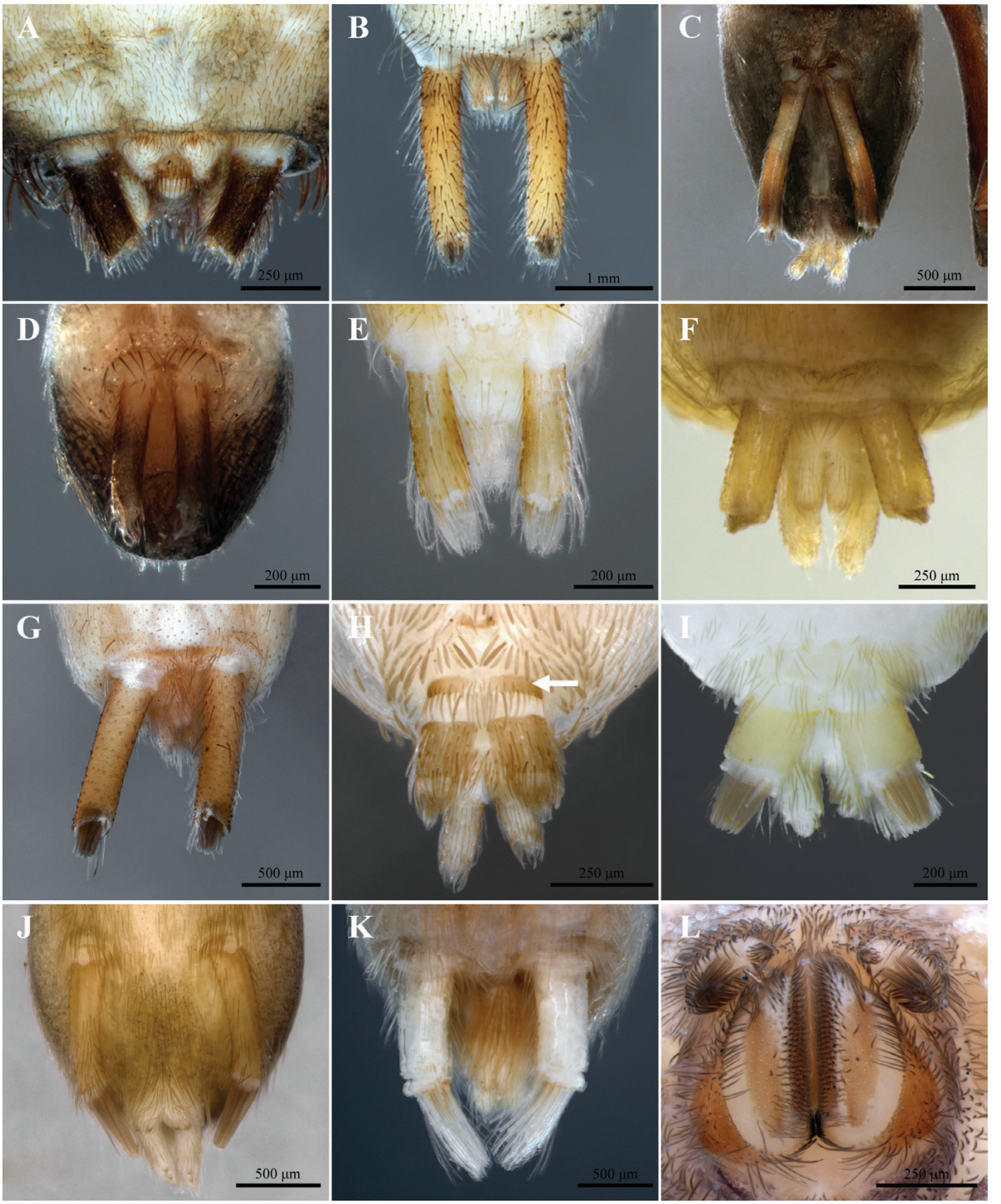

Figure 21. Spinnerets, ventral (except figure L). A, *Vectius niger*, female; B, *Pterotricha lentiginosa*, female; C, *Molycria mammosa*, female; D, *Myandra cambridgei*, female; E, *Lygromma gasnieri*, male; F, *Chilongius palmas*, female; G, *Theuma* sp.1, male; H, *Eleleis* sp., female, arrow to sclerotization close to base of ALS; I, *Austrodomus zuluensis*, female; J, *Namundra* sp., female; K, *Zimiris doriai*, female; L, *Prodidomus simoni*, female, apical.

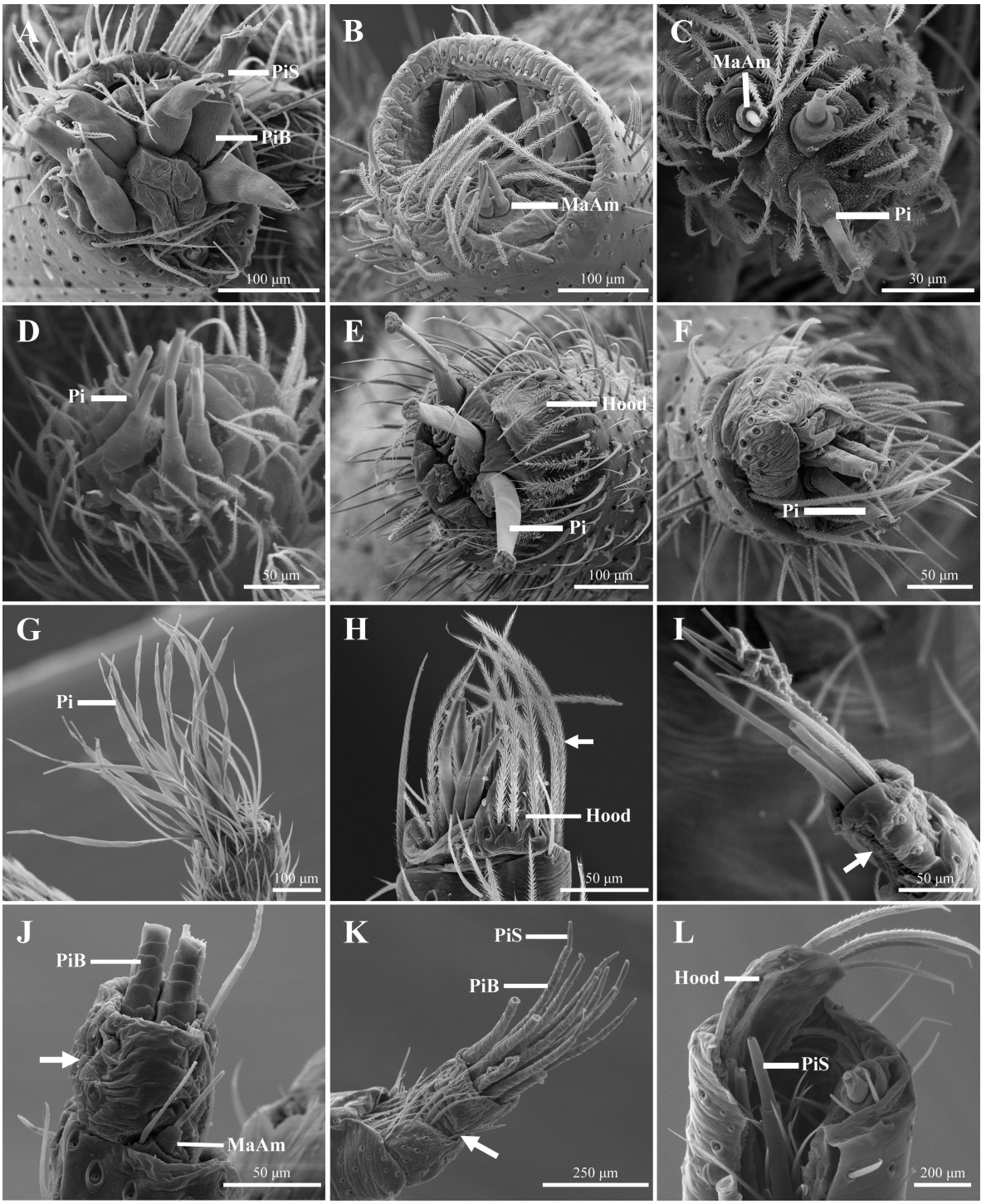

Figure 22. Spinnerets, ALS. A, *Urozelotes rusticus*, male; B, *Latonigena auricomis*, female; C, *Leptodrassex* sp., male; D, *Anagrina* sp., male; E, *Asemesthes* sp., female; F, *Cryptoerithus occultus*, female; G, *Molycrina mammosa*, female; H, *Myandra cambridgei*, male, arrow to setae covered by barbs; I, *Nomindra kinchega*, female, arrow to retractile area of ALS; J, *Wesmaldra bidgemia*, male, arrow to retractile area of ALS; K, *Wydundra osbourne*, female, arrow to retractile area of ALS; L, same, detail of hood. MaAm, major ampullate gland spigots; Pi, piriform gland spigots; PiB, piriform spigot base; PiS, piriform spigot shaft.

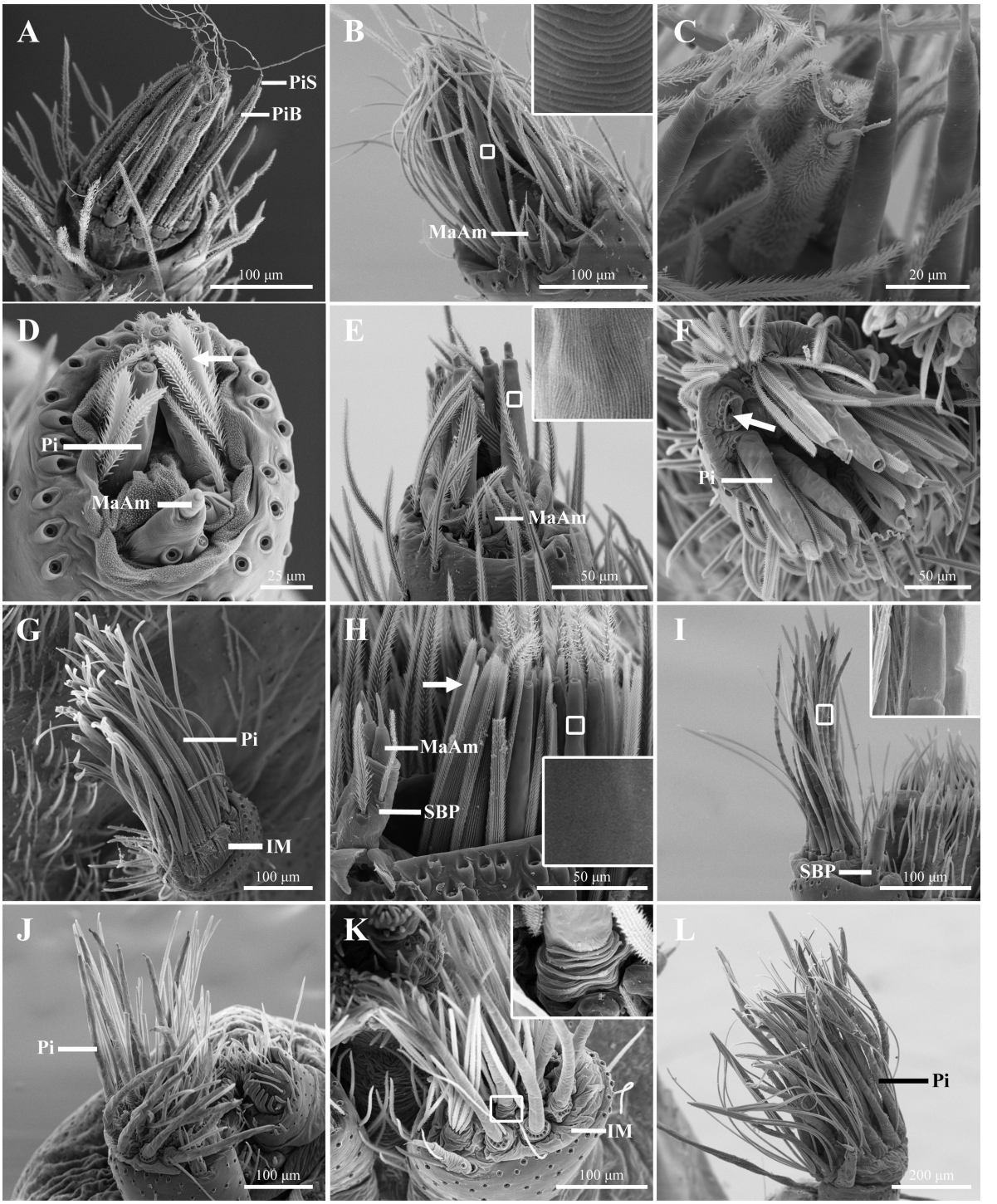

Figure 23. Spinnerets, ALS. A, *Lygromma gasnieri*, male; B, same, female, detail texture of base of piriform gland spigots; C, same, female, central spigot with plumose base; D, *Nopyllus* sp., male; E, *Tricongius beltraoe*, male, detail texture of base of piriform gland spigots; F, *Theuma* sp.3, female, arrow to well-defined base of Pi; G, *Namundra* sp., female; H, *Eleleis* sp., male, detail texture of base of piriform gland spigots; I, Gen.2 AFR. sp.1, female, detail texture of base of piriform gland spigots; J, *Neozimiris* sp., female; K, *Zimirina hirsuta*, female, detail insertion annulate of piriform gland spigots; L, *Zimiris doriai*, female. IM, inflatable membrane; MaAm, major ampullate gland spigots; Pi, piriform gland spigots; PiB, piriform spigot base; PiS, piriform spigot shaft; SBP, setae bearing projection.

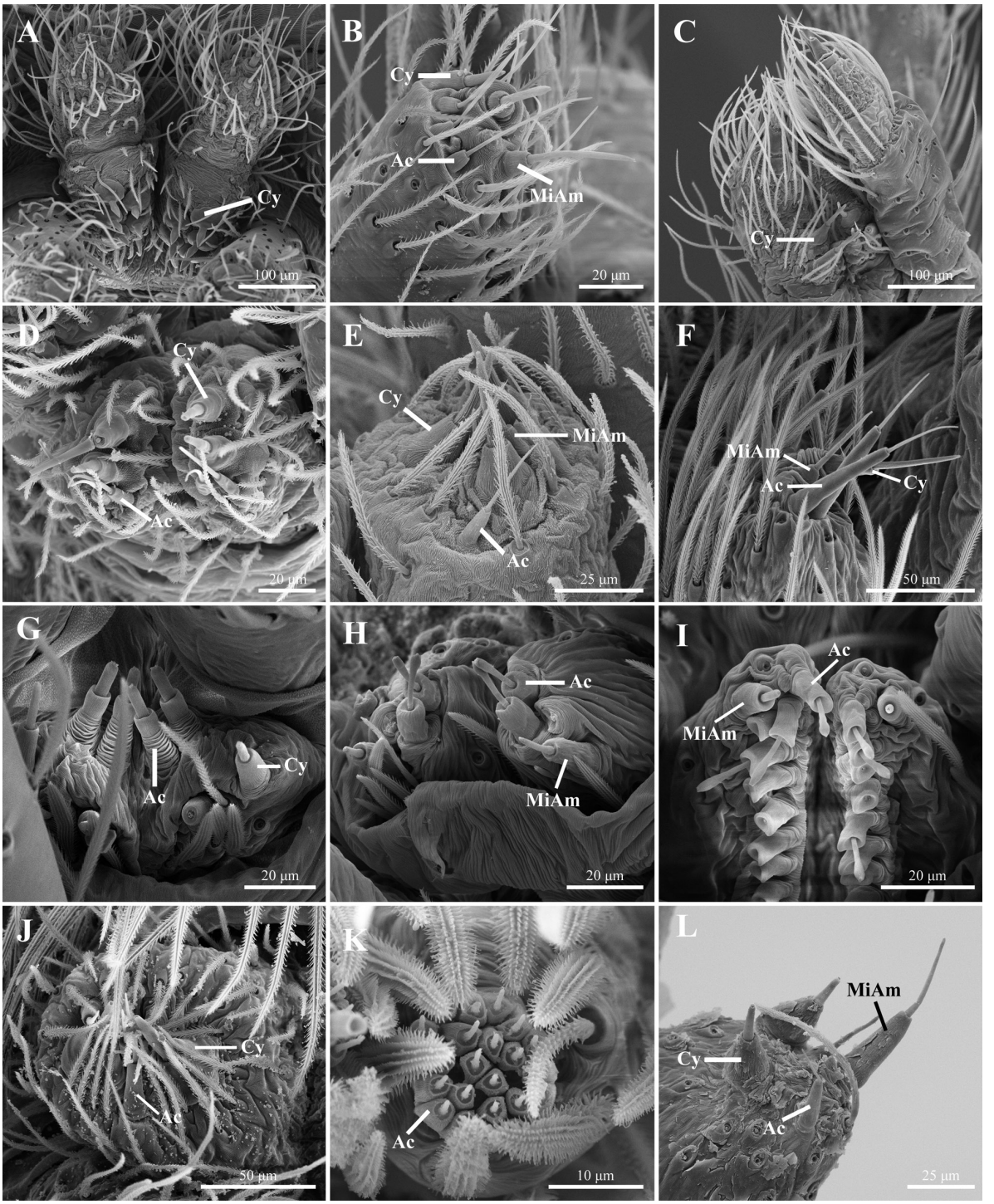

Figure 24. Spinnerets, PMS, female. A, *Apopyllus silvestrii*; B, *Leptodrassex* sp.; C, *Cryptoerithus occultus*; D, *Myandra cambridgei*; E, *Tricongius amazonicus*; F, *Theuma* sp.1; G, Neozimiris sp.; H, Austrodomus scaber; I, Prodidomus wooldleigh; J, *Namundra* sp.; K, *Zimirina hirsuta*; L, *Zimiris doriai*. Ac, aciniform gland spigot; MiAm, minor ampullate gland spigot; Cy, cylindrical gland spigot.

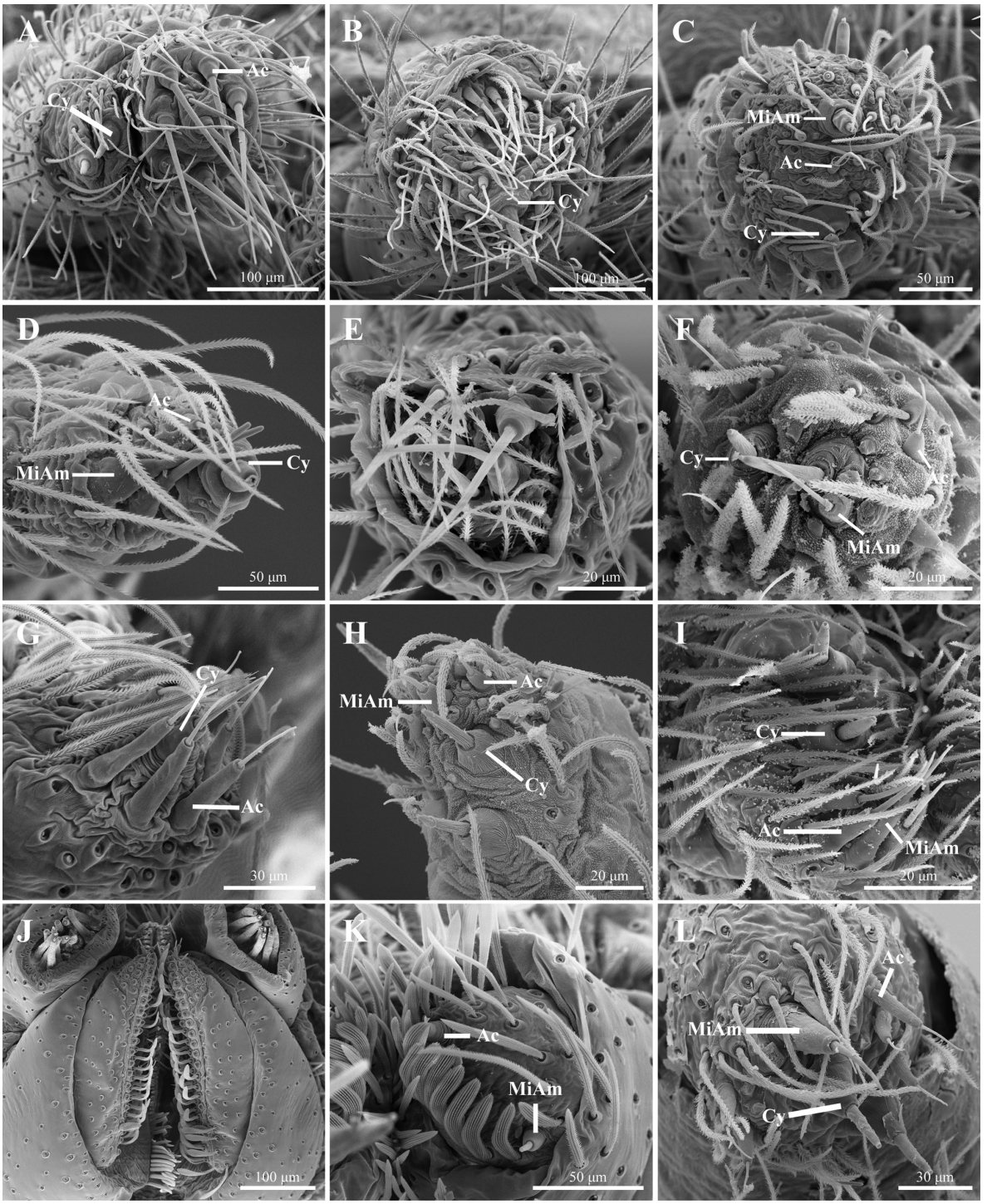

Figure 25. Spinnerets, PLS, female. A, *Asemesthes* sp.; B, *Latonigena auricomis*; C, *Apopyllus silvestrii*; D, *Cryptoerithus occultus*; E, *Wesmaldra bidgemia*; F, *Lygromma gasnieri*; G, *Theuma* sp.1; H, *Tricongius amazonicus*; I, *Namundra* sp.; J, *Prodidomus wooldleigh*; K, *Neozimiris* sp.; L, *Zimiris doriai*. Ac, aciniform gland spigot; MiAm, minor ampullate gland spigot; Cy, cylindrical gland spigot.

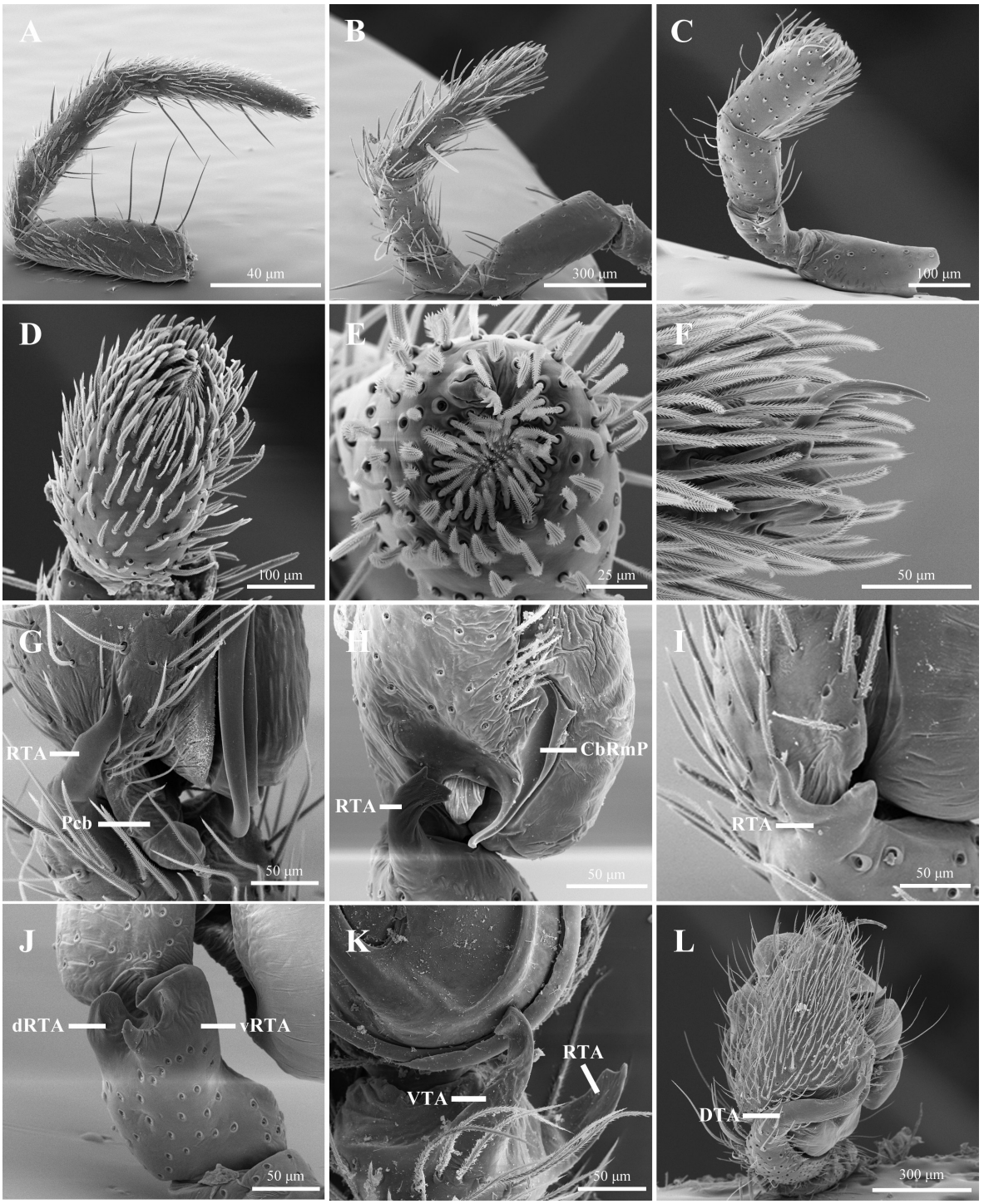

Figure 26. Female pedipalp. A, *Wesmaldra bidgemia*, retrolateral; B, *Namundra* sp., retrolateral; C, Gen.2 AFR. sp.1, retrolateral; D, *Eleleis* sp., tarsus; E, *Neozimiris* sp., tarsus; F, Theuma sp.3, tarsus. Male palp, RTA. G, *Paracymbiomma carajas*; H, *Zimirina hirsuta*; I, *Moreno ramirezi*; J, *Prodidomus wooldleigh*; K, *Lygromma gasnieri*; L, *Asemesthes* sp. CbRmP, cymbial retromedian process; dRTA, dorsal retrolateral tibial apophysis; DTA, dorsal tibial apophysis; Pcb, paracymbium; RTA, retrolateral tibial apophysis; vRTA, ventral retrolateral tibial apophysis; VTA, ventral tibial apophysis.

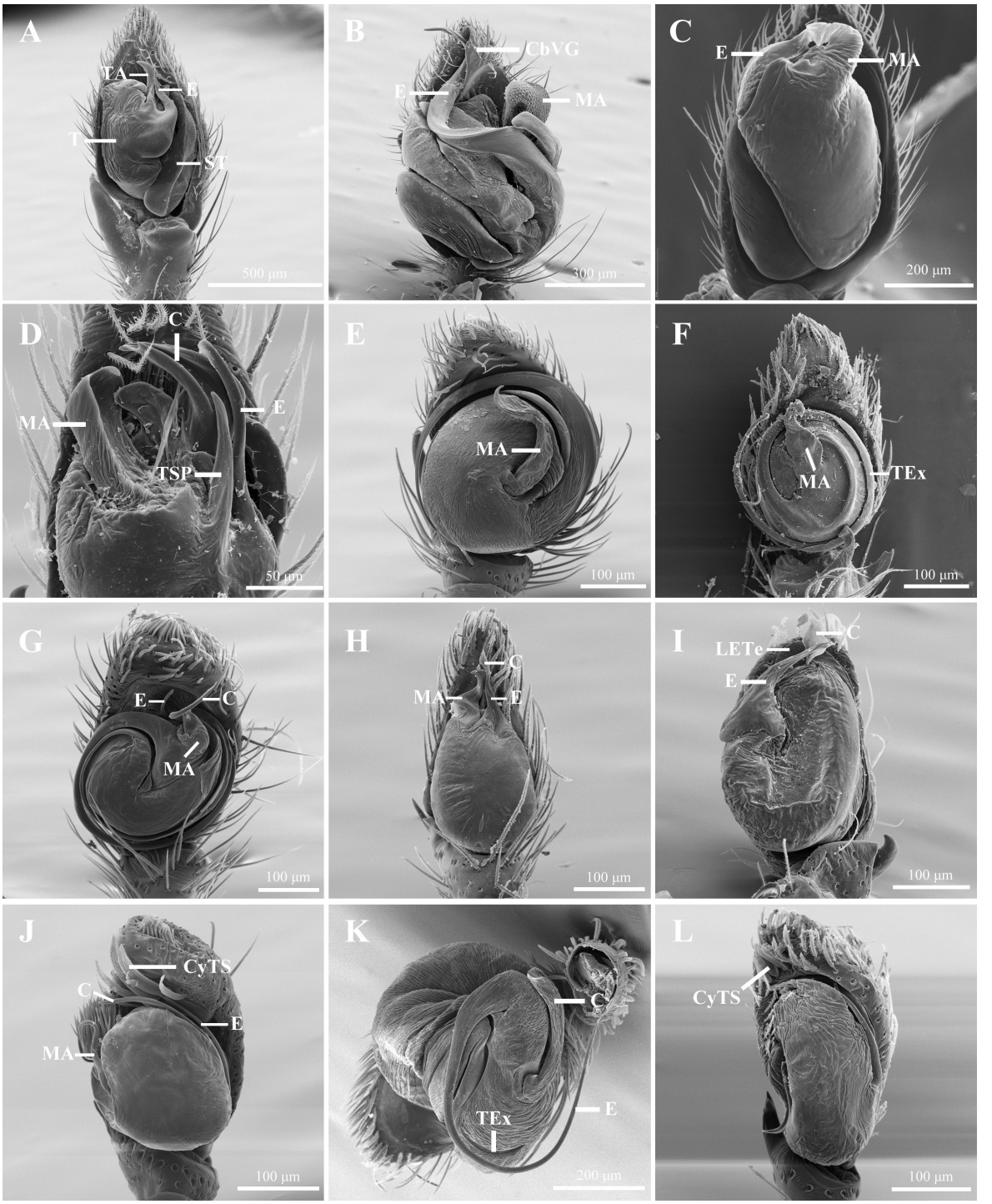

Figure 27. Male palp, ventral. A, *Urozelotes rusticus*; B, *Asemesthes* sp.; C, *Anagrina* sp.; D, *Myandra cambridgei*; E, *Tricongius beltraoe*; F, *Lygromma gasnieri*; G, *Paracymbiomma carajas*; H, *Moreno ramirezi*; I, *Austrodomus scaber*; J, *Neozimiris* sp.; K, *Eleleis* sp.; L, *Zimirina hirsuta*. C, conductor; CbTS, cymbial thick setae; CbVG, cymbial ventral groove; E, embolus; LETe, laminar extension of tegulum; MA, median apophysis; T, tegulum; TA, terminal apophysis; TEx, tegular excavation; TSP, tegular spine-like process.

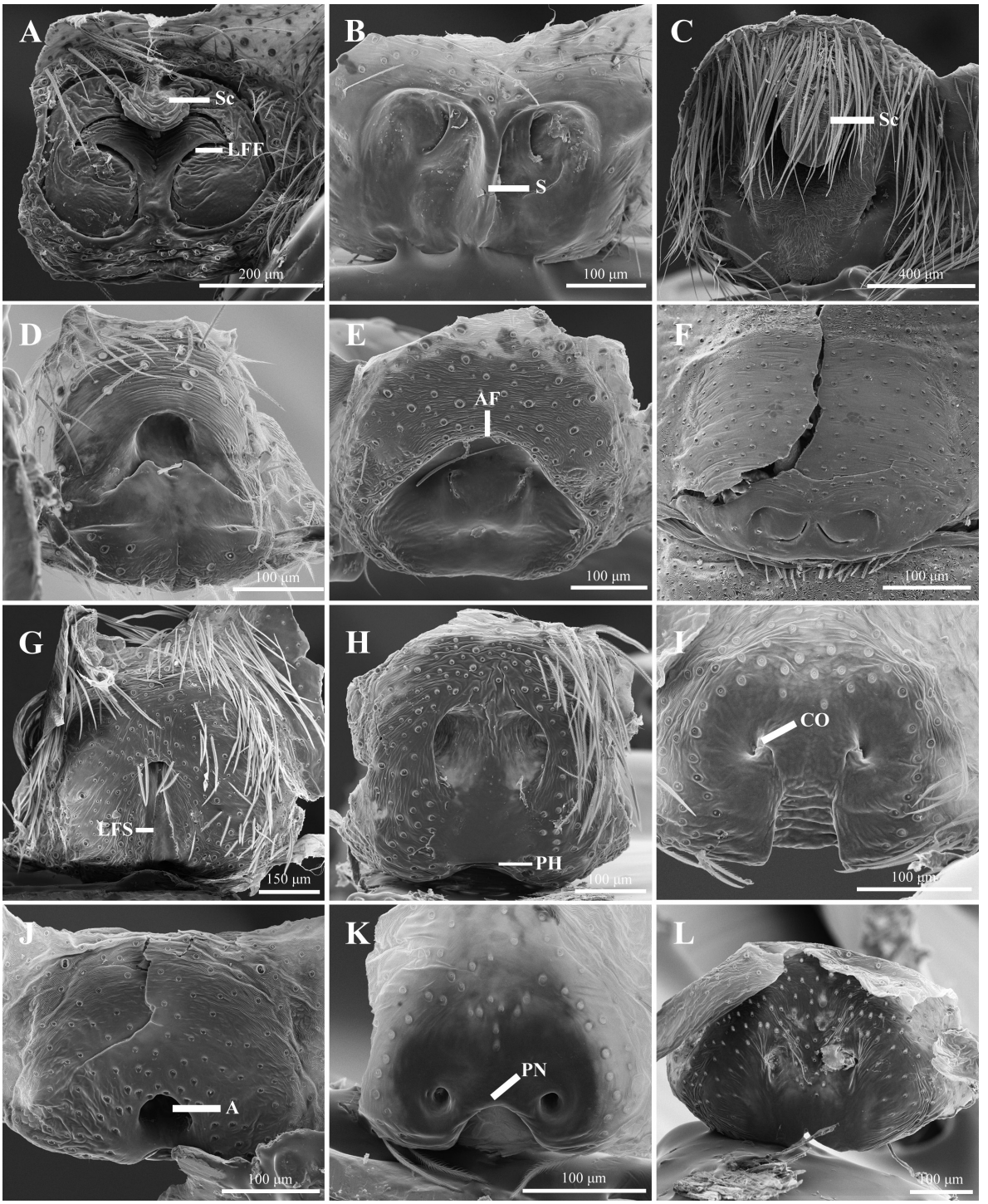

Figure 28. Female epigyne. A, *Asemesthes* sp.; B, *Leptodrassex* sp.; C, *Xerophaeus appendiculatus*; D, *Myandra cambridgei*; E, *Wesmaldra bidgemia*; F, *Lygromma gasnieri*; G, *Theuma* sp.1; H, *Theuma* sp.3; I, *Purcelliana* sp.; J, *Eleleis* sp.; K, *Zimirina hirsuta*; L, *Zimiris doriai*. A, atrium; AF, anterior fold; AFH, anterior fold hood; CO, copulatory opening; LFF, lateral fold furrow; LFS, lateral fold suture; PH, posterior hood; PN, posterior notched; S, septum; Sc, Scape.

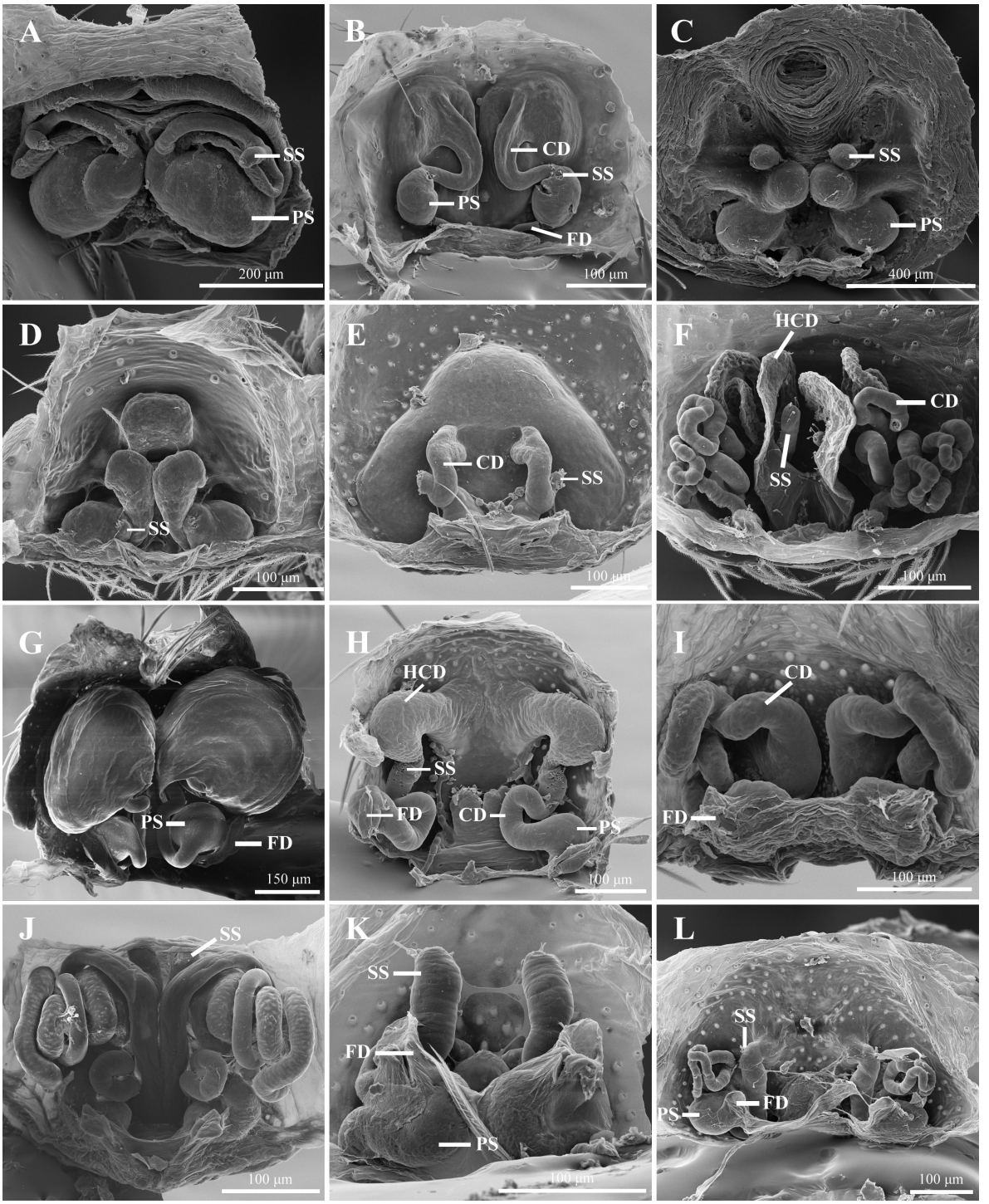

Figure 29. Female vulva. A, *Asemesthes* sp.; B, *Leptodrassex* sp.; C, *Xerophaeus appendiculatus*; D, *Myandra cambridgei*; E, *Wesmaldra bidgemia*; F, *Paracymbiomma carajas*; G, *Theuma* sp.1; H, *Theuma* sp.3; I, *Purcelliana* sp.; J, *Eleleis* sp.; K, *Zimirina hirsuta*; L, *Zimiris doriai*. CD, copulatory duct; FD, fertilization duct; HCD, hyaline duct copulatory; PS, primary spermathecae; SS, secondary spermathecae.

claw slit suture complete, forming onychium: absent ➔ present; ***char. 137—Legs***, tarsus, apical, claws, pointed solid clasper: absent ➔ present; ***char. 165—Spinnerets***, ALS, length relative to abdomen length: less than 22% to abdomen ➔ 1 = more than 22% to abdomen; ***char. 167—Spinnerets***, ALS, distance between them in relation to their diameter diameter: separated by approximately one ALS diameter or more ➔ contiguous to separated by less than one ALS; ***char. 190—Spinnerets***, ALS, distal article, incomplete ring, type: semicircle in the anterior margin ➔ retractile area; ***char. 209—Spinnerets***, ALS, dorsal hood: absent ➔ present; ***char. 276—Epigyne***, median field, plate surface, atrium: absent ➔ present.

PRODIDOMINAE SIMON, 1884

Prodidomidae Simon, 1884: 302. Platnick 1990: 4.
Prodidominae: Platnick & Shadab, 1976: 3. Azevedo *et al.*, 2018: 24.

Type genus: Prodidomus Hentz, 1847.

Genera included: Austrodomus Lawrence, 1947; *Brasilomma* Brescovit, Ferreira & Rheims, 2012; *Caudalia* Alayon, 1980; *Chileomma* Platnick et al., 2005; *Chileuma* Platnick et al., 2005; *Chilongius* Platnick et al., 2005; *Eleleis* Simon, 1893; *Indiani* Rodrigues et al., 2020; *Katumbea* Cooke, 1964; *Lygromma* Simon, 1893; *Lygrommatoides* Strand, 1918; *Moreno* Mello-Leitão, 1940; *Namundra* Platnick & Bird, 2007; *Neozimiris* Simon, 1903; Nopyllus Ott, 2014; *Paracymbiomma* Rodrigues et al., 2018; *Plutonodomus* Cooke, 1964; *Prodidomus*; *Purcelliana* Cooke, 1964; *Theuma* Simon, 1893; *Theumella* Strand, 1906; *Tivodrassus* Chamberlin & Ivie, 1936; *Tricongius* Simon, 1893; *Zimirina* Dalmas, 1919; *Zimiris* Simon, 1882.

Diagnosis: ALS with pyriform gland spigots elongated with base longer than shaft and with long setae around these spigots (Fig. 23); presence of large protrusion between coxae IV with erect setae and unsclerotized margin (Fig. 11I–P).

Shared characters: ***char. 24—Eyes***, AME, size relative to ALE: as large as or larger than ALE ➔ smaller than ALE; ***char. 122—Legs***, tarsus, tarsal organ, opening, shape: round to oval ➔ teardrop or keyhole; ***char. 127—Legs***, tarsus, cuticle, texture: smooth ➔ fingerprint; ***char. 147—Abdomen***, pedicel, ventral, anterior margin, shape: pointed ➔ truncate; ***char. 190—Spinnerets***, ALS, distal article, incomplete ring, type: semicircle in the anterior margin ➔ patches of setae at the base of the gland spigots; ***char. 197—Spinnerets***, ALS, major ampullate gland spigots field, conical setae-bearing projection: absent ➔ present; ***char. 246—Palp***, cymbium, dorsal, terminal, chemosensory patch: absent ➔ present.

TRICONGIUS SIMON, 1893

Tricongius Simon, 1893: 453.
Oltacloea Mello-Leitão, 1940: 254, **syn. nov.**

Type species: Tricongius collinus Simon, 1893.

Species included: Tricongius amazonicus Platnick & Hofer, 1990; *T. beltraoe* (Brescovit & Ramos, 2003) **comb. nov.**; *T. collinus*; *T. mutilata* (Mello-Leitão, 1940) **comb. nov.**; *T. ribaslangei* (Bonaldo & Brescovit, 1997) **comb. nov.**; *T. ybyguara* (Rheims & Brescovit, 2004) **comb. nov.**

Misplaced species: Tricongius granadensis Mello-Leitão, 1941.

Diagnosis: Eyes (when present) widely separated with AME–AME shorter than AME–ALE, sternum with anterior margin less than half maximum width (Fig. 11K) and cymbium with a bunch of thick setae on the ventral-terminal part (Fig. 27E).

Shared characters: ***char. 2—Carapace***, dorsal, posterior margin shape: notched ➔ truncated; ***char. 35—Sternum***, anterior margin, width relative to maximum width: more than half ➔ equal or less than half; ***char. 200—Spinnerets*** (M), ALS, major ampullate gland spigots, mesal spigot: absent ➔ present; ***char. 201—Spinnerets*** (M), ALS, major ampullate gland spigots, mesal spigot, type: nubbin ➔ normal; ***char. 245—Palp***, cymbium, ventral, terminal, bunch of thick setae: absent ➔ present.

PRODIDOMUS HENTZ, 1847

Prodidomus Hentz, 1987: 466.
Hyltonia Birabén, 1954: 13. Platnick & Baehr, 2006: 9 [Syn.].

Prodida Dalmas 1919: 324**, syn. nov.**

Type species: Prodidomus rufus Hentz 1847.

Species included: Prodidomus longivetris (Dalmas, 1919) **comb. nov.**; *P. stella* (Saaristo, 2002) **comb. nov.**. For complete composition see https://wsc.nmbe.ch/specieslist/2459 (World Spider Catalog, 2020).

Diagnosis: Presence of PLS massive, much thicker than the anterior spinnerets (Figs 21L, 25J).

Shared characters: ***char. 54—Chelicerae***, paturon, retromargin, escort setae: present ➔ absent; ***char. 168—Spinnerets***, ALS, sclerotizaton close to base: present ➔ absent; ***char. 182—Spinnerets***, base spigot, Ac, insertion articulation, type: simple ➔ insertion annulate, flexible; ***char. 203—Spinnerets*** (F), ALS, major ampullate gland spigots, mesal spigot: absent ➔ present; ***char. 224—Spinnerets***, massive PLS: absent ➔ present; c***har. 289—Epigyne***, vulva, fertilization duct, position: well advanced from the epigastric furrow ➔ posterior, close to the epigastric furrow.

ACKNOWLEDGEMENTS

We thank the curators of all museum collections that provided material for our studies: G. A. Milledge (AM); L. Prendini (AMNH); R. Lyle (ARC.LNR); A. D. Brescovit (IBSP); E. Florez (ICN); L. F. Armas (IES); A. L. Henriques (INPA); M. Ramírez (MACN); R. Ott (MCN); G. Giribet (MCZ); C. Rollard (MNHN); A. B. Bonaldo (MPEG); L. Lotz (NMBA); B. Muramba (NMNW); Z. M. Simmons (OUMNH); R. Teixeira (PUCRS); R. Raven (QMB); P. Jäger (SMF); R. Jocque (RMCA); D. Larson (SAMC); P. Mota (UNB); M. Harvey (WAM) and Beatriz Mauricio (Laboratório de Biologia Celular, Instituto Butantan, São Paulo) for helping with SEMs. This study was financially supported by 'Fundação de Amparo à Pesquisa do estado de São Paulo' (FAPESP grant no. 2014/23533–7 to B.V.B. Rodrigues and 2015/18982-0 to C.A. Rheims) and by 'Coordenação de Aperfeçoamento de Pessoal de Nível Superior' Nacional do Desenvolvimento Científico e Tecnológico' (CAPES to B. V. B. Rodrigues).

REFERENCES

Alayón GG. 1980. Nuevo género y nueva especie de Prodidominae (Araneae: Gnaphosidae) de Isla de Pinos, Cuba. *Poeyana* **208:** 1–8.

Azevedo GHF, **Griswold CE**, **Santos AJ. 2018.** Systematics and evolution of ground spiders revisited (Araneae, Dionycha, Gnaphosidae). *Cladistics* **34:** 579–626.

Birabén M. 1954. Nuevo genero de la rara familia Prodidomidae. *Neotropica* **1:** 13–16.

Bremer K. 1994. Branch support and tree stability. *Cladistics* **10:** 295–304.

Cooke JAL. 1964. A revisionary study of some spiders of the rare family Prodidomidae. *Proceedings of the Zoological Society of London* **142:** 257–305.

Cooke JAL. 1977. Fam. Prodidomidae. In: La faune terrestre de l'île de Sainte-Hélène IV. Annales, Musée Royal de l'Afrique Centrale. *Sciences Zoologiques (Zool. Ser. 8)* **220:** 49–51.

Dalmas R. 1919. Synopsis des araignées de la famille des Prodidomidae. *Annales de la Société Entomologique de France* **87:** 279–340.

Deeleman-Reinhold CL. 2001. *Forest spiders of South East Asia: with a revision of the sac and ground spiders (Araneae: Clubionidae, Corinnidae, Liocranidae, Gnaphosidae, Prodidomidae and Trochanterriidae)*. Leiden: Brill, 551–564.

Dippenaar-Schoeman AS. 2014. *Field guide to the spiders of South Africa*. Pretoria: LAPA Uitgewers.

Dippenaar-Schoeman AS, **Jocqué R. 1997.** *African spiders: an identification manual*. Pretoria: Agricultural Research Council, 392.

Fernández R, **Kallal RJ**, **Dimitrov D**, **Ballesteros JA**, **Arnedo MA**, **Giribet G**, **Hormiga G. 2018.** Phylogenomics, diversification dynamics, and comparative transcriptomics across the spider tree of life. *Current Biology* **28:** 1489–1497.

Foelix R. 2011. *Biology of spiders*, *3rd edn*. Oxford: Oxford University Press.

Garrison NL, **Rodriguez J**, **Agnarsson I**, **Coddington JA**, **Griswold CE**, **Hamilton CA**, **Hedin M**, **Kocot KM**, **Ledford JM**, **Bond JE. 2016.** Spider phylogenomics: untangling the spider tree of life. *PeerJ* **4:** e1719.

Goloboff PA. 1993. Estimating character weights during tree search. *Cladistics* **9:** 83–91.

Goloboff PA. 1999. Analyzing large data sets in reasonable times: solutions for composite optima. *Cladistics* **15:** 415–428.

Goloboff PA. 2008. Calculating SPR distances between trees. *Cladistics* **24:** 591–597.

Goloboff PA, **Catalano SA. 2016.** TNT version 1.5, including a full implementation of phylogenetic morphometrics. *Cladistics* **32:** 1–18.

Goloboff PA, **Farris JS. 2001.** Methods for quick consensus estimation. *Cladistics* **17:** S26–S34.

Goloboff PA, **Farris S**, **Nixon K. 2008.** TNT, a free program for phylogenetic analysis. *Cladistics* **24:** 774–786.

Hentz NM. 1847. Descriptions and figures of the araneides of the United States. *Boston Journal of Natural History* **5:** 443–478.

Hilbrant M. 2008. *Development and evolution of the spider silk production system*. Dissertation. University of Cologne, Germany.

Labarque FM, **Wolff JO**, **Michalik P**, **Griswold CE**, **Ramírez MJ. 2017.** The evolution and function of spider feet (Araneae: Arachnida): multiple acquisitions of distal articulations. *Zoological Journal of the Linnean Society* **181:** 308–341.

Lawrence RF. 1947. A collection of Arachnida made by Dr. I. Trägårdh in Natal and Zululand (1904–1905). *Göteborgs Kungliga Vetenskaps och Vitterhets Samhälles Handlingar (B)* **5:** 1–41.

Magalhaes ILF, **Santos AJ. 2012.** Phylogenetic analysis of *Micrathena* and *Chaetacis* spiders (Araneae: Araneidae) reveals multiple origins of extreme sexual size dimorphism and long abdominal spines. *Zoological Journal of the Linnean Society* **166:** 14–53.

Mello-Leitão CF. 1940. Tres géneros extraños de arañas argentinas. *Notas del Museo de la Plata* **5:** 251–258.

Murphy J. 2007. *Gnaphosid genera of the world*. St. Neots, Cambridgeshire: British Arachnological Society 1, i–xii, 1–92; 2, i–ii, 93–605.

Nixon KC. 2002. *WinClada v.1.00.08*. Ithaca: published by the author.

Ott R. 2014. *Nopyllus*, um novo gênero de Drassodinae sul-americano (Araneae, Gnaphosidae). *Iheringia Serie Zoologia* **104:** 252–261.

Pechmann M, **Khadjeh S**, **Sprenger F**, **Prpic NM. 2010.** Patterning mechanisms and morphological diversity of spider appendages and their importance for spider evolution. *Arthropod Structure & Development* **39:** 453–467.

Platnick NI. 1990. Spinneret morphology and the phylogeny of ground spiders (Araneae, Gnaphosoidea). *American Museum Novitates* **2978:** 1–42.

Platnick NI. 2000. A relimitation and revision of the Australasian ground spider family Lamponidae (Araneae: Gnaphosoidea). *Bulletin of the American Museum of Natural History* **245:** 1–328.

Platnick NI. 2002. A revision of the Australasian ground spiders of the families Ammoxenidae, Cithaeronidae, Gallieniellidae, and Trochanteriidae (Araneae: Gnaphosoidea). *Bulletin of the American Museum of Natural History* **271:** 1–244.

Platnick NI, **Baehr B. 2006.** A revision of the Australasian ground spiders of the family Prodidomidae (Araneae, Gnaphosoidea). *Bulletin of the American Museum of Natural History* **298:** 1–287.

Platnick NI, **Bird TL. 2007.** On the first African spiders of the subfamily Molycriinae (Araneae, Prodidomidae). *American Museum Novitates* **3552:** 1–8.

Platnick NI, **Penney D. 2004.** A revision of the widespread spider genus *Zimiris* (Araneae, Prodidomidae). *American Museum Novitates* **3450:** 1–12.

Platnick NI, **Shadab MU. 1976.** A revision of the spider genera *Lygromma* and *Neozimiris* (Araneae, Gnaphosidae). *American Museum Novitates* **2598:** 1–23.

Platnick NI, **Shadab MU**, **Sorkin LN. 2005.** On the Chilean spiders of the family Prodidomidae (Araneae, Gnaphosoidea), with a revision of the genus *Moreno* Mello-Leitão. *American Museum Novitates* **3499:** 1–31.

Pollard SD. 1990. The feeding strategy of a crab spider, *Diaea* sp. indet. (Araneae: Thomisidae): post-capture decision rules. *Journal of Zoology* **222:** 601–615.

Purcell WF. 1904. Descriptions of new genera and species of South African spiders. *Transactions of the South African Philosophical Society* **15:** 115–173.

Ramírez MJ. 2014. The morphology and phylogeny of dionychan spiders (Araneae: Araneomorphae). *Bulletin of the american Museum of Natural History* **390:** 1–374.

Rheims CA, **Brescovit AD. 2004.** A new cave spider of the genus *Lygromma* Simon (Araneae, Prodidomidae) from Minas Gerais, Brazil. *Revista Ibérica de Aracnología* **9:** 325–327.

Robinson DF, **Foulds LR. 1981.** Comparison of phylogenetic trees. *Mathematical Biosciences* **53:** 131–147.

Rodrigues BVB, **Cizauskas I**, **Rheims CA. 2018.** *Paracymbiomma* gen. nov., a new genus of prodidomid spiders from the Neotropical region (Araneae: Prodidomidae): description of one troglobitic species and notes on adaptations and specializations to the subterranean environment. *Zootaxa* **4514:** 301–331.

Rodrigues BVB, **Cizauskas I**, **Lemos Y. 2020.** A new genus of cave spider from Neotropical region (Gnaphosidae: Prodidominae). *Zootaxa* **4722:** 77–83.

Sereno PC. 2007. Logical basis for morphological characters in phylogenetics. *Cladistics* **23:** 565–587.

Simon E. 1884. Note synonomique sur les genres *Prodidomus* Hentz et *Miltia* E. S. *Annales de la Société Entomologique de Belgique* **28:** 302.

Simon E. 1893. Voyage de M. E. Simon au Venezuela (Décembre 1887–Avril 1888). 21e Mémoire. Arachnides (1). Familles des Uloboridae, Zoropsidae, Dictynidae, Oecobiidae, Filistatidae, Sicariidae, Leptonetidae, Oonopidae, Dysderidae, Caponiidae, Prodidomidae, Drassidae, Palpimanidae et Zodariidae. *Annales de la Société Entomologique de France* **61:** 423–462, pl. 9.

Simon E. 1897. Histoire naturelle des araignées. *Paris* **2:** 1–192.

Ubick D, Paquin P, Cushing PE, Roth VD. 2005. *Spiders of North America: an identification manual*. Keene, NH: American Arachnological Society, 377.

Wheeler WC, **Coddington JA**, **Crowley LM**, **Dimitrov D**, **Goloboff PA**, **Griswold CE**, **Hormiga G**, **Prendini L**, **Ramírez MJ**, **Sierwald P**, **Almeida-Silva LM**, **Álvarez-Padilla F**, **Arnedo MA**, **Benavides LR**, **Benjamin SP**, **Bond JE**, **Grismado CJ**, **Hasan E**, **Hedin M**, **Izquierdo MA**, **Labarque FM**, **Ledford J**, **Lopardo L**, **Maddison WP**, **Miller JA**, **Piacentini LN**, **Platnick NI**, **Polotow D**, **Silva-Dávila D**, **Scharff N**, **Szűts T**, **Ubick D**, **Vink C**, **Wood HM**, **Zhang JX. 2017.** The spider tree of life: phylogeny of Araneae based on target-gene analyses from an extensive taxon sampling. *Cladistics* **33:** 576–616.

Wolff JO, **Řezáč M**, **Krejčí T**, **Gorb SN. 2017.** Hunting with sticky tape: functional shift in silk glands of araneophagous ground spiders (Gnaphosidae). *Journal of Experimental Biology* **220:** 2250–2259.

World Spider Catalog. **2020.** *World spider catalog, v.20.5*. Bern: Natural History Museum Bern. Available at: http://wsc.nmbe.ch (accessed 15 January 2020).

Wunderlich J. 2011. Spiders of the family Prodidomidae (Araneae) from Europe and Madagascar. *Beiträge zur Araneologie* **6:** 98–107.

SUPPORTING INFORMATION

Additional Supporting Information may be found in the online version of this article at the publisher's web-site.

Figure S1. Strict consensus of phylogenetic hypothesis of Prodidominae under implied weighting (k=9), showing clade synapomorphies optimized according to delayed transformation series (DELTRAN) criteria. Numbers

above and below branches indicate the character and respective state. Black circles indicate non-homoplastic synapomorphies and white circles indicate homoplastic synapomorphies.
Data S1. Morphological data matrix used for phylogenetic analysis of Prodidominae.
Data S2. List of the vouchers used for the morphological phylogenetic analysis of Prodidominae.

APPENDIX

LIST OF CHARACTERS

Characters with '(F)' were scored for females and characters with '(M)' for males.

Carapace

The carapace can have different types of setae. The clavate setae are stout tactile setae that can be distributed throughout the body. In our dataset the presence of these setae was coded separately for carapace and abdomen (char. 7, 8 154 and 155). These setae also show different sizes throughout the body. The holotype of *E. crinita* Simon, does not have visible setae on the carapace; however, the original description clearly mentions the presence these long clavate setae (Simon, 1893). In addition, it is possible to see the stout insertions of these setae on the carapace. Scales (plumose setae and squamose setae) are another type of setae with small sockets, parallel to the cuticular surface (Ramírez, 2014). Plumose setae are scales with cylindrical shafts and lateral appendages, while squamose setae are flattened scales that show a wide morphological diversity. Morphology of scales follows Azevedo *et al.* (2018) and was coded independently for carapace, abdomen, legs and anterior lateral spinnerets. All pictures in Figure 21 are scales from the abdomen, but in order to identify the characters, we indicate these figures for the first character mentioned, in this case the carapace.

0. **Carapace, dorsal, fovea: (**Ramírez, 2014**, char. 0):** 0 = absent (Fig. 8H, N–P); 1 = present (Fig. 8A–G, I–M).
1. **Carapace, dorsal, anterior margin shape (**Azevedo *et al.* 2018**, char. 322):** 0 = with a moderate cephalic constriction and a convex anterior margin (Fig. 8I–M); 1 = without a cephalic constriction and a straight to concave anterior margin (Fig. 8N–O). Azevedo *et al.* (2018) defined this character using morphometric data and coded *Neozimiris pubenscens* as having no constriction. In our dataset, some species share this condition with *N. pubenscens*, and were coded similarly.
2. **Carapace, dorsal, posterior margin shape:** 0 = truncated (Fig. 8B, E); 1 = notched (Fig. 8F, K, L).
3. **Carapace, flatness (**Ramírez, 2014**, char. 3):** 0 = domed or slightly flattened (Fig. 9A); 1 = extremely flat, straight dorsal profile (Fig. 9B).
4. **Carapace, anterior, clypeus, margin profile in frontal view (**Ramírez, 2014**, char. 29):** 0 = straight or slightly curved (Fig. 9G–I); 1 = produced in a median lobe anteriorly (Fig. 9D); 2 = strongly curved, forming an arch (Fig. 9F).
5. **Carapace, anterior, chilum (**Ramírez, 2014**, char. 30)**: 0 = absent; 1 = present (Fig. 9E, H).
6. **Carapace, anterior, chilum, configuration (**Ramírez, 2014**, char. 31):** 0 = single median sclerite (Fig. 9E); 1 = paired isolated sclerites (Fig. 9H).
7. **Carapace, surface, clavate setae:** 0 = absent; 1 = present (Fig. 8O, P). The holotype of *E. crinita* Simon, 1893 does not have visible setae on the carapace; however, the original description clearly mentions the presence of these long clavate setae (Simon, 1893). In addition, it is possible to see the stout insertions of these setae on the carapace.
8. **Carapace, surface, clavate setae, size:** 0 = all similar sized (Fig. 8P); 1 = variable sizes (Fig. 8O).
9. **Carapace, surface, plumose setae (scales) (**Azevedo *et al.*, 2018**, char. 26)**: 0 = absent; 1 = present (Fig. 20A, B).
10. **Carapace, surface, plumose setae, appendages (brachia) arrangement (**Azevedo *et al.*, 2018**, char. 27)**: 0 = only on proximal part (Fig. 20A); 1 = reaching terminal half (Fig. 20B).
11. **Carapace, surface, squamose setae (**Azevedo *et al.*, 2018**, char. 29)**: 0 = absent; 1 = present (Fig. 20C–L).
12. **Carapace, surface, squamose setae, lateroventral appendages (**Azevedo *et al.*, 2018**, char. 30)**: 0 = absent; 1 = present (Fig. 20C, E, F).
13. **Carapace, surface, squamose setae, dorsolateral spines (**Azevedo *et al.*, 2018**, char. 31)**: 0 = absent; 1 = present (Fig. 20D, H).
14. **Carapace, surface, squamose setae, dorsolateral spines, type (**Azevedo *et al.*, 2018**, char. 32)**: 0 = on both sides (Fig. 20D); 1 = on one side (Fig. 20H).

15. **Carapace, surface, squamose setae, number of axes (shafts) (**Azevedo *et al.*, 2018**, char. 33)**: 0 = zero (Fig. 20H); 1 = one (Fig. 20C); 2 = two (Fig. 20J).

Eyes

The occurrence of eyes was not scored in our dataset, since their presence or absence can be the result of different selective pressures, such as adaptations for life in subterranean environments (Rodrigues *et al.*, 2018). Four cavernicolous species, *Brasilomma enigmatica*, *Lygromma ybyguara*, *Plutonodomus kungwensis* and *Indiani gaspar*, do not have eyes and were coded non-applicable (-) for all eye characters (char. 16–28). *Chileomma ruiles* Platnick *et al.*, 2005 and *Lygromma gasnieri* Brescovit & Höfer, 1993 do not have AME and were coded non-applicable (-) for characters 17, 24 and 25.

16. **Eyes, posterior eye row, shape: (**Azevedo *et al.*, 2018**, char. 324):** 0 = procurved (Figs 8N–P, 10C); 1 = straight to recurved (Fig 8A, B, K, M). Azevedo *et al.* (2018) used morphometric data to define the limits of the posterior eye row curvature, and determined two states, 'procurved' and 'straight to recurved'. Since the extreme condition, defined by the authors as 'procurved', was observed in some Prodidominae, we choose to use this character, even without a morphometric analysis. We scored according to Azevedo *et al.* (2018) for the same terminal taxa. The authors used the same method to define the limits of the anterior eye row curvature in frontal view; however, the results were not significant. For this reason, we did not score the anterior eye row curvature for our dataset.
17. **Eyes, anterior eyes row, interdistances:** 0 = AME–AME longer or equal to AME–ALE (Fig. 9E, F); 1 = AME–AME shorter than AME–ALE (Fig. 9D).
18. **Eyes, PME, lens curvature (**Ramírez, 2014**, char. 19)**: 0 = convex (Fig. 10E); 1 = flattened (Fig. 10F).
19. **Eyes, PME, lens limits (**Ramírez, 2014**, char. 20):** 0 = lens raised from surrounding cuticle (Fig. 10C, D); 1 = lens not raised, totally flat (Ramírez, 2014, fig. 10C, E).
20. **Eyes, PME–PME distance (**Azevedo *et al.*, 2018**, char. 47):** 0 = separated (Fig. 8L–N); 1 = close, almost touching (Fig. 8J, K).
21. **Eyes, PME–PLE distance:** 0 = separated (Fig. 8A–D); 1 = close, almost touching (Figs 8L, N–P, 10C, D).
22. **Eyes, ALE–ALE distance:** 0 = separated (Figs 9H, I, 10A, B); 1 = close, almost touching (Figs 9G, 10D).
23. **Eyes, ALE–PLE distance:** 0 = separated (Figs 9D, E, 10A, E); 1 = close, almost touching (Figs 8N–P, 9F, G, 10C, D, F).
24. **Eyes, AME, size relative to ALE (**Azevedo *et al.*, 2018**, char. 48, mod.):** 0 = as large as or larger than ALE (Figs 9I, 10A); 1 = smaller than ALE (Figs 9H, 10B).
25. **Eyes, AME, black surrounds (**Azevedo *et al.*, 2018**, char. 39):** 0 = absent (Fig. 9E); 1 = present (Fig. 9F). As described by Azevedo *et al.* (2018), the black surrounds are only considered present when they are connected.
26. **Eyes, ALE, tapetum symmetry axis (**Ramírez, 2014**, char. 23)**: 0 = vertical or oblique down to external; 1 = horizontal.
27. **Eyes, PME, tapeta, symmetry axes (**Ramírez, 2014**, char. 26):** 0 = parallel to each other; 1 = orthogonal to each other (Fig. 9C).
28. **Eyes, PLE and PME, tapeta axes orthogonal (**Ramírez, 2014**, char. 28)**: 0 = absent; 1 = present.

Mouthparts

29. **Endites, distal margin, width relative to basal margin:** 0 = wider or similar to basal margin (Fig. 10G, I); 1 = smaller than basal margin (Fig. 10H).
30. **Endites, ventral surface, oblique depression (**Platnick, 2000**, char. 10):** 0 = absent; 1 = present (Fig. 10G–I). This is a traditional character of the former superfamily Gnaphosoidea. The depressions are sometimes difficult to observe under the stereomicroscope but with SEM it is possible to have a better definition.
31. **Endites, prolateral edge, longitudinal groove (**Platnick, 2000**, char. 207)**: 0 = absent; 1 = present (Fig. 10G).
32. **Endites, dorsal, branched setae (Ramirez, 2000, char. 73)**: 0 = absent; 1 = present (Fig. 10L).
33. **Endites, serrula (**Ramírez, 2014**, char. 74)**: 0 = absent (Fig. 10K); 1 = present (Fig. 10J).

Sternum

Sternum characters were not scored considering their shape or proportion, as in other studies (Ramírez, 2014; Azevedo *et al.*, 2018). Instead, we scored the morphology of each margin independently, since their differences are easily observed.

34. **Sternum, anterior margin, shape:** 0 = truncate (Fig. 11C–E); 1 = rounded (Fig. 11M–O).
35. **Sternum, anterior margin, width relative to maximum width:** 0 = more than half (Fig. 11J); 1 = equal or less than half (Fig. 11K).
36. **Sternum, posterior margin, shape:** 0 = truncated (Fig. 11A); 1 = pointed (Fig. 11B–P).
37. **Sternum, posterior margin, large protrusion between coxae IV:** 0 = absent (Fig. 11B–F); 1 = present (Fig. 11G–P). This character was traditionally used to characterize the former subfamily Theuminae. Here, this protrusion is present in all members of the ingroup, except *Nomindra kinchega*.
38. **Sternum, posterior margin, large protrusion between coxae IV, erect setae:** 0 = absent; 1 = present (Fig. 11N). *Leptodrassex* sp. and *Neodrassex aureus*, that have the protrusion but without the erect setae.
39. **Sternum, posterior margin, protrusion, sclerotization marginal:** 0 = unsclerotized (Fig. 11I–N); 1 = sclerotized (Fig. 11G, H). Molycriinae have the protrusion margins sclerotized, while most Prodidominae have the margins unsclerotized. *Namundra* sp. and *Zimiris doriai* have the protrusion margins slightly sclerotized, scored 1.
40. **Sternum, posterior margin, protrusion, size:** 0 = wide (Fig. 11I–K); 1 = narrow (Fig. 11L). Usually the protrusion of the sternum is large and robust. However, the African genera *Theuma* and *Theumella* have this protrusion narrow and elongate.
41. **Sternum, intercoxal extensions (Ramírez, 2014, char. 96, mod.)**: 0 = absent; 1 = present (Fig. 11C, L).
42. **Sternum, precoxal triangles (Ramírez, 2014, char. 95, mod.)**: 0 = absent; 1 = present (Fig. 11G, H, O).
43. **Sternum, precoxal triangles fused to sternum (Platnick, 2000, char. 8)**: 0 = absent; 1 = present.

Chelicerae

The treatment of the morphology of cheliceral setae (char. 50–55) follows Ramírez (2014). The projections of the cheliceral margins were coded according to Azevedo *et al.* (2018), where all projections are considered homologous. The authors established homology for each tooth, since Ramírez (2014) showed that to code only teeth numbers can be incongruent in the analysis. We did not evaluate the homology of the teeth due to the difficulty in determining their limits, and we did not code teeth numbers because of the instability caused in the analysis. In our dataset, only the occurrence and the morphology of teeth were considered. We considered a tooth reduced when the margins of the chelicerae have a small protuberance instead of a well-defined tooth (char. 58, 61).

44. **Chelicerae, paturon, boss: (Ramírez, 2014, char. 38)**: 0 = absent; 1 = present (Fig. 9A).
45. **Chelicerae, paturon, promarginal depression**: 0 = absent; 1 = present (Fig. 12A).
46. **Chelicerae, fang, shaft serrula (Ramírez, 2014, char. 59)**: 0 = absent; 1 = present (Fig. 12D).
47. **Chelicerae, fang, venon gland opening size:** 0 = small, tiny opening (Fig. 12B); 1 = large, wide opening forming a canal (Fig. 12C).
48. **Chelicerae, fang, length (Platnick, 2002, char. 22):** 0 = normal (Fig. 12A); 1 = elongated, with tip almost reaching paturon base (Fig. 12E).
49. **Chelicerae, paturon, anterior surface, tuft of macrosetae (Azevedo *et al.*, 2018, char. 63)**: 0 = absent; 1 = present.
50. **Chelicerae, paturon, promargin, whisker setae (Ramírez, 2014, char. 51)**: 0 = absent; 1 = present (Fig. 12F).
51. **Chelicerae, paturon, promargin, escort setae (Ramírez, 2014, char. 52)**: 0 = absent; 1 = present (Fig. 12F).
52. **Chelicerae, paturon, promargin, rake setae (Azevedo *et al.*, 2018, char. 69)**: 0 = absent; 1 = present (Fig. 12F).
53. **Chelicerae, paturon, retromargin, whisker setae (Azevedo *et al.*, 2018, char. 84)**: 0 = absent; 1 = present (Fig. 12E).
54. **Chelicerae, paturon, retromargin, escort setae (Azevedo *et al.*, 2018, char. 83)**: 0 = absent; 1 = present (Fig. 12E).
55. **Chelicerae, paturon, promargin, rake setae (Azevedo *et al.*, 2018, char. 82)**: 0 = absent; 1 = present.
56. **Chelicerae, paturon, retromargin, projections (Azevedo *et al.*, 2018, char. 80)**: 0 = absent; 1 = present (Fig. 12A, I).
57. **Chelicerae, paturon, retromargin, projections type (Azevedo *et al.*, 2018, char. 81)**: 0 = teeth (Fig. 12B, H); 1 = serrated keel (Fig. 12I).
58. **Chelicerae, paturon, retromargin, teeth:** 0 = normal, well-defined teeth (Fig. 12B); 1 = reduced to small protuberance (Fig. 12H).
59. **Chelicerae, paturon, promargin, projections**: 0 = absent; 1 = present.
60. **Chelicerae, paturon, promargin, projections type**: 0 = teeth; 1 = keel.

61. **Chelicerae, paturon, promargin, teeth**: 0 = normal; 1 = reduced
62. **Chelicerae, paturon, shape (**Platnick, 2002**, char. 8):** 0 = conical, longer than wide (Fig. 9E); 1 = rounded, as long as wide (Fig. 9D).

Legs

63. **Legs, orientation (**Platnick, 2002**, char. 14)**: 0 = prograde; 1 = laterigrade.
64. **Leg IV, trochanter, length relative to trochanter III (**Platnick, 2002**, char. 23)**: 0 = similar to trochanter III; 1 = longer than trochanter III (Fig. 13J).
65. **Legs I–II, patellae, indentation (**Ramírez, 2014**, char. 107)**: 0 = absent; 1 = present (Fig. 14I).
66. **Leg I–II, femur, dorsal, macrosetae (**Ramírez, 2014**, char. 146, mod.)**: 0 = absent; 1 = present.
67. **Legs I–II, tarsus, ventral, macrosetae (**Ramírez, 2014**, char. 152, mod.)**: 0 = absent; 1 = present (Fig. 14J).
68. **Leg I, ventral, macrosetae with apical tenent surface (**Ramírez, 2014**, char. 155)**: 0 = absent; 1 = present (Fig. 14L).
69. **Legs, metatarsus, dorsal, stopper with setae**: 0 = absent; 1 = present (Fig. 14G).
70. **Leg I, patella, length relative to tibia:** 0 = short, less than tibia length (Fig. 13B); 1 = long, similar to tibia length (Fig. 13A).
71. **Legs I–II, trochanters, distal rim (**Azevedo *et al.*, 2018**, char. 174):** 0 = straight (Fig. 13E); 1 = shallow indentation (Fig. 13F); 2 = notched (Fig. 13G).
72. **Legs III–IV, trochanters, distal rim (**Azevedo *et al.*, 2018**, char. 193)**: 0 = straight; 1 = shallow indentation; 2 = notched.
73. **Legs I–II, tibia and metatarsus, ventral, parallel row of macrosetae (**Azevedo *et al.*, 2018**, char. 182)**: 0 absent; 1 = present (Fig. 14K).
74. **Leg III, tarsus, ventral, paired row of macrosetae (**Azevedo *et al.*, 2018**, char. 189)**: 0 = absent; 1 = present.
75. **Leg IV, tarsi, ventral, paired row of macrosetae (**Azevedo *et al.*, 2018**, char. 198)**: 0 = absent; 1 = present.
76. **Legs III–IV, metatarsi, distal, preening bush (**Azevedo *et al.*, 2018**, char. 183)**: 0 = absent; 1 = present (Fig. 13C).
77. **Legs III–IV, metatarsi, distal, preening comb (**Azevedo *et al.*, 2018**, char. 184)**: 0 = absent; 1 = present (Fig. 13D).
78. **Legs, surface, plumose setae (**Azevedo *et al.*, 2018**, char. 120)**: 0 = absent; 1 = present.
79. **Legs, surface, plumose setae, appendages (brachiae) arrangement (**Azevedo *et al.*, 2018**, char. 121)**: 0 = only on proximal part; 1 = reaching terminal half.
80. **Legs, surface, squamose setae (**Azevedo *et al.*, 2018**, char. 123)**: 0 = absent; 1 = present.
81. **Legs, surface, squamose setae, lateroventral appendages (**Azevedo *et al.*, 2018**, char. 124)**: 0 = absent; 1 = present.
82. **Legs, surface, squamose setae, dorsolateral spines (**Azevedo *et al.*, 2018**, char. 125)**: 0 = absent; 1 = present.
83. **Legs, surface, squamose setae, dorsolateral spines, arrangement (**Azevedo *et al.*, 2018**, char. 127)**: 0 = on both sides; 1 = only on one side.
84. **Legs, surface, squamose setae, number of axes (shafts) (**Azevedo *et al.*, 2018**, char. 128)**: 0 = zero; 1 = one; 2 = two.
85. **Legs I–II, tarsus, ventral, scopulae of tenent setae (**Azevedo *et al.*, 2018**, char. 171)**: 0 = absent; 1 = present (Fig. 14A–E).
86. **Legs I–II, tarsus, ventral, scopulae of tenent setae, density (**Azevedo *et al.*, 2018**, char. 172)**: 0 = sparse (Fig. 14C); 1 = dense (Fig. 14B).
87. **Legs I–II, tarsus, ventral, scopulae of tenent setae, type (**Azevedo *et al.*, 2018**, char. 173)**: 0 = continuous (Azevedo *et al.*, 2018, fig. 22F); 1 = divided (Azevedo *et al.*, 2018, fig. 22A).
88. **Legs I–II, metatarsus, ventral, scopulae of tenent setae (**Azevedo *et al.*, 2018**, char. 162)**: 0 = absent; 1 = present (Fig. 14A).
89. **Legs I–II, metatarsus, ventral, scopulae of tenent setae, density (**Azevedo *et al.*, 2018**, char. 163)**: 0 = sparse; 1 = dense.
90. **Legs I–II, metatarsus, ventral, scopulae of tenent setae, longitudinal extension (**Azevedo *et al.*, 2018**, char. 164)**: 0 = restricted to distal part; 1 = reaching proximal third (Fig. 14A).
91. **Legs I–II, metatarsus, ventral, scopulae of tenent setae, type (**Azevedo *et al.*, 2018**, char. 165)**: 0 = continuous; 1 = divided.
92. **Legs I–II, tibia, ventral, scopulae of tenent setae:** 0 = absent; 1 = present (Fig. 14A). Azevedo *et al.* (2018) coded scopula of tenent setae only on tarsi and metatarsi I–II. Here we observe some species that also show scopula on tibiae I–II.
93. **Legs I–II, tibia, ventral, scopulae of tenent setae, density:** 0 = sparse; 1 = dense.

94. **Legs I–II, tibia, ventral, scopulae of tenent setae, longitudinal extension:** 0 = restricted to distal part (Fig. 14A); 1 = reaching proximal third.
95. **Legs I–II, tibia, ventral, scopulae of tenent setae, type:** 0 = continuous; 1 = divided; 2 = only on prolateral side.
96. **Leg III, tarsus, ventral, scopulae of tenent setae (Azevedo *et al.*, 2018, char. 190):** 0 = absent; 1 = present.
97. **Leg III, tarsus, ventral, scopulae of tenent setae, density (Azevedo *et al.*, 2018, char. 191):** 0 = sparse; 1 = dense.
98. **Leg III, tarsus, ventral, scopulae of tenent setae, type (Azevedo *et al.*, 2018, char. 192):** 0 = continuous; 1 = divided.
99. **Leg III, metatarsus, ventral, scopulae of tenent setae (Azevedo *et al.*, 2018, char. 185):** 0 = absent; 1 = present.
100. **Leg III, metatarsus, ventral, scopulae of tenent setae, density (Azevedo *et al.*, 2018, char. 186):** 0 = sparse; 1 = dense.
101. **Leg III, metatarsus, ventral, scopulae of tenent setae, longitudinal extension (Azevedo *et al.*, 2018, char. 187):** 0 = restricted to distal part; 1 = reaching proximal third.
102. **Leg III, metatarsus, ventral, scopulae of tenent setae, type (Azevedo *et al.*, 2018, char. 188):** 0 = continuous; 1 = divided; 2 = only on prolateral side.
103. **Leg IV, tarsus, ventral, scopulae of tenent setae (Azevedo *et al.*, 2018, char. 200):** 0 = absent; 1 = present.
104. **Leg IV, tarsus, ventral, scopulae of tenent setae, density (Azevedo *et al.*, 2018, char. 201):** 0 = sparse; 1 = dense.
105. **Leg IV, tarsus, ventral, scopulae of tenent setae, type (Azevedo *et al.*, 2018, char. 202):** 0 = continuous; 1 = divided.
106. **Leg IV, metatarsus, ventral, scopulae of tenent setae (Azevedo *et al.*, 2018, char. 194):** 0 = absent; 1 = present.
107. **Leg IV, metatarsus, ventral, scopulae of tenent setae, setae, longitudinal extension (Azevedo *et al.*, 2018, char. 196):** 0 = restricted to distal part; 1 = reaching proximal third.
108. **Leg IV, metatarsus, ventral, scopulae of tenent setae, type (Azevedo *et al.*, 2018, char. 197):** 0 = continuous; 1 = divided; 2 = only on prolateral side.
109. **Legs I–II, scopula of tenent setae, socket indented (Ramírez, 2014, char. 162):** 0 = absent (Fig. 14E); 1 = present (Fig. 14D).
110. **Legs I–II, tarsus, pseudosegmentation (Azevedo *et al.*, 2018, char. 175):** 0 = absent; 1 = present (Fig. 14F).
111. **Leg III, tarsus, pseudosegmentation (Azevedo *et al.*, 2018, char. 176):** 0 = absent; 1 = present.
112. **Leg IV (F), tarsus, pseudosegmentation (Azevedo *et al.*, 2018, char. 177):** 0 = absent; 1 = present.
113. **Leg IV (M), tarsus, pseudosegmentation (Azevedo *et al.*, 2018, char. 178):** 0 = absent; 1 = present.
114. **Legs, tarsus, pseudosegmentation, dorsal extension (Azevedo *et al.*, 2018, char. 179):** 0 = absent; 1 = present.
115. **Legs, tarsus, pseudosegmentation, longitudinal extension (Azevedo *et al.*, 2018, char. 180):** 0 = only on terminal half (Fig. 14F); 1 = reaching proximal.
116. **Legs, tarsus, pseudosegmentation, type (Azevedo *et al.*, 2018, char. 181):** 0 = rings; 1 = cracked (Fig. 14F).
117. **Legs, tarsus, trichobothria, proximal and distal plate limit (Ramírez, 2014, char. 176):** 0 = well differentiated (Fig. 15A–L); 1 = not well differentiated (Ramírez, 2014, fig. 94D).
118. **Legs, tarsus, trichobothria, proximal plate (Ramírez, 2014, char. 178):** 0 = smooth (Fig. 15A); 1 = with transverse ridges (Fig. 15B–L).
119. **Legs, tarsus, trichobothria, distal plate (Ramírez, 2014, char. 182):** 0 = smooth, distal plate is continuous with the surrounding cuticle, or slightly elevated (Fig. 15C); 1 = distal plate embedded below transverse ridge (Fig. 15A, B); 2 = distal ridge continuous in a closed alveolus (Fig. 15E).
120. **Legs, tarsus, trichobothria, proximal and distal plates medial differentiation (Ramírez, 2014, char. 177):** 0 = hood entire, differentiated (Fig. 15F); 1 = hood not differentiated medially (Fig. 15B).
121. **Legs, tarsus, trichobothria, setae base thickness (Ramírez, 2014, char. 183):** 0 = thin (Fig. 15A–C); 1 = thickened as a basal bulb (Fig. 15G, H, K, L).
122. **Legs, tarsus, tarsal organ, opening, shape (Ramírez, 2014, char. 127):** 0 = round to oval (Fig. 16B, I, K); 1 = teardrop or keyhole (Fig. 16D, F, H, J).
123. **Legs, tarsus, tarsal organ, capsule elevation (Azevedo *et al.*, 2018, char. 150):** 0 = absent, the capsule is contiguous with surrounding cuticle, not clearly differentiated

(Fig. 16A, B); 1 = present, the capsule is elevated (Fig. 16C, D).

124. **Legs, tarsus, tarsal organ, capsule, marginal sulci** (Azevedo *et al.*, 2018, **char. 151):** 0 = absent; 1 = present (Fig. 16D).
125. **Legs, tarsus, tarsal organ, capsule, texture** (Azevedo *et al.*, 2018, **char. 152):** 0 = same as surrounding cuticle (Fig. 16A–C); 1 = different (Fig. 16F).
126. **Legs, tarsus, tarsal organ, opening, rim, type** (Azevedo *et al.*, 2018, **char. 153):** 0 = depressed; 1 = elevated (Fig. 16C).
127. **Legs, tarsus, cuticle, texture** (Ramírez, 2014, **char. 100, mod.):** 0 = smooth (Fig. 15A, B); 1 = fingerprint (Fig. 15D, E); 2 = rough (Fig. 15I). This character was proposed by Ramírez (2014) and modified by Azevedo *et al.* (2008) who defined two states, 'smooth to rugose' and 'fingerprint'. Here we further modified it to include three separate states.
128. **Legs, tarsus, apical, claw tuft** (Ramírez, 2014, **char. 163):** 0 = absent (Fig. 17A); 1 = present (Figs 17B–I, 18A–I).
129. **Legs, tarsi, apical, claw tuft, density:** 0 = sparse (Fig. 18A–D); 1 = dense (Fig. 18G–I).
130. **Legs, tarsus, apical, claw tuft, insertion** (Azevedo *et al.*, 2018, **char. 140):** 0 = continuous with lateral cuticle (Fig. 18A–D); 1 = well-delimited plate (Fig. 18E–I).
131. **Legs, tarsus, distal, ventral, claw slit suture (CSS)** (Azevedo *et al.*, 2018, **char. 147):** 0 = absent; 1 = present (Figs 17I, 18C).
132. **Legs, tarsus, distal, claw slit suture complete, forming onychium (podotarsite)** (Azevedo *et al.*, 2018, **char. 148):** 0 = absent (Fig. 18C); 1 = present (Fig. 17F–I). This terminology was proposed by Labarque *et al.* (2017) to define the structure delimited by an arthrodial membrane in place of the slit suture that extends forming an additional joint. Coded only for terminals with claw slit suture.
133. **Legs, tarsus, apical, claws, dorsal scales (velvety texture)** (Azevedo *et al.*, 2018, **char. 137):** 0 = absent (Fig. 17C); 1 = present (Fig. 18F, G).
134. **Legs, tarsus, apical, claws, classic clasper** (Azevedo *et al.*, 2018, **char. 131):** 0 = absent; 1 = present, claw tuft clasping mechanism of teeth appressed together (Fig. 18A–D). The characters involving the claw tuft clasping mechanism were defined considering the hypothesis of multiple homologies of Azevedo *et al.* (2018).
135. **Legs, tarsus I–II, apical, claws, classic clasper, teeth number:** 0 = two (Fig. 18C); 1 = three (Fig. 18D); 2 = four.
136. **Legs, tarsus, apical, claws, folded clasper** (Azevedo *et al.*, 2018, **char. 132):** 0 = absent; 1 = present, claw tuft clasping mechanism formed by a developed basal fold (Azevedo *et al.*, 2018, fig. 4A).
137. **Legs, tarsus, apical, claws, pointed solid clasper** (Azevedo *et al.*, 2018, **char. 133):** 0 = absent; 1 = present, claw tuft clasping mechanism formed by solid projection of basal fold (Fig. 18F, G).
138. **Legs, tarsus, apical, claws, flexible single clasper:** 0 = absent; 1 = present, claw tuft clasping mechanism formed by single projection of basal fold (Fig. 18H, I). This new claw tuft clasping mechanism was observed in *Namundra* sp. and *Zimiris doriai*. In *Namundra* sp. this clasper arises laterally from the base of the claw, while in *Z. doriai* the clasper arises ventrally from the base of the claw.
139. **Legs, tarsus, apical, claws, teeth** (Azevedo *et al.*, 2018, **char. 134):** 0 = absent (Fig. 18E–I); 1 = present (Fig. 18A–D).
140. **Legs I–II, tarsus, apical, claws, teeth, size** (Azevedo *et al.*, 2018, **char. 135):** 0 = reduced, teeth shorter than superior tooth (fig. 5E, F); 1 = normal, teeth longer than half superior tooth length (Fig. 17A–C).
141. **Legs, tarsus, apical, claws, teeth tip:** 0 = pointed (Fig. 17B); 1 = truncate (Fig. 17H, I).
142. **Legs, tarsus, apical, claw tuft, seta, tenent surface, orientation** (Ramírez, 2014, **char. 172):** 0 = facing ventrally (Fig. 17C); 1 = facing mesally (Fig. 17B).
143. **Legs, tarsus, apical, claw tuft, seta, basal section, shape** (Ramírez, 2014, **char. 164):** 0 = basal section nearly cylindrical or flattened without folds (Fig. 17C, D); 1 = basal section with folds or ribs (Fig. 18C).
144. **Legs, tarsus, apical, claw tuft, seta, base, packing** (Ramírez, 2014, **char. 166):** 0 = bases inserted in individual sockets (Fig. 18E–I); 1 = bases packed together (Fig. 18A–D).
145. **Legs, tarsus, apical, modified ventral setae:** 0 = absent; 1 = present (Fig. 14H). These modified setae are larger tactile setae located on ventro-apical tarsus. Platnick & Penney (2004) already had observed these setae in *Zimiris*.

Abdomen

146. **Abdomen, ventral, internally invaginated postepigastric sclerites** (Platnick, 2000, **char. 11):** 0 = absent; 1 = present (Figs 13K, 19E).

147. **Abdomen, pedicel, ventral, anterior margin, shape (Ramírez, 2014, char. 199):** 0 = pointed (Fig. 13H); 1 = truncate (Fig. 13I).
148. **Abdomen, anterodorsal tuft of setae (Ramírez, 2014, char. 213, mod.):** 0 = absent; 1 = present (Fig. 13L).
149. **Abdomen (M), dorsal, scutum (Ramírez, 2014, char. 205):** 0 = absent; 1 = present (Fig. 13L).
150. **Abdomen (M), dorsal, scutum, size (Ramírez, 2014, char. 206):** 0 = small, limited to anterior half of abdomen; 1 = large, extending beyond anterior half of abdomen.
151. **Abdomen (M), ventral, epiandrum, epiandrous spigots (Ramírez, 2014, char. 214):** 0 = absent; 1 = present (Fig. 19A).
152. **Abdomen (M), ventral, epiandrum, epiandrous spigots, arrangement (Ramírez, 2014, char. 215, mod.):** 0 = dispersed (Ramírez, 2014, fig. 103A); 1 = two groups in separated cavities (Fig. 19A); 2 = two groups in single cavity.
153. **Abdomen, openings of posterior respiratory system, position (Ramírez, 2014, char. 221):** 0 = close to spinnerets (Fig. 19B); 1 = slightly separated from spinnerets (Fig. 21A); 2 = well advanced, closer to epigastrium (Fig. 19C). The openings of the posterior respiratory system are usually located close to the spinnerets, except in many Anyphaenidae genera, in which they are well advanced. Here we observe the well-advanced condition of the opening in *Namundra* sp. and *Zimiris doriai*. Apparently, the advance of the opening is associated with the advance of the ALS in these genera.
154. **Abdomen, surface, clavate setae: 0** = absent; 1 = present (Figs 13M, 19F).
155. **Abdomen, surface, clavate setae, arrangement:** 0 = dorsal and ventral; 1 = only ventral.
156. **Abdomen, surface, plumose setae (Azevedo *et al.*, 2018, char. 9):** 0 = absent; 1 = present.
157. **Abdomen, surface, plumose setae, appendages (brachia) arrangement (Azevedo *et al.*, 2018, char. 10):** 0 = only on proximal part; 1 = reaching terminal half.
158. **Abdomen, surface, squamose setae (Azevedo *et al.*, 2018, char. 12):** 0 = absent; 1 = present.
159. **Abdomen, surface, squamose setae, lateroventral appendages (Azevedo *et al.*, 2018, char. 13):** 0 = absent; 1 = present.
160. **Abdomen, surface, squamose setae, dorsolateral spines (Azevedo *et al.*, 2018, char. 14):** 0 = absent; 1 = present.
161. **Abdomen, surface, squamose setae, dorsolateral spines, arrangement (Azevedo *et al.*, 2018, char. 16):** 0 = on both sides; 1 = only on one side.
162. **Abdomen, surface, squamose setae, number of axes (shafts) (Azevedo *et al.*, 2018, char. 17):** 0 = zero; 1 = one; 2 = two.
163. **Abdomen, ventral, posterior, colulus (Ramírez, 2014, char. 237):** 0 = absent; 1 = present.

Spinnerets

164. **Spinnerets, ALS, length relative to width:** 0 = longer than wide (Fig. 21E); 1 = approximately equal or wider than long (Fig. 21I).
165. **Spinnerets, ALS, length relative to abdomen length (Platnick & Baehr, 2006, char. 5):** 0 = less than 22% to abdomen (Fig. 21A); 1 = more than 22% to abdomen (Fig. 21B–D). This character was originally proposed by Platnick & Baehr (2006) to characterize the greatly elongated anterior lateral spinnerets of the former Molycriinae.
166. **Spinnerets, ALS, anteroposterior position (Platnick & Baehr, 2006, char. 6, mod.):** 0 = close to PMS and PLS (Fig. 21F); 1 = slightly advanced from PMS and PLS (Fig. 21K); 2 = extremely advanced from PMS and PLS (Fig. 21C, D, J). This is also a character proposed by Platnick & Baehr (2006) to characterize the position of the ALS in the former Molycriinae. We modified the character and included one additional state, since some species have the ALS slightly advanced. We considered this new condition as ALS separated from the spinnerets but still located on the distal third of the abdomen.
167. **Spinnerets, ALS, distance between them in relation to their diameter (Ramírez, 2014, char. 243):** 0 = contiguous to separated by less than one ALS diameter (Fig. 21E–G); 1 = separated by approximately one ALS diameter or more (Fig. 21H, I).
168. **Spinnerets, ALS, sclerotizaton close to base:** 0 = absent; 1 = present (Fig. 21H).
169. **Spinnerets, long and erect setae between ALS and posterior spinnerets: 0** = absent; 1 = present (Fig. 21G, K).
170. **Spinnerets, ALS, surface, plumose setae:** 0 = absent; 1 = present. Azevedo *et al.* (2018)

described the scales for carapace, legs and abdomen. We identified that some species also have scales on the ALS. All species with scales on the ALS also had them in other parts.

171. **Spinnerets, ALS, surface, plumose setae, appendages (brachia) arrangement:** 0 = only on proximal part; 1 = reaching terminal half.
172. **Spinnerets, ALS, surface, squamose setae:** 0 = absent; 1 = present.
173. **Spinnerets, ALS, surface, squamose setae, lateroventral appendages:** 0 = absent; 1 = present.
174. **Spinneres, ALS, surface, squamose setae, dorsolateral spines:** 0 = absent; 1 = present.
175. **Spinnerets, ALS, surface, squamose setae, dorsolateral spines, arrangement:** 0 = on both sides; 1 = only on one side.
176. **Spinnerets, ALS, surface, squamose setae, number of axes (shafts):** 0 = zero; 1 = one; 2 = two.
177. **Spinnerets (M), ALS, pyriform gland spigots (**Ramírez, 2014**, char. 300):** 0 = absent; 1 = present (Figs 22A, C, D, 23A, D, E).
178. **Spinnerets (F), ALS, pyriform gland spigots (**Ramírez, 2014**, char. 301):** 0 = absent; 1 = present (Figs 22E–G, 23F, J, L).
179. **Spinnerets, ALS, pyriform gland spigots, central spigot with plumose base (**Ramírez, 2014**, char. 270):** 0 = absent; 1 = present (Fig. 23C). Character proposed by Ramírez (2014) to show the morphology of one central pyriform spigot found in *Lygromma*. In *Lygromma gasnieri*, we observed three central pyriform spigots, scored 1. This is not observed in all species of *Lygromma* (pers. obs.) and a more detailed examination of the genus is necessary to elucidate this condition.
180. **Spinnerets, base spigot, Pi, insertion articulation, type (**Azevedo *et al.*, 2018**, char. 319):** 0 = simple; 1 = insertion annulate, flexible (Fig. 23K).
181. **Spinnerets, base spigot, MaAm, insertion articulation, type (**Azevedo *et al.*, 2018**, char. 319):** 0 = simple; 1 = insertion annulate, flexible.
182. **Spinnerets, base spigot, Ac, insertion articulation, type (**Azevedo *et al.*, 2018**, char. 319):** 0 = simple; 1 = insertion annulate, flexible.
183. **Spinnerets, base spigot, MiAm, insertion articulation, type (**Azevedo *et al.*, 2018**, char. 319):** 0 = simple; 1 = insertion annulate, flexible.
184. **Spinnerets, base spigot, Cy, insertion articulation, type (**Azevedo *et al.*, 2018**, char. 319):** 0 = simple; 1 = insertion annulate, flexible.
185. **Spinnerets, ALS, pyriform gland spigots, texture of base (**Ramírez, 2014**, char. 261, mod.):** 0 = longitudinal ridges (Fig. 23E); 1 = concentric ridges (Fig. 23B, C); 2 = smooth (Fig. 23H); 3 = imbricate (Fig. 22J); 4 = cracked (Fig. 23I). We modified this character proposed by Ramírez (2014) to include other states.
186. **Spinnerets, ALS, pyriform gland spigots, shaft fused to base (**Ramírez, 2014**, char. 263):** 0 = absent, shaft and base delimited (Fig. 22C, D); 1 = present, fused (Fig. 22A, B, E).
187. **Spinnerets, ALS, pyriform gland spigots, insertion:** 0 = insertion simple, continuous with cuticle (Fig. 22C); 1 = on well-defined base (Fig. 23F). A well-defined base is determined when enough aligned plumose setae are on the outside margin of each pyriform gland spigot, giving the base a 'wagon wheel' appearance when the setae fall off (Platnick, 1990).
188. **Spinnerets (F), ALS, pyriform gland spigots, position (**Azevedo *et al.*, 2018**, char. 302):** 0 = only on the edge (Fig. 22A); 1 = on the edge and in the middle of the spinneret (Fig. 23K).
189. **Spinnerets, ALS, distal article (**Azevedo *et al.*, 2018**, char. 273):** 0 = completely sclerotized ring; 1 = incomplete ring (Figs 22A, B, 23D, G).
190. **Spinnerets, ALS, distal article, incomplete ring, type (**Azevedo *et al.*, 2018**, char. 274):** 0 = semicircle in the anterior margin (Fig. 22A, B); 1 = patches of setae at the base of the gland spigots (Fig. 23); 2 = retractile area (Fig. 22I–L).
191. **Spinnerets, ALS, pyriform gland spigots, base length:** 0 = moderately short (Fig. 23D, E); 1 = extremely elongated (Fig. 23J–L). Applicable only to taxa with ALS pyriform gland spigots associated with plumose setae.
192. **Spinnerets, ALS, spinning field, inflatable membrane (**Ramírez, 2014**, char. 268):** 0 = absent; 1 = present (Fig. 23G, K).
193. **Spinnerets, ALS, pyriform gland spigots, base length relative to shaft (**Azevedo *et al.*, 2018**, char. 283):** 0 = shorter than or as short as (Fig. 22A–E); 1 = longer (Fig. 22F–K).
194. **Spinnerets, ALS, pyriform gland spigots, base width in relation to major ampullate gland spigots (**Azevedo *et al.*, 2018**, char. 284):** 0 = about the same; 1 = greatly widened (Figs 22B, C, 23D, L).

195. **Spinnerets, ALS, pyriform gland spigots, length relative to the major ampullate gland spigots (Azevedo *et al.*, 2018, char. 285):** 0 = shorter or about the same; 1 = longer (Figs 22B, 23H).
196. **Spinnerets, ALS, pyriform gland spigots, shaft width relative to base (Azevedo *et al.*, 2018, char. 288):** 0 = narrower (Fig. 22C, D); 1 = as wide as base, with broad openings (Fig. 22A, B, E).
197. **Spinnerets, ALS, major ampullate gland spigots field, conical setae-bearing projection (Ramírez, 2014, char. 257):** 0 = absent, field on a flat or slightly domed area (Fig. 22B, C); 1 = present, field on a conical, well-defined, setae-bearing article (Fig. 23D, H, I).
198. **Spinnerets, ALS, major ampullate gland spigots field, conical setae-bearing projection, length:** 0 = short (Fig. 23D, E); 1 = extremely elongated (Fig. 23I, K, L).
199. **Spinnerets (M), ALS, major ampullate gland spigots, ectal spigot (Azevedo *et al.*, 2018, char. 297):** 0 = absent; 1 = present, functional or as a nubbin (Fig. 23D).
200. **Spinnerets (M), ALS, major ampullate gland spigots, mesal spigot (Azevedo *et al.*, 2018, char. 298):** 0 = absent (Fig. 23D); 1 = present (Fig. 23H).
201. **Spinnerets (M), ALS, major ampullate gland spigots, mesal spigot, type (Azevedo *et al.*, 2018, char. 299):** 0 = normal (Fig. 23H); 1 = nubbin (Fig. 22C).
202. **Spinnerets (F), ALS, major ampullate gland spigots, ectal spigot (Azevedo *et al.*, 2018, char. 294):** 0 = absent; 1 = present, functional or as a nubbin (Fig. 23B).
203. **Spinnerets (F), ALS, major ampullate gland spigots, mesal spigot (Azevedo *et al.*, 2018, char. 295):** 0 = absent (Fig. 23L); 1 = present (Fig. 23B).
204. **Spinnerets (F), ALS, major ampullate gland spigots, mesal spigot, type (Azevedo *et al.*, 2018, char. 296):** 0 = normal (Fig. 23B); 1 = nubbin.
205. **Spinnerets (F), ALS, anterior (ectal) major ampullate gland spigots, shaft and base, thickness relative to posterior (mesal) (Ramírez, 2014, char. 254):** 0 = ectal thinner (Fig. 23B); 1 = same size (Fig. 22B); 2 = ectal thicker.
206. **Spinnerets, major ampullate and aciniform gland spigots, shaft, shape (Ramírez, 2014, char. 250):** 0 = cylindrical or tapering (Fig. 24F); 1 = clavate, widened at the tip (Fig. 24H, I).
207. **Spinnerets (F), ALS, spinning field, furrow between major ampullate and pyriform gland spigots (Azevedo *et al.*, 2018, char. 303)**: 0 **=** absent; 1 = present.
208. **Spinnerets (M), ALS, spinning field, furrow between major ampullate and pyriform gland spigots (Azevedo *et al.*, 2018, char. 304):** 0 = absent; 1 = present.
209. **Spinnerets, ALS, dorsal hood:** 0 = absent; 1 = present (Fig. 22E, F, H, L). The hood of the dorsoapical extension of ALS is probably used to protect the pyriform spigots tips. All species with this structure have elongate pyriform spigots without associated setae, except *Asemesthes* sp. that has a hood and pyriform spigots not elongate.
210. **Spinnerets, PMS insertion:** 0 = directly on cuticle; 1 = high on a cuticular base (Fig. 19B).
211. **Spinnerets (F), PMS, aciniform gland spigots (Azevedo *et al.*, 2018, char. 310):** 0 = absent; 1 = present (Fig. 24B, E, J).
212. **Spinnerets (M), PMS, aciniform gland spigots (Azevedo *et al.*, 2018, char. 311):** 0 = absent; 1 = present.
213. **Spinnerets (F), PMS, minor ampullate gland spigots (Azevedo *et al.*, 2018, char. 316):** 0 = absent; 1 = present (Fig. 24F, L).
214. **Spinnerets (M), PMS, minor ampullate gland spigots (Azevedo *et al.*, 2018, char. 317):** 0 = absent; 1 = present.
215. **Spinnerets (F), PMS, cylindrical gland spigots (Azevedo *et al.*, 2018, char. 312):** 0 = absent; 1 = present (Fig. 24A–E).
216. **Spinnerets, PMS, aciniform gland spigot, arrangement:** 0 = scattered (Fig. 24E, J); 1 = clustered (Fig. 24K).
217. **Spinnerets (F), PMS, cylindrical gland spigots, forming separated field (Ramírez, 2014, char. 284):** 0 = absent; 1 = present, the cylindrical spigots are not mixed with other spigots (Fig. 24A, C).
218. **Spinnerets, PMS–PLS, claviform setae (Ramírez, 2014, char. 292):** 0 = absent; 1 = present (Fig. 25J, K).
219. **Spinnerets (F), PLS, aciniform gland spigots (Azevedo *et al.*, 2018, char. 305):** 0 = absent; 1 = present (Fig. 25A, C, E).
220. **Spinnerets (M), PLS, aciniform gland spigots (Azevedo *et al.*, 2018, char. 306):** 0 = absent; 1 = present.
221. **Spinnerets (F), PLS, minor ampullate gland spigots (Azevedo *et al.*, 2018, char. 308):** 0 = absent; 1 = present (Fig. 25F, H, L).
222. **Spinnerets (M), PLS, minor ampullate gland spigots (Azevedo *et al.*, 2018, char. 309):** 0 = absent; 1 = present.

223. **Spinnerets (F), PLS, cylindrical gland spigots (**Azevedo *et al.*, 2018**, char. 307):** 0 = absent; 1 = present (Fig. 25B, D, G).
224. **Spinnerets, massive PLS:** 0 = absent; 1 = present (Figs 21L, 25J).

Female palp

225. **Female palp, tarsus, dorsal, chemosensory setae, distribution (**Ramírez, 2014**, char. 83):** 0 = scattered (Fig. 26A); 1 = in a defined patch (Fig. 26C).
226. **Female palp, tarsus, dorsal, chemosensory patch, configuration (**Ramírez, 2014**, char. 84):** 0 = on dorsoapical surface; 1 = on apical truncation (Fig. 26C–E).
227. **Female palp, tarsus, terminal, claw (**Azevedo *et al.* 2018**, char. 213):** 0 = absent (Fig. 26C); 1 = present, normal (Fig. 26F); 2 = present, reduced (Fig. 26E). We consider the claw reduced when it is small, poorly formed (with or without teeth) and inserted on the basal margin of the apical truncated patch. Probably, some of them are nonfunctional.
228. **Female palp, tarsus, terminal, claw, teeth (**Azevedo *et al.*, 2018**, char. 214):** 0 = absent; 1 = present (Fig. 26E, F).
229. **Female palp, femur, lateroventral row of long and strong spines (**Platnick & Baehr, 2006**, char. 10):** 0 = absent (Fig. 26B, C); 1 = present (Fig. 26A).

Male Palp

230. **Palp, femur, ventral median apophysis (**Ramírez, 2014**, char. 306):** 0 = absent; 1 = present.
231. **Palp, tibia, size:** 0 = short, less than cymbium length; 1 = long, equal or longer than cymbium length (Azevedo *et al.*, 2018, fig. 21C).
232. **Palp, tibia, RTA (**Ramírez, 2014**, char. 311):** 0 = absent; 1 = present (Fig. 26G–K). We consider any apophysis located retrolaterally on the tibia an RTA, regardless if the position is distal, basal or displaced to a dorsal or ventral position. Only *Gallianoela* sp. do not have an RTA. *Wesmaldra bidgemia* was described as lacking an RTA, but we consider the slight retrolateral projection on tibia as RTA, scored 1.
233. **Palp, tibia, vRTA:** 0 = absent (Fig. 26G–I); 1 = present (Fig. 26J). Some species have two RTAs and here we separated them into ventral RTA (vRTA) and dorsal RTA (dRTA). We considered the dRTA present in all species of our dataset, except *Gallianoela* sp., and therefore the vRTA was considered an extra apophysis.
234. **Palp, tibia, vRTA conformation:** 0 = simple; 1 = bifid (Fig. 26J).
235. **Palp, tibia, dRTA position:** 0 = apical; 1 = median.
236. **Palp, tibia, dRTA conformation:** 0 = simple (Fig. 26G); 1 = bifid (Fig. 26I).
237. **Palp, tibia, RTA sclerotization (**Ramírez, 2014**, char. 315):** 0 = all sclerotized; 1 = with membranous area (Ramírez, 2014, fig. 145A).
238. **Palp, tibia, VTA (**Azevedo *et al.*, 2018**, char. 266):** 0 = absent; 1 = present (Fig. 26K).
239. **Palp, tibia, DTA (**Azevedo *et al.*, 2018**, char. 268):** 0 = absent; 1 = present (Fig. 26L).
240. **Palp, cymbium, apical, conformation (**Ramírez, 2014**, char. 325):** 0 = elongate, extending beyond distal margin of alveolus (Fig. 27G, H); 1 = short, wide, not extending beyond distal margin of alveolus (Fig. 27K).
241. **Palp, cymbium, apical, ventral groove (**Ramírez, 2014**, char. 323):** 0 = absent; 1 = present (Fig. 27B). This is a conductor-like structure proposed by Ramirez (1995) to characterize some Anyphaenidae spiders. In this dataset, only *Xiruana gracilipes* and *Asemesthes* sp. have ventral grooved cymbium.
242. **Palp, cymbium, retromedian process (**Azevedo *et al.*, 2018**, char. 254):** 0 = absent; 1 = present (Fig. 26H).
243. **Palp, cymbium, retromedian process, type (**Azevedo *et al.*, 2018**, char. 255):** 0 = without incision; 1 = with incision, forming a conductor canal-like (Fig. 26H).
244. **Palp, cymbium, retrobasal process (paracymbium) (**Azevedo *et al.*, 2018**, char. 256):** 0 = absent; 1 = present (Fig. 26G).
245. **Palp, cymbium, ventral, terminal, bunch of thick setae (**Ramírez, 2014**, char. 326):** 0 = absent; 1 = present (Fig. 27J–L).
246. **Palp, cymbium, dorsal, terminal, chemosensory patch (**Ramírez, 2014**, char. 324):** 0 = absent; 1 = present (Fig. 27G, J).
247. **Palp, cymbium, dorsal, trichobothria (**Ramírez, 2014**, char. 329):** 0 = absent; 1 = present.
248. **Palp, copulatory bulb, median apophysis (**Ramírez, 2014**, char. 356):** 0 = absent (Fig. 27I, K, L); 1 = present (Fig. 27E–H).
249. **Palp, copulatory bulb, median apophysis, numerous small spines (granulation) (**Azevedo *et al.*, 2018**, char. 236):** 0 = absent; 1 = present (Fig. 27B).

250. Palp, copulatory bulb, median apophysis, sclerotization (Azevedo *et al.*, 2018**, char. 237):** 0 = completely sclerotized (Fig. 27A, B); 1 = partially sclerotized (Fig. 27C); 2 = not sclerotized.

251. Palp, copulatory bulb, median apophysis, shape (Azevedo *et al.*, 2018**, char. 238):** 0 = elongate (Fig. 27E); 1 = rounded, or irregularly shaped, but approximately as long as wide (Fig. 27B).

252. Palp, copulatory bulb, median apophysis, terminal hook (Azevedo *et al.*, 2018**, char. 239):** 0 = absent (Fig. 27B, C); 1 = present (Fig. 27E, J).

253. Palp, copulatory bulb, conductor (Ramírez, 2014**, char. 359):** 0 = absent (Fig. 27B, C); 1 = present (Fig. 27I, K).

254. Palp, copulatory bulb, conductor, sclerotization (Ramírez, 2014**, char. 360):** 0 = hyaline (Fig. 27I); 1 = sclerotized (Fig. 27G).

255. Palp, copulatory bulb, conductor, shape (Azevedo *et al.*, 2018**, char. 218, mod.):** 0 = robust, rounded, folds; 1 = simple, thin, elongated (Fig. 27G, H).

256. Palp, copulatory bulb, embolus, insertion on tegulum in unexpanded bulb (Azevedo *et al.*, 2018**, char. 225):** 0 = retrolateral (Fig. 27G, K); 1 = prolateral (Fig. 27H, I).

257. Palp, copulatory bulb, embolus, fused to tegulum (Ramírez, 2014**, char. 351):** 0 = fixed; 1 = flexibly attached.

258. Palp, copulatory bulb, embolus, embolar base proximal projection (Azevedo *et al.*, 2018**, char. 221):** 0 = absent; 1 = present (Azevedo *et al.*, 2018, fig. 15F).

259. Palp, copulatory bulb, embolus, embolar locking lobe (Azevedo *et al.*, 2018**, char. 223):** 0 = absent; 1 = present (Azevedo *et al.*, 2018, fig. 21G).

260. Palp, copulatory bulb, embolus, shape: 0 = robust with folds (Fig. 27A); 1 = tubular, simple, thin, elongated (Fig. 27D–L).

261. Palp, copulatory bulb, tegulum, distal tegular spine-like process (Azevedo *et al.*, 2018**, char. 247):** 0 = absent; 1 = present (Fig. 27D). Sclerotized process found in some Molycriinae. Same as terminal apophysis in Platnick & Baehr (2006).

262. Palp, copulatory bulb, tegulum, laminar extension: 0 = absent; 1 = present (Fig. 27I).

263. Palp, copulatory bulb, tegulum, proximal part, covered by subtegulum (Azevedo *et al.*, 2018**, char. 248):** 0 = absent; 1 = present (Fig. 27B).

264. Palp, copulatory bulb, terminal apophysis (Azevedo *et al.*, 2018**, char. 249):** 0 = absent; 1 = present (Azevedo *et al.*, 2018, fig. 23A).

265. Palp, copulatory bulb, tegular excavation (embolus accommodation): 0 = absent; 1 = present (Fig. 27F, G, K). Some Prodidominae have a groove in the tegulum that accommodates the embolus.

Epigyne

266. Epigyne, posterior extension (Ramírez, 2014**, char. 367):** 0 = not extending much beyond the epigastric furrow; 1 = evidently projecting posteriorly.

267. Epigyne, posterior notch: 0 = absent; 1 = present (Fig. 28I, K, L).

268. Epigyne, posterior hood: 0 = absent; 1 = present (Fig. 28G, H). The epyginal plate has a sclerotized structure, here termed posterior hood, that is not homologous to the hood formed by the anterior fold.

269. Epigyne, anterior fold (Azevedo *et al.*, 2018**, char. 96)**: 0 = absent; 1 = present (Fig. 28D, E).

270. Epigyne, anterior fold, posterior extension forming a secondary lateral fold (Azevedo *et al.*, 2018**, char. 97)**: 0 = absent; 1 = present (Fig. 28E).

271. Epigyne, anterior fold, hood (Azevedo *et al.*, 2018**, char. 98)**: 0 = absent; 1 = present.

272. Epigyne, anterior fold, scape (Azevedo *et al.*, 2018**, char. 99)**: 0 = absent; 1 = present (Fig. 28A, C).

273. Epigyne, lateral folds (Azevedo *et al.*, 2018**, char. 100):** 0 = absent, the epigyne is an undivided plate (Fig. 28F); 1 = present, there are sutures or furrows delimiting the epigynal fields (Fig. 28A, G).

274. Epigyne, lateral folds, type (Azevedo *et al.*, 2018**, char. 101)**: 0 = suture (Fig. 28G); 1 = furrow (Fig. 28A).

275. Epigyne, median field, septum (Azevedo *et al.*, 2018**, char. 103):** 0 = absent; 1 = present (Fig. 28B).

276. Epigyne, median field, plate surface, atrium (Azevedo *et al.*, 2018**, char. 104)**: 0 = absent, median field on same plane as lateral field; 1 = present, there is an excavation on the median field (Fig. 28J).

277. Epigyne, vulva, primary spermathecae (Azevedo *et al.*, 2018**, char. 111):** 0 = inconspicuous (Fig. 29F, I); 1 = conspicuous (Fig. 29A–C). The primary spermathecae is the receptacle to which the fertilization duct is connected. Usually this structure is

well-defined in the vulva, but some species do not have this spermathecae distinct, the copulatory duct is continuous.

278. Epigyne, vulva, primary spermathecae, position (Azevedo *et al.*, 2018**, char. 112):** 0 = paramedian, separated by less than half of the epigyne width (Fig. 29G); 1 = lateral, separated by more than half of the epigyne width (Fig. 29H).

279. Epigyne, vulva primary spermathecae, shape (Azevedo *et al.*, 2018**, char. 119):** 0 = rounded (Fig. 29L); 1 = elongated; 2 = reniform (Fig. 29K).

280. Epigyne, vulva, secondary spermathecae (Azevedo *et al.*, 2018**, char. 114):** 0 = absent (Fig. 29G, I); 1 = present (Fig. 29A–F). The secondary spermathecae is a receptacle with glandular pores. This spermathecae can be a blind sac or reduced to a patch of gland pores, usually emerging from the copulatory ducts, but can also emerge from the primary spermathecae.

281. Epigyne, vulva, secondary spermatheca, location (Azevedo *et al.*, 2018**, char. 115):** 0 = copulatory duct (Fig. 29A, H, J); 1 = spermathecae (Fig. 29B).

282. Epigyne, vulva, secondary spermatheca, well-defined lumen (Azevedo *et al.*, 2018**, char. 116):** 0 = absent, reduced to a patch of gland pores in the copulatory duct or in the primary spermathecae (Fig. 29B, H); 1 = present, a blind sac with well-defined lumen (Fig. 29C, J, K).

283. Epigyne, vulva, secondary spermathecae, size relative to primary spermathecae (Azevedo *et al.*, 2018**, char. 117):** 0 = smaller (Fig. 29A–C); 1 = as large as (Fig. 29J); 2 = larger.

284. Epigyne, vulva, secondary spermathecae, long duct (at least twice the spermathecae diameter) (Azevedo *et al.*, 2018**, char. 118):** 0 = absent; 1 = present (Fig. 29F, K).

285. Epigyne, vulva, secondary spermathecae, position: 0 = closer to copulatory opening (Fig. 29L); 1 = closer to primary spermathecae (Fig. 29D); 2 = approximately median, between PS and CO (Fig. 29A).

286. Epigyne, vulva, copulatory ducts, shape (Azevedo *et al.*, 2018**, char. 106)**: 0 = highly convoluted (Fig. 29F); 1 = spiral; 2 = curved or with some curls (Fig. 29I).

287. Epigyne, vulva, copulatory ducts, sclerotization (Azevedo *et al.*, 2018**, char. 107):** 0 = completely sclerotized (Fig. 29A, I); 1 = partially sclerotized (Fig. 29F, H).

288. Epigyne, vulva, copulatory ducts, width: 0 = similar width along the ducts (Fig. 29J); 1 = wider closest to the copulatory opening (Fig. 29H); 2 = wider closest to the PS.

289. Epigyne, vulva, fertilization duct, position (Ramírez, 2014**, char. 379):** 0 = posterior, close to the epigastric furrow (Fig. 29G, H); 1 = well advanced from the epigastric furrow (Fig. 29K).

290. Epigyne, vulva, fertilization duct, direction (Azevedo *et al.*, 2018**, char. 109):** 0 = ventrally directed (Fig. 29G); 1 = posteriorly directed (Fig. 29B).